

***Ministry of Higher Education  
and Scientific Research  
University of Kerbala  
College of Engineering  
Mechanical Engineering Department***



***Investigation of Thermal performance of Phase Change  
Material Heat Exchanger***

***A Thesis***

***Submitted to the Mechanical Engineering Department at  
the University of Kerbala in a Partial Fulfillment of the  
Requirements for the Degree of Master of Science in  
Mechanical Engineering.***

***By***

***Wisam Abbas Dukhan  
(B.Sc. University of Babylon 2004)***

***Supervisors***

***Prof.Dr.Tahseen Ali H. AL-Hattab  
Asst.Prof.Dr.Nabeel S. Dhaidan***

بِسْمِ اللّٰهِ الرَّحْمٰنِ الرَّحِیْمِ

قُلْ لَوْ كَانُ الْبَحْرُ مَدَادًا لَّكَلِمَاتِ رَبِّي لَنَفَذَ الْبَحْرُ قَبْلَ

أَنْ تَنْفَدَ كَلِمَاتُ رَبِّي وَلَوْ جِئْنَا بِمِثْلِهِ مَدَدًا

صدق الله العظيم

سوره الكهف آیه (۱۰۹)

## **Supervisors' certification**

We certify that this thesis entitled “*Investigation of Thermal performance of Phase Change Material Heat Exchanger*” was prepared by *Wisam Abbas Dukhan* under our supervision at the Mechanical Engineering Department /College of Engineering/University of Kerbala, in partial fulfillment of the requirements for the Master Degree in Sciences of Mechanical Engineering.

### **Signature**

**Prof.Dr.Tahseen Ali H. .AL-Hattab**

**College of Engineering**

**University of Babylon**

**Date: / / 2019**

### **Signature:**

**Asst.Prof.Dr.Nabeel S. Dhaidan.**

**College of Engineering**

**University of Kerbala**

**Date: / /2019**

## **Acknowledgments**

First, I would like to express my sincere gratitude and thanks to Almighty ALLAH for the guidance through this work and for all the blessings bestowed upon me.

I would like to express my deep thanks and sincere gratitude to my supervisors **Prof.Dr.Tahseen A.AL-Hattab** and **Asst.Prof.Dr.Nabeel S. Dhaidan** for their assistance, guidance, encouragement and endless help throughout the steps of this work.

I am grateful to **Mr. Hussein H. Rashid**/mechanical engineering laboratories at Babylon university for helping me during the experimental work.

Thanks are also due to the head and staff of Mechanical Engineering Department University of Kerbala for all the assistance they present through the courses.

My sincere thanks also go to **Mr. Mohamed Raof** for his assistance with regard to the Ansys Fluent program.

I am also thankful to all who helped me directly or indirectly to accomplish this work.

## *Dedication*

*To those who supported me (my mother, brothers, and sisters).*

*To the one who supported me and walked with me step by step (my wife).*

*To my love and my joy (my daughters).*

*To those who gave me help, courage, and strength (my friends).*

*To the person who helped me getting my academic leave (my cousin Essam).*

*To my nephew Hussein.*

*Wisam*

*2019*

## Abstract

The present study includes an experimental and numerical investigation of the thermal performance of a phase change material (PCM) inside a concentric two pipes heat exchanger. The RT-42 Rubitherm PCM paraffin wax was used to fill the annular space between the hot copper inner pipe of 25 mm diameter and the external insulated acrylic shell of 75 mm diameter. The experimental setup involves twelve thermocouples to record the transient temperatures of PCM at desired locations. Also, the progress of solid-liquid front during the melting process is tracked photographically by a digital camera. A 2D numerical simulation applied the enthalpy-porosity method was used to solve the problem of PCM melting. The effect of the different temperatures (60, 70 and 80 °C) of hot water as heat transfer fluid (HTF) which flows inside the inner tube on the melting process is examined. Also, the impact of the two orientations (horizontal and vertical) of the heat exchanger on the behavior of melting PCM is researched.

The experimental and numerical results revealed that the melt layer of PCM is formed symmetrically around the inner pipe for both orientations of heat transfer due to the conduction domination at the first stage of melting process. Later, the melt layer of PCM grows and the influence of natural convection is developed causing a higher melting rate at the upper portion of the cavity. It has appeared that the melting time is clearly reduced by increasing the inlet temperature of water in both cases of the heat exchanger, horizontal and vertical. Also, the melting rate of PCM in the vertical direction is faster than the melting rate in the horizontal direction. The experimental results revealed that the melting time in horizontal PCM-annular cavity heat exchanger reduced about 27.5% and 46.3% when the temperature increased from 60 to 70 °C and from 60 to 80 °C, respectively. For the same temperature increase, the melting time is

accelerated by about 32.6% and 50.2% in the vertical heat exchanger. Also, the amounts of energy stored by PCM in the vertical heat exchanger are higher about 4, 14.2 and 16.3% than that obtained in the horizontal orientation at 140 min for 60, 70 and 80 °C respectively. In addition, the transient Nusselt number has the same behavior for the two orientations and changes positively with the amount of transferred thermal energy from HTF which in turns varies proportionally with an inlet temperature of HTF.

The numerical and experimental results showed a good agreement. The maximum differences between the numerical and experimental results for melting time, Nusselt number and energy storage is found to be 12.4, 22.5 and 22.1% for horizontal heat exchanger at 70 °C of inlet water temperature. While those differences are 10.7, 14.9 and 15.4% for vertical heat exchanger.

## Table of contents

<b><u>Subject</u></b>	
<b><u>page</u></b>	
Abstract .....	I
Table of contents .....	III
Nomenclatures .....	VII
<b>Chapter One – Introduction .....</b>	<b>1-7</b>
1.1 Overview .....	1
1.2 Thermal energy storage .....	1
1.3 Phase Change Materials (PCMs).....	2
1.3.1 PCMs classification.....	4
1.3.2 Properties of PCM.....	5
1.3.3 Applications of PCM .....	6
1.4 General description of the present work .....	6
<b>Chapter Two- Literature review.....</b>	<b>8-32</b>
2.1 PCM melting in cylindrical vessel heat exchanger.....	8
2.1.1 Melting of PCM inside Vertical cylindrical enclosures.....	8
2.1.2 Melting of PCM inside Horizontal cylindrical enclosures.....	10
2.2 PCM melting in rectangular cavity heat exchanger.....	14
2.3 PCM melting inside spherical vessel.....	19
2.4 PCM melting in annular heat exchanger.....	24
2.5 Scope of Present Study.....	32



<b>Chapter Three- Numerical Study</b> .....	33-48
3.1 Physical Model.....	33
3.2 Mathematical formulation of the problem.....	35
3.2.1 Model assumptions.....	36
3.2.2 The Governing Equations.....	36
3.2.3 Enthalpy–porosity method.....	37
3.2.4 Boundary and Initial Condition.....	38
3.3 Computational model .....	40
3.4 Validation of the Numerical model.....	41
3.5 Grid- independence test.....	43
3.6 Time-step independence test.....	45
3.7 The influence of the mushy zone constant .....	46
<b>Chapter Four – The experimental work</b> .....	49-63
4.1 Experimental setup .....	49
4.2 The components of the experimental setup.....	51
4.2.1 Hot water tank with an electric heater.....	51
4.2.2 Automatic temperature controller .....	51
4.2.3 Water pump .....	52
4.2.4 Water flowmeter .....	52
4.2.5 Thermocouples and temperature data logger .....	53
4.2.6 Thermal storage unit.....	56

4.2.7 Ball Valves and PVC piping system.....	57
4.3 Phase change material (RT-42).....	57
4.4 Experimental Procedure.....	58
4.5 Dimensionless parameters and data reduction.....	59
4.6 Error Analysis and Uncertainty .....	60
4.7 Repeatability Check .....	62
<b>Chapter Five- Result and Discussion.....</b>	<b>64-97</b>
5.1 The Experimental Results.....	64
5.1.1 PCM melting in the horizontal heat exchanger.....	64
5.1.1.1 Temperature Distribution of PCM.....	65
5.1.1.2 Transient Evolution of Solid-Liquid Interface and Melt Fraction .....	68
5.1.1.3 Variations of the Nusselt number. ....	70
5.1.1.4 Stored energy by PCM.....	71
5.1.2 PCM melting inside the vertical heat exchanger.....	73
5.1.2.1 Temperatures distribution of PCM.....	73
5.1.2.2 Transient Melting Front and Melt Fraction .....	75
5.1.2.3 The Time-Behavior of the Nusselt number .....	78
5.1.2.4 Stored Energy .....	79
5.2 The Numerical Results.....	81
5.2.1 Predicted melting front and temperature contours of PCM.....	81
5.2.2 Numerical results of the liquid fraction.....	84
5.2.3 The velocity vector of the PCM melt .....	86
5.2.4 Numerical results of the Nusselt number .....	89

5.2.5 Numerical energy stored by PCM.....	90
5.3 Comparison between Experimental findings and Numerical result....	92
<b>Chapter Six -Conclusion and Recommendation .....</b>	<b>98-99</b>
6.1 Conclusions .....	98
6.2 Recommendations for future works.....	99
<b>Reference.....</b>	<b>100- 105</b>
<b>Appendix-A (Calibration of Thermocouples and Data Logger.....</b>	<b>A1-A3</b>
<b>Appendix-B Evaluation of the effect of water flow rate on the melting process .....</b>	<b>B1-B2</b>

## NOMENCLATURES

SYMBOL	DESCRIPTION	UNITS
$C_p$	Specific heat	$\text{J kg}^{-1} \text{K}^{-1}$
$D$	Characteristic length storage cell	m
$f$	Melt fraction	
$h$	Average heat transfer coefficient	$\text{W m}^{-2} \text{K}^{-1}$
$k$	Thermal conductivity	$\text{W m}^{-1} \text{K}^{-1}$
$L$	Latent heat of melting	$\text{kJ kg}^{-1}$
$Q_s$	Stored thermal energy	kJ
$T$	Temperature	$^{\circ}\text{C}$
$r_i$	Radius of inner pipe	mm
$r_o$	Radius of outer cylinder	mm
$\Theta$	Angle of melting PCM	degree $^{\circ}$
$g$	Gravitational acceleration	$\text{m/s}^2$
$f$	Liquid fraction	
$V$	Velocity of liquid PCM ,	m/s
$k$	Thermal conductivity,	$\text{w.m}^{-1} .^{\circ}\text{C}^{-1}$
$H$	Total enthalpy	J/kg
$h$	Sensible enthalpy	J/kg
$L$	Latent heat of material.	J/kg
$Pr$	Prandtl number = $\frac{c_p \mu}{k}$	
$Ste$	Stefan number = $\frac{c_p (T_w - T_m)}{L}$	
$Ra$	Rayleigh number = $\frac{\rho^2 D^3 g \beta c_p (T_w - T_m)}{\mu k}$	
$Nu$	Nusselt number = $\frac{h D}{k}$	
$U, V$	Velocity components	
$\Theta, r$	Polar coordinates, degree, and m	

### Greek symbols

SYMBOL	DESCRIPTION	UNITS
$\rho$	Density of PCM	$\text{Kg/m}^3$
$\mu$	Dynamic viscosity	$\text{Kg/m.s}$
$\nu$	Kinematics viscosity	$\text{m}^2/\text{s}$
$\alpha$	Thermal diffusivity	$\text{m}^2/\text{s}$
$\beta$	Thermal expansion coefficient	$1/\text{k}$

### Subscripts

SYMBOL	DESCRIPTION
w	heated wall
l	liquid PCM
s	solid PCM
M	Melting
PCM	phase change material
I	initial , inner pipe
O	Outer cylinder
Ref	Reference value

# CHAPTER ONE

## INTRODUCTION

## 1.1 Overview

Energy is an extremely important aspect of our daily life, and the need for energy is continuously increasing with the development of life. People depend on fossil fuels to provide energy for life requirements for long periods of time. The combustion products of fossil fuels cause environmental pollution and global warming that has led researchers to use renewable energy. The problem of renewable energy is how to keep energy available and sustainable which attracting the attention of many researchers. Studies were carried out on renewable energy such as solar energy, wind and tidal energy to avoid the depletion and the pollution produced by using fossil fuel.

## 1.2 Thermal energy storage

The unavailability of renewable energy at all times becomes a major obstacle of increasing the investments of renewable resources. For example, solar energy exists during the day and lost at night [1]. For this reason, energy storage becomes an insisting necessity to keep energy when it is needed. The thermal energy can be stored as sensible, latent and chemical as shown in Fig. (1.1). In thermal systems, the energy can be stored in two forms: sensible and latent. The sensible storage occurs by changing the temperature and phase stability and can be inferred through thermocouples. While the latent heat storage occurs when the phase changes from phase to another phase at an approximately constant temperature. The latent heat has the following conversions; solid-to-liquid with expansion volume, solid-gaseous, solid-solid as a change in the molecular structure of the material occurs as a result of thermal gain. The thermal energy can be stored/released during the chemical reactions.

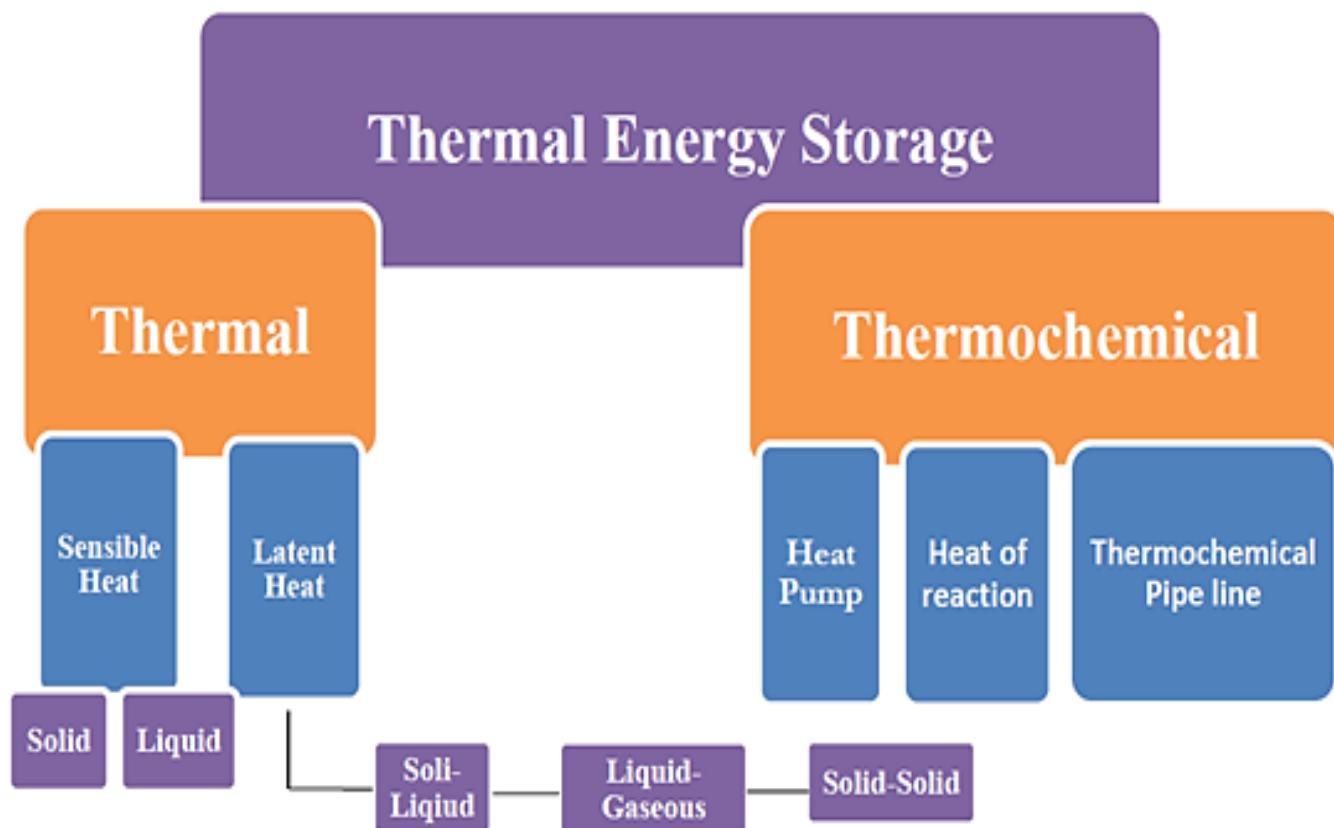


Fig. (1.1) Illustrated the kind of thermal storage [2].

### 1.3 Phase Change Materials (PCMs)

Recently, the phase change materials have taken considerable interest from researchers because they have the ability to store (charging) and release (discharging) a large amount of thermal energy compared to sensible energy storage system. In charging (melting) process, the heat is absorbed by PCM and changes it from the solid phase to the liquid phase. Conversely, in discharging (solidification) process, the transition from a liquid phase to solid phase requires the releasing of heat. The thermal energy is stored inside the PCM in two stages: the sensible heat and the latent heat as described by Fig. (1.2). It is worth noting that the thermal energy storage systems consist of three main parts: PCM, suitable heat exchanger (container) and the surface of a thermal conductor between the PCM and the source of heat. Therefore, researchers studied the three parts to improve storage capacity and energy release by understanding the



melting behavior of the phase change materials in different geometrical shapes of heat exchangers such as rectangular, cylindrical, spherical, and annular [3].

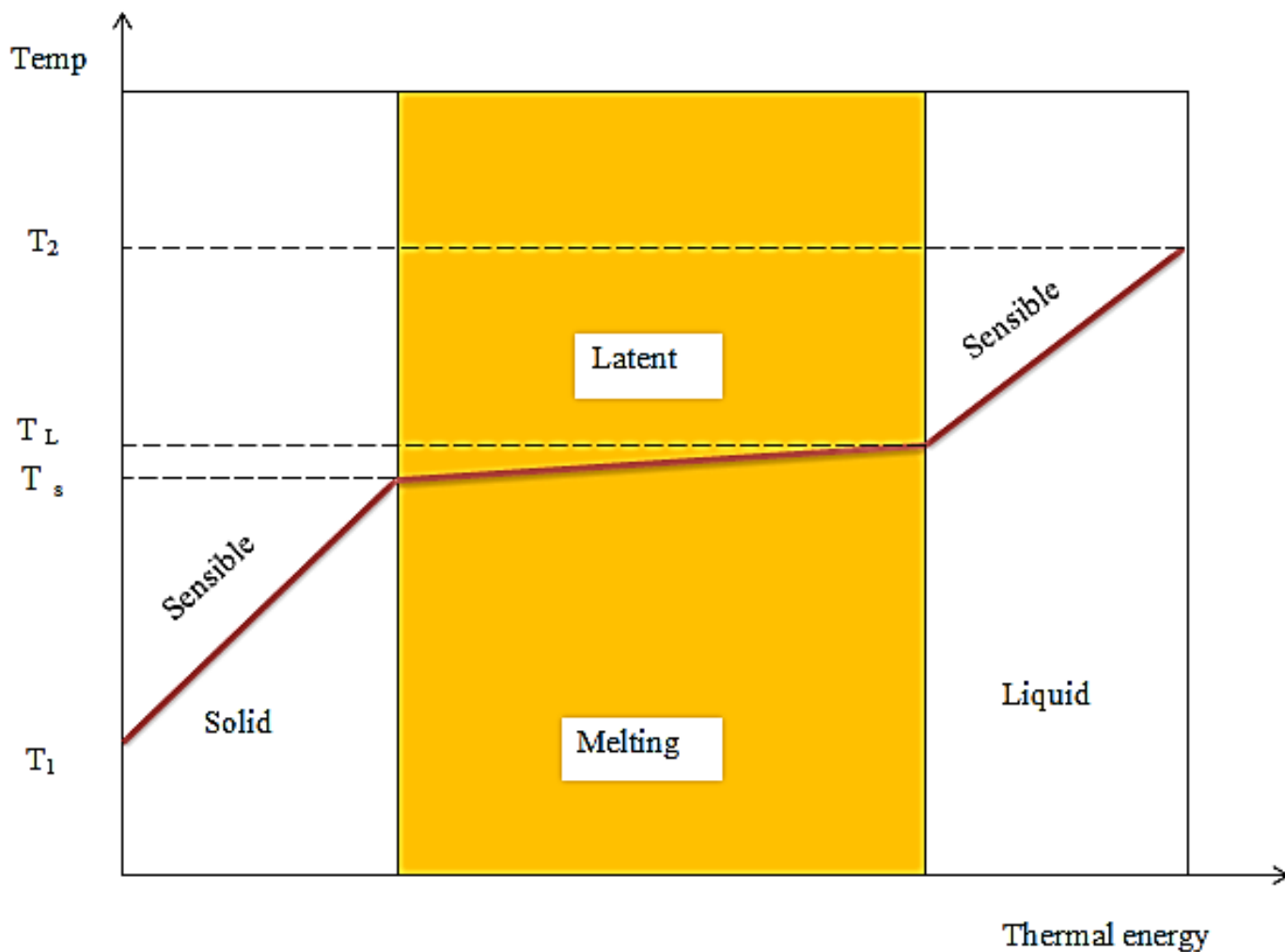


Fig. (1.2) Energy stored by PCM vs. temperature during the sensible and latent stage.

### 1.3.1 PCMs classification

In general, PCM is classified into three main groups such as organic, inorganic and eutectics materials. Therefore, PCMs have characteristics that differ between them such as the melting point, expansion coefficient, latent heat and heat storage capacity [2]. The classification of PCM according to groups is depicted in Fig. (1.3), while the range of the melting point for each group is introduced in Fig. (1.4).

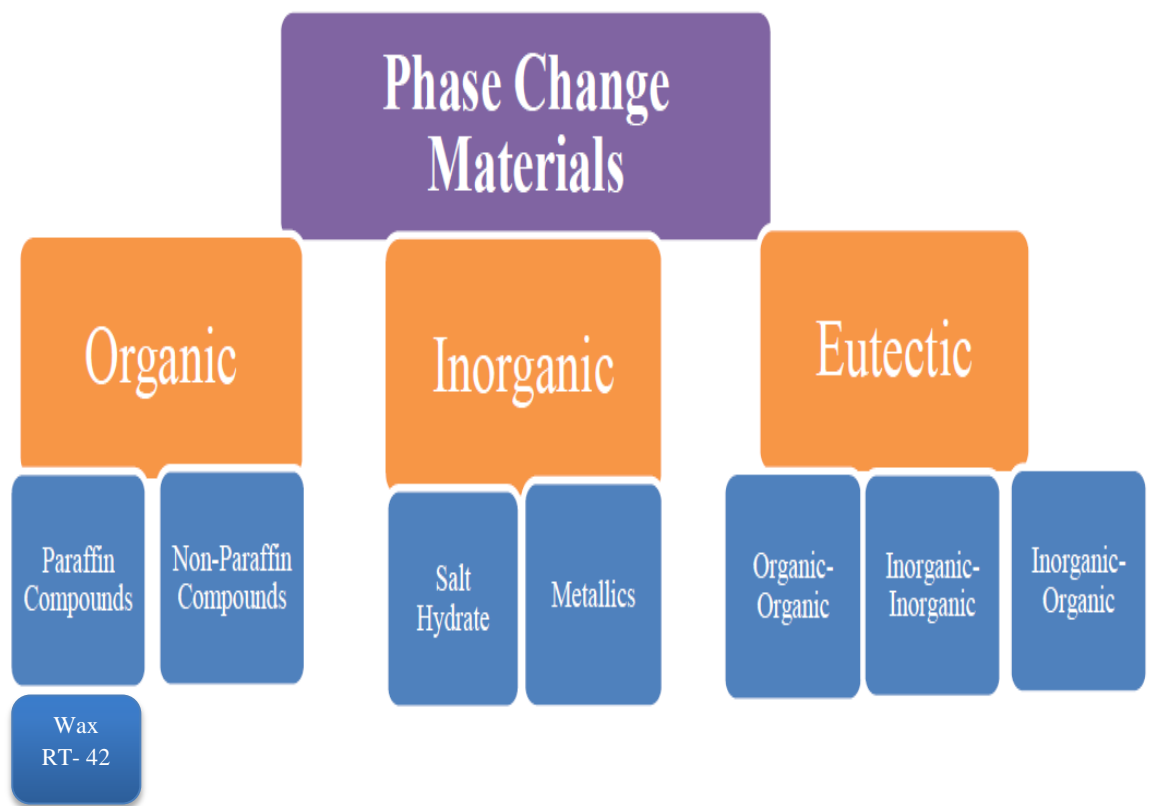


Fig. (1.3) The classifications of PCM[2].

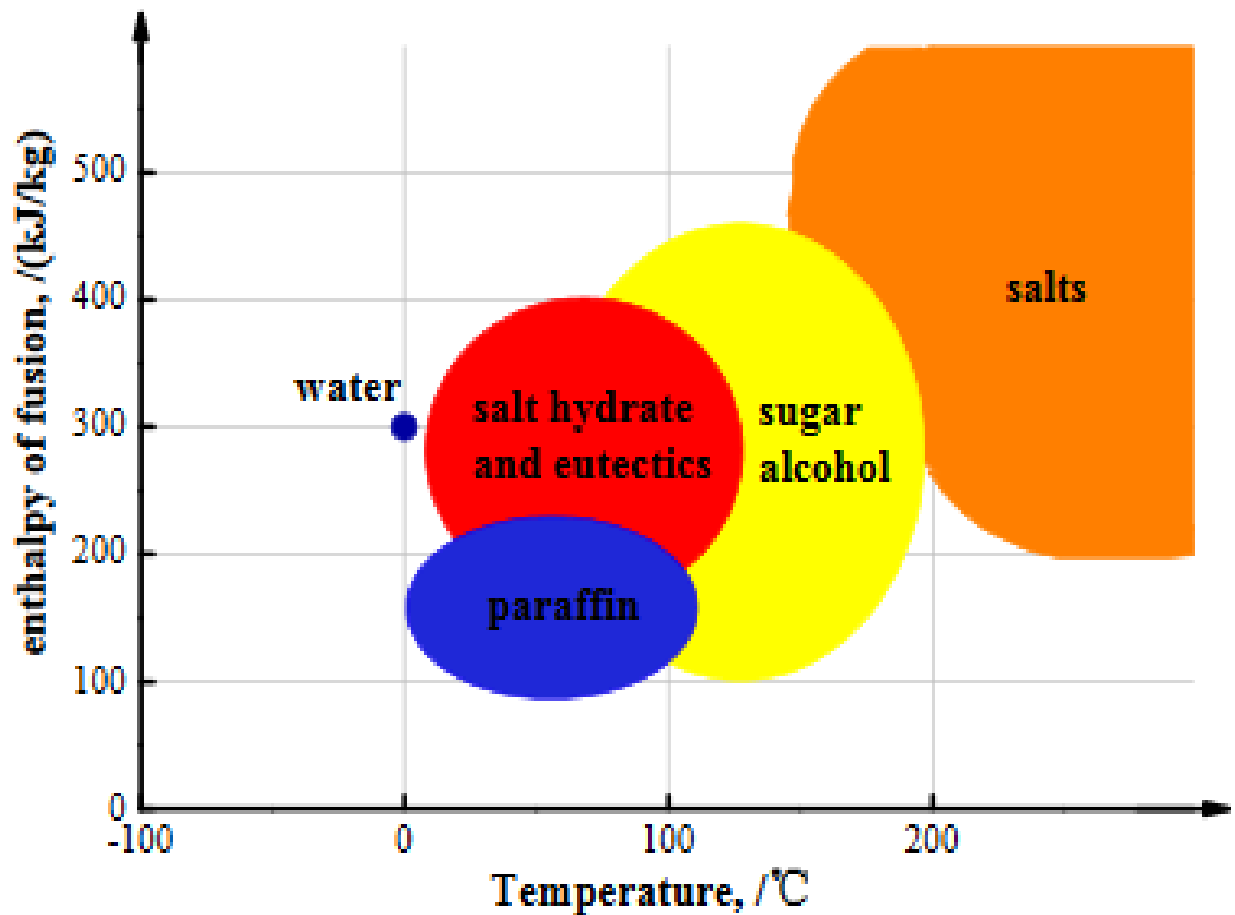


Fig. (1.4) Range of melting temperature and latent Heat for each group of PCMs [4] .

### 1.3.2 Properties of PCM ([2], [4])

- Thermo-physical properties
  - High energy storage with low volume change.
  - Limited thermal conductivity.
  - The phase change of PCM occurs at a constant temperature.
  - Service life is high (stable for more cycles).
- Chemical properties
  - Environment-friendly.
  - Non- toxic, non- explosive, non-corrosives.
  - Chemically stable.

### 1.3.3 Applications of PCM

Applications of phase change materials (Fig. (1.5)) include, but are not limited to:

- Thermal energy storage.
- Removing and dissipating the heat from electronic devices in spacecraft and clothing of astronauts.
- Cooling of battery.
- Clothing industry for firefighters.
- Medical fields such as blood container.
- Cooling of electronic elements such as processors, chips, etc.
- Insulation of buildings.

### 1.4 General description of the present work

The PCM is used as a medium of absorbing excessive heat when it is available and releasing it at another time when it is needed. The present study investigates experimentally and numerically the PCM-assisted heat exchanger of two orientations: horizontal and vertical. The PCM contained inside annular cavity receives heat from the hot water passing inside the inner tube. The effects of orientation of heat exchanger and the water temperature on the thermal behavior of melting of PCM are studied.

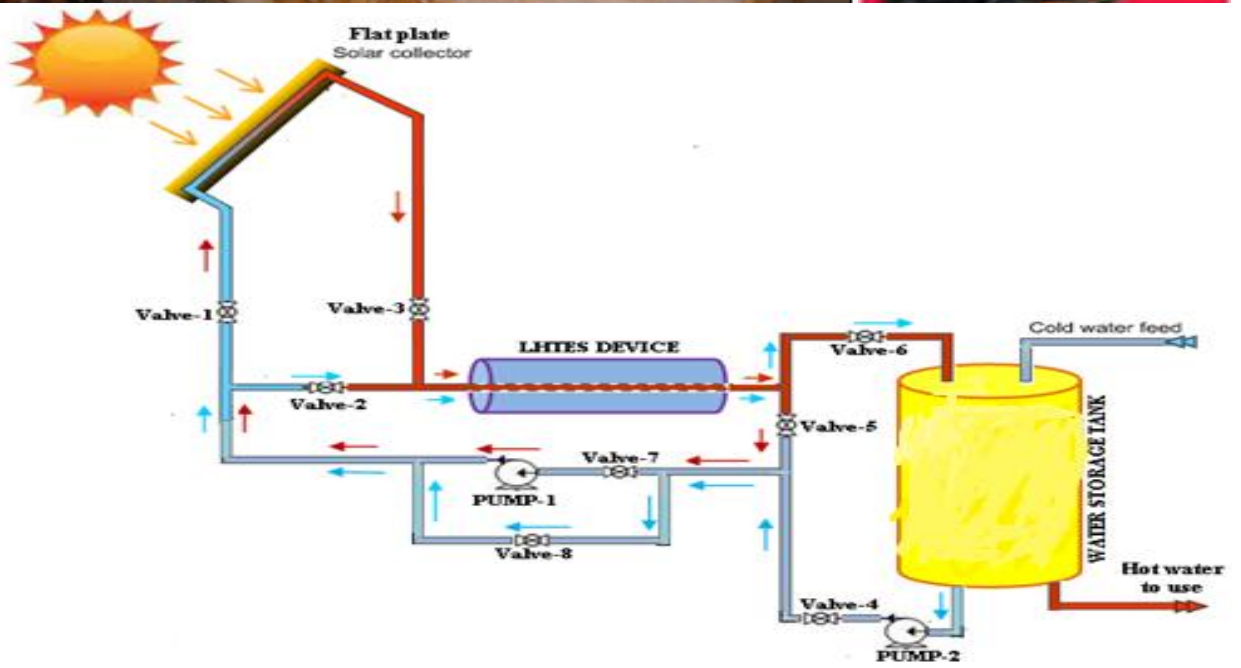


Fig. (1.5) Applications of PCM.

**CHAPTER TWO**  
**LITERATURE REVIEW**

## **Chapter Two: Literature Review**

This chapter introduces a review of the previous studies related to phase change materials (PCM) melting behavior in different shapes of heat exchangers (e.g. rectangular, cylindrical, spherical and annular).

### **2.1 PCM melting in the cylindrical vessel heat exchanger.**

The melting of PCM in the cylindrical cavity is affected by the orientation of the cavity (horizontal or vertical), type of melting, geometrical of a container and operating conditions.

#### **2.1.1 Melting of PCM inside Vertical cylindrical enclosures.**

For the melting of PCM inside vertical cylinders occurs due to the heat supplied either from the outer wall of the cylinder or from the inside through a tube or rod passing through the cylinder.

Shmueli et al. [5] investigated experimentally and numerically the melting of RT-27 Rubitherm PCM inside a vertical cylinder. The cylinder was opened from the top and the PCM was exposed to the atmosphere. The enthalpy porosity formulation was adopted as a numerical solution. It is evident that the conduction dominates at the beginning of melting. As time travels, the natural convection dominates which leads to the change of solid PCM to a conical shape. This shape shrinks in size from top to the bottom. After PCM melted, the PCM layer which is exposed to air ascends as a result of the increase in volume during melting. Moreover, the temperature gradient of the upper part drops faster compared with the lower part due to the earlier solid melting in the upper part.

Waghmare and Pise [6] carried out a numerical study to investigate the effect of gravity and buoyancy on the melting PCM inside concentric vertical cylinders. Enthalpy porosity and volume of fluid

methods were used to solve the transient behavior of PCM melting problem. The numerical solution was validated through experimental findings. The results revealed that the heat is transported to PCM by conduction at the beginning of the melting process. Then, the liquid fraction is expanded and the convection becomes dominated heat transfer. It is observed that the effect of both gravity and buoyancy starts close to the hot tube, and the melt moves upward; then it descends to the bottom. Moreover, without gravity and buoyancy effects, the PCM melt moves from the tube in a radial direction and reaches the cylinder wall.

Bechiri and Mansouri [7] numerically and experimentally studied the melting of RT- 27 PCM inside a vertical cylinder. The upper part of the cylinder contains about 15% of the air to accommodate the PCM expansion during melting as exhibited in Fig. (2.1). The enthalpy-porosity methods, the finite volume technique, and the volume of fluid (VOF) model were used numerically to solve the PCM melting problem. The effect of different parameters (Fourier number, Grashof number, wall conductivity, and aspect ratio) were investigated, and it was found that all these parameters clearly affect the PCM melting rate. Also, the increase in wall temperature results in expediting the melting process while there is an inverse relationship between the melting rate and the size of the storage unit. In addition, it is noticed that longer melting time is occurred by increasing the wall thickness. Also, the initial temperature effected on the sensible and latent heating process. Decreasing the shell-to-tube diameter ratio leads to expediting the melting process.

Wang et al. [8] experimentally studied the melting of paraffin inside a vertical cylinder container. The PCM was heated by electric heater rod located in the center of the cylinder. The readings of the thermocouples located inside PCM and the interpolation method were used to obtain the phase front and liquid fraction during the melting process. In the initial



melting stages, the paraffin close to the heater rod melts first due to conduction and then natural convection develops causing the acceleration of melting rate in the upper region of the container. The result revealed that the melting rate is directly affected by the amount of heating power.

Alsiyabi et al. [9] numerically and experimentally investigated melting of PCM (RT-35) inside a cylindrical container. The study focused on the effect of inclination from vertical to horizontal with three inclination angles; 0, 45 and 90 degrees. The result showed that the melting rate is directly affected by inclination angles where natural convection develops by increasing the inclination angle. It is noted that the melting rate is faster with 45° in comparison with the 0° and 90° inclination angles. Also, the inclination influences on the direction of the melt where the PCM melts in axial direction faster than radial direction at 0° degree (vertical position), while in a horizontal position, the direction of the melt is reversed. At 45° degree inclination angle, the rate of melting was faster than horizontal and vertical directions.

### **2.1.2 Melting of PCM inside Horizontal cylindrical enclosures.**

Generally, the melting in horizontal cylindrical and spherical capsules is classified into constrained and unconstrained modes. In the constrained melting, the solid part melts by convection from the top and the bottom, since the thermocouples prevent the solid part of PCM from falling in liquid PCM. The unconstrained melting occurs when there is no obstruction to solid movement inside the liquid melt. Thus, the solid PCM remains in contact with the container wall.

Chung and Lee [10] investigated numerically by the enthalpy-porosity method the effect of a wide range of Rayleigh numbers on the heat transfer and shape of flow liquid melt during constrained melting of n-octadecane

PCM. The results revealed that before the start of the Benard convection, there is a stability of the flow in the molten gap at the low Rayleigh number. Also, at intermediate Rayleigh number, the flow tends to take different patterns when the viscose force and thermal buoyancy force are balanced. At the high Rayleigh number, the base flow does not affect the Benard convection.

Kawanami et al. [11] investigated experimentally the unconstrained melting of the slush ice (a mixture of fine ice particles and ethylene glycol aqueous solution) inside a horizontal cylindrical container heated isothermally. The study showed that the movement of the liquid is caused by both convection and the motion of the floating ice. Also, it is noticed that the motion of slush ice during the process of melting to the top leads to an increase in the melting rate resulted from the contact of the slush ice with the hot wall of the cylinder as shown in Fig. (2.2). As time travels, the convection effect is generated from stratified layers formed between the slush ice and the cylinder hot wall. Moreover, the melting front is clearly affected by the location and the height of the stratified layers as well as their number. The melting rate increases monotonically with time regardless of heat flux and concentration of the primary solution.

Regin et al. [12] experimentally and numerically studied the unconstrained melting behavior of PCM (paraffin wax) in a horizontal cylindrical container utilized as latent thermal energy in a solar heating collector. The enthalpy method was adopted to solve the PCM melting problem. The results revealed that melting is governed by the value of Stefan number, PCM melting point, and the radius of the container. At the beginning of melting, the heat flux is high because the solid PCM is in direct contact with the hot wall of the cylinder. Furthermore, the formation of a liquid PCM layer between the wall of the cylinder and solid PCM

causes a quick decrease in the heat flux. In addition, the melting rate varies inversely with the radius of the cylinder for the same volume of the cavity.

Hlimi et al. [13] investigated the role of natural convection on the unconstrained melting motion of the PCM (gallium) inside a horizontal-cylindrical capsule. The enthalpy porosity method and finite volume technique were adopted to solve the phase-change problem. The different melting shapes and the predicted PCM temperatures showed the importance of natural convection on heat transfer in the melting region. The conduction and paralleled solid-liquid front to the shape of the container wall were dominated at the beginning of the melting process. It is observed that with the progress of time, the natural convection becomes dominant so the shape of melting become nonsymmetrical between the upper part and lower part of melting.

Ansyah et al. [14] experimentally investigated the constrained melting of paraffin wax RT-52 in a horizontal cylindrical capsule surrounded by HTF (water). The effect of temperatures of 60, 65, 70 °C on PCM melting was studied. At the early stages of the melting process, conduction is dominated heat transfer between the wall of the cylinder and the solid PCM. In addition, convection is dominated and responsible for temperature rise in liquid PCM in the upper region. It is also observed that melting time is reduced by about 34% with an increase of 5 °C in temperature of HTF.

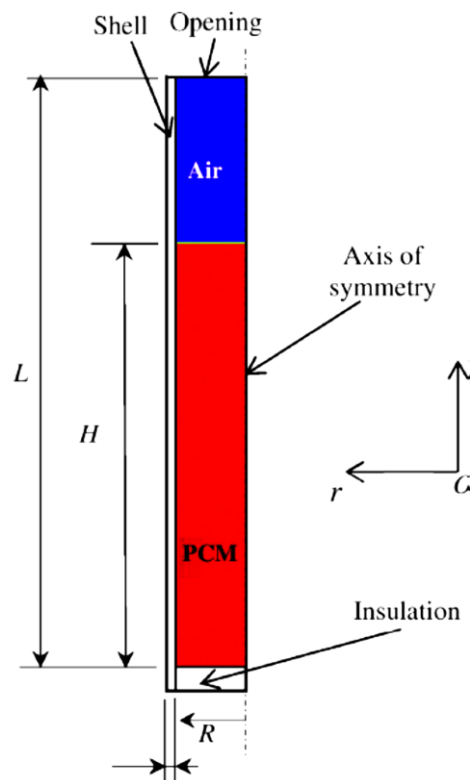


Fig. (2.1) Schematic of geometry (Bechiri and Mansouri et al.[7].).

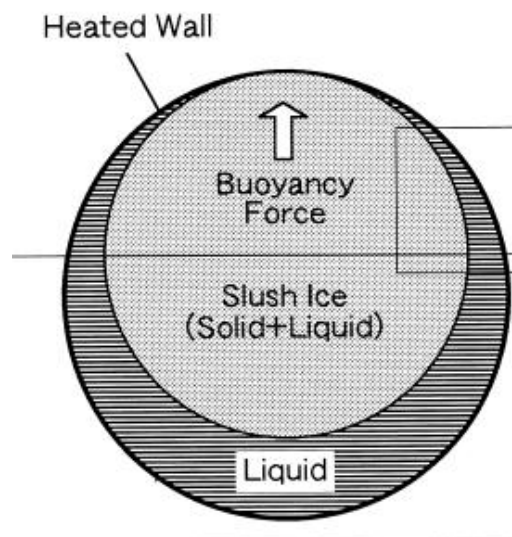


Fig. (2.2) Unconstrained melting of slush ice inside the cylindrical capsule (Kawanami et al. [11]).

## 2.2 PCM melting in the rectangular cavity heat exchanger.

Rectangular PCM-heat exchangers are considered as the solution to some of the engineering applications such as casting, cooling of electronic equipment, crystal growth, photocell, heat storage unit and transport of thermal energy.

Ghasemi and Molki et al. [15] numerically studied the unfixed solid melting of gallium as PCM in a square container heated isothermally on its walls. A fixed-grid enthalpy method was adopted to solve the melting process. The results revealed that as Archimedes ( $Ar$ ) and Rayleigh ( $Ra$ ) numbers equal zero, the melting is dominated by conduction only and symmetrical melting shape is observed. The role of natural convection appears as a result of the increase in Rayleigh number which leads to melting enhancement and an asymmetrical melting shape. The role natural convection is more effective when  $Ar \neq 0$  due to the downward motion of solid PCM which causes induced liquid flow. Also, the flow is more active, and more melting of PCM is noticed in the upper part of the square cavity.

Yanxia et al. [16] experimentally studied the melting of the ethanolamine-water binary mixture as PCM in a closed rectangular cavity with heated vertical walls. It showed that the natural convection effect increases the melting rate as a comparison with conduction alone. Moreover, at the beginning of melting, the heat conduction is dominated, so the shape of the melting front is parallel with the heated walls. Although the wall temperature is constant, the liquid temperatures are higher in the upper part due to the currents of natural convection. Furthermore, it was noticed that the Nusselt number decreases in all cases with the progress of time, and it is stable in convection domination as compared with conduction domination.

Younsi et al. [17] numerically studied the melting of PCM (RT-27) in a rectangle cavity heated differentially at vertical walls, while the horizontal walls are adiabatic. The finite volume and enthalpy method was adopted numerically to solve the PCM melting. At the beginning of melting, the solid-liquid interface is flat and parallel to the hot wall as a result of prevailing heat conduction. With the progress of time, the melting at the top is increased as a result of the buoyancy effect as shown in Fig. (2.3). Moreover, the heat conduction has a short transient phase as a comparison with natural convection.

Qarnia et al. [18] presented a numerical study to examine the melting of n-eicosane in a rectangular container. The container was heated by three discrete protruding which were put on one vertical wall to simulate the heat source in the electronic component as introduced in Fig. (2.4). To solve the melting problem, the enthalpy-fixed-grid method was adopted. It was noticed that the rate of heat absorption becomes higher whenever the discrete protruding heaters were closer to the bottom wall. According to the correlation which combines the maximum working time with the melting fraction, it is found that the approach can be utilized in the design of PCM cooling system.

Kousksou et al. [19] numerically studied the melting of gallium in a rectangular capsule with a wavy bottom, isothermal hot wall and the other walls are adiabatic as shown in Fig. (2.5). The finite volume and enthalpy methods were used to solve the melting problem of PCM. It was found that the melting rate and the distribution of the local heat flux along the wavy surface are affected by the amplitude of the wavy surface.

Kamkari and Amlashi [20] experimentally and numerically studied PCM melting inside a vertical inclined rectangular container. The bottom wall of the rectangular is heated and the other walls are insulated as

presented in Fig. (2.6). In order to solve the problem of PCM melting, the enthalpy-porosity method was used. The study included investigation the effect of inclination angles ( $0^\circ$ ,  $45^\circ$  and  $90^\circ$ ) on the melting rate. At the beginning of the melting process, the solid PCM which is in contact with the hot wall melts as a result of conduction. With the progress of time, the melt ascends to the upper part due to natural convection. It can be observed that the melting time reduces about 52% and 37% for the inclination angles  $0^\circ$  and  $45^\circ$  respectively as a comparison with the vertical position regardless of Stephan number.

Wang et al. [21] presented a numerical and experimental investigation of melting of PCM (RT-60) inside a rectangular container with different inclination angles as shown in Fig (2.7). One of the walls was isothermally heated and the rest of the walls were insulated. A fixed-grid enthalpy method was adopted to solve the melting problem. Heat conduction is dominant at the beginning of melting at all inclination angles. The results revealed that the inclination angles have a significant effect on the melting performance of PCM. An increase of angles from  $0^\circ$  to  $180^\circ$  leads to a nonlinear reduction in melting rate.

Hong et al. [22] utilized enthalpy-porosity approach to numerically study the melting process of PCM in the differentially-heated rectangular cavity as shown in Fig. (2.8). The effect of the mushy zone constant and acceleration of gravity was investigated. The results showed that the melting rate is affected by the mushy zone constant and acceleration of gravity. As the mushy zone constant increases, the convection of the liquid PCM decreases, and the melting time is increased. At the same time, the liquid fraction increases with the increase in acceleration of gravity since the increase in Rayleigh number and consequence development of natural convection.

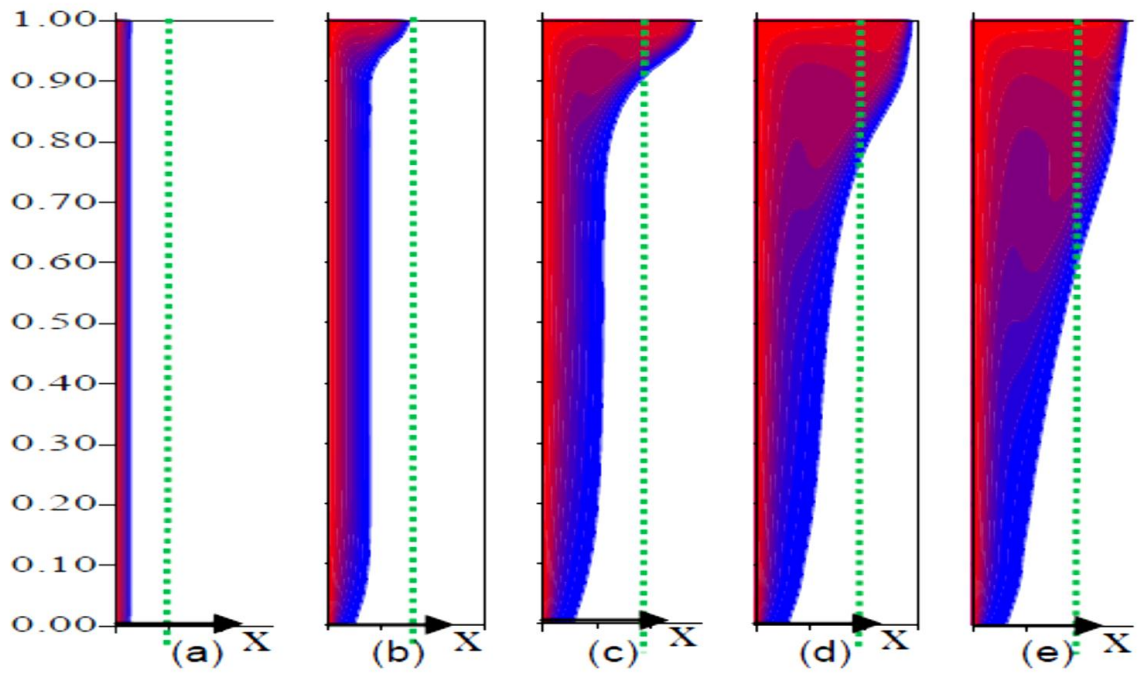


Fig. (2.3) Contour progress of melting front (Younsi et al. [17]).

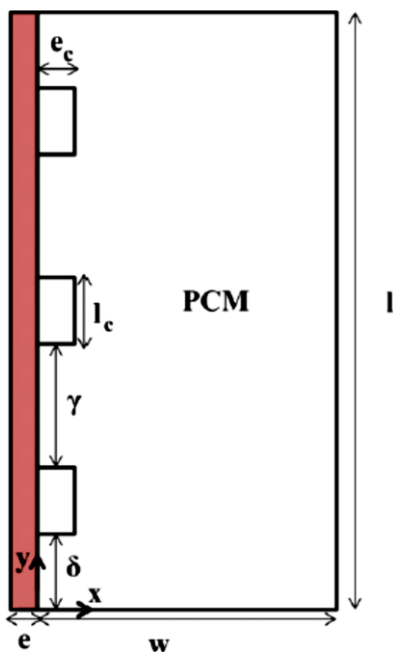


Fig. (2.4) The schematic view of model (Qarnia et al. [18]).

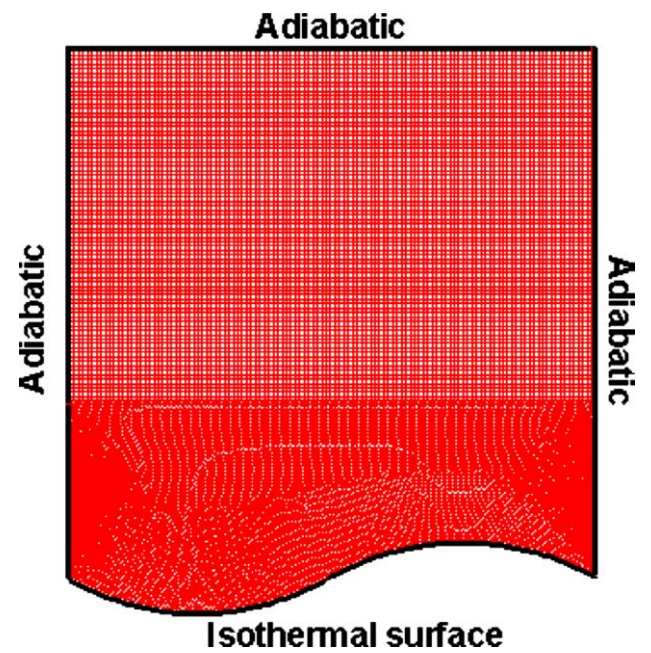


Fig. (2.5) layout of model (Kousksou et al. [19]).



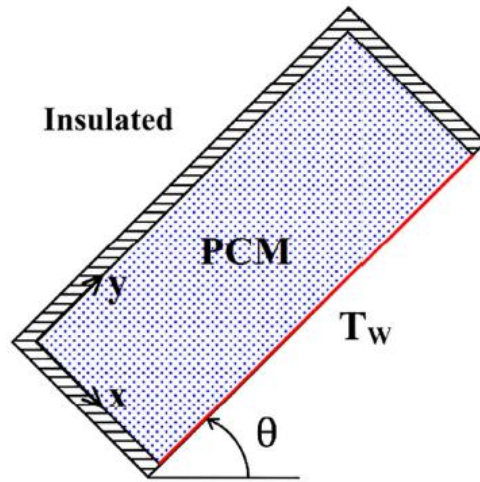


Fig. (2.6) schematic view of PCM container (Kamkari and Amlashi [20]).

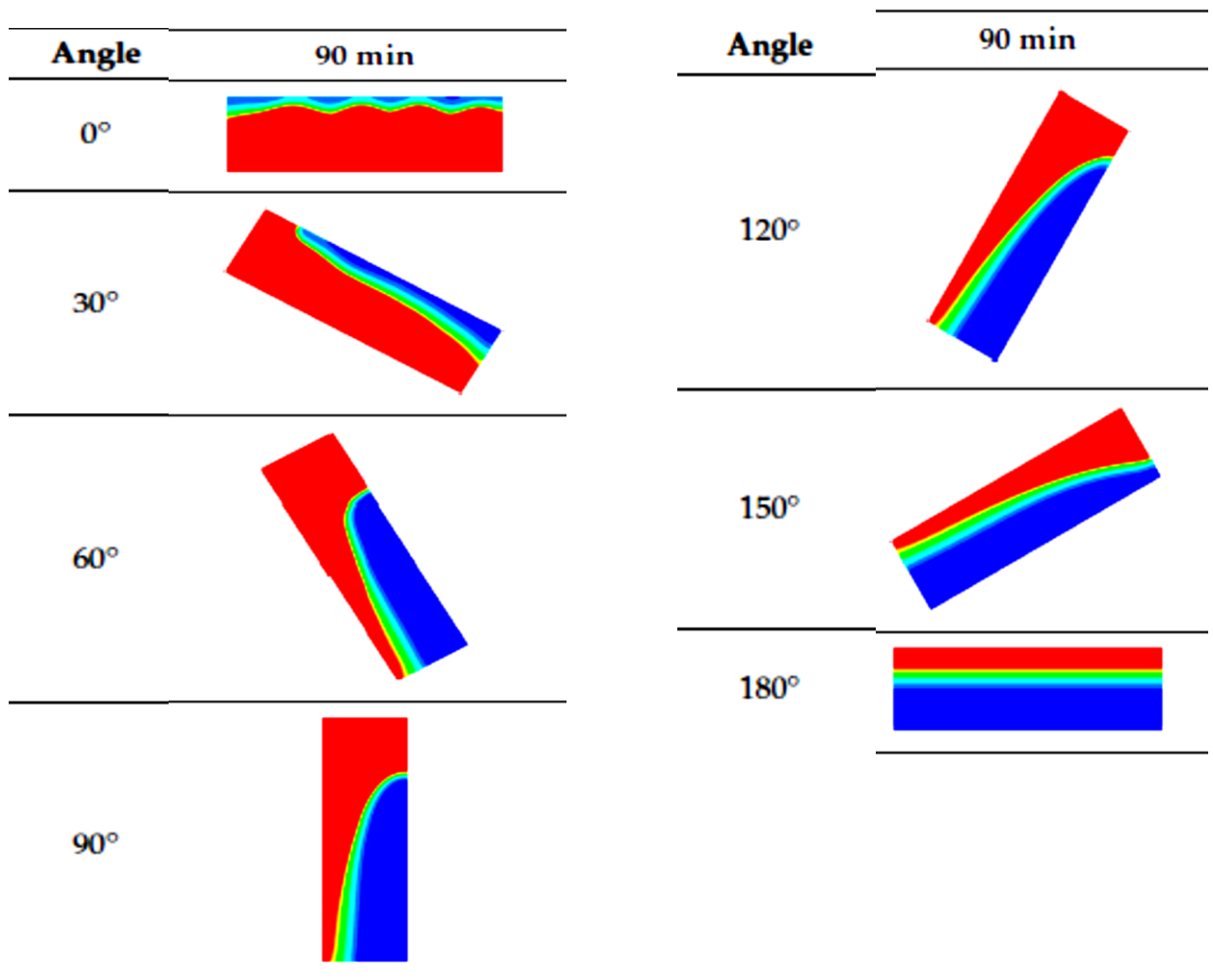


Fig. (2.7) Effect the inclination on the melting rate (Wang et al. [21]).

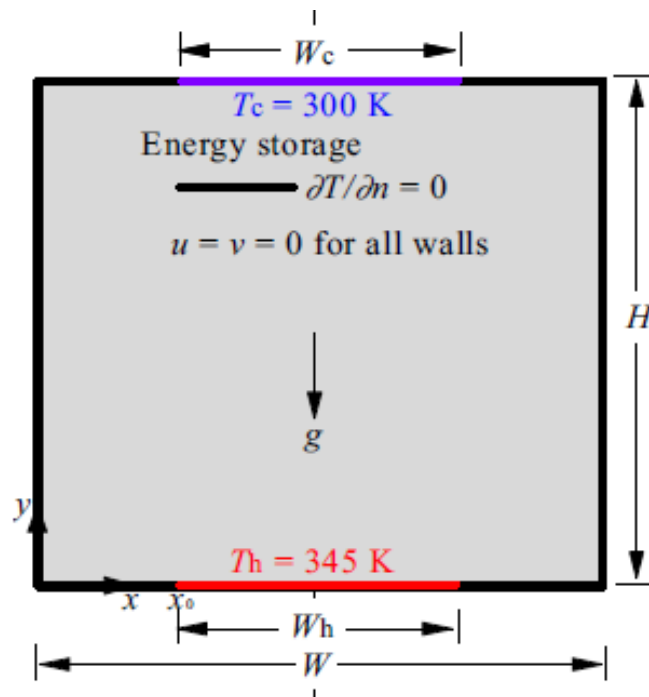


Fig. (2.8) Physical model (Hong et al. [22])

### 2.3 PCM melting inside the spherical vessel

The spherical container is one of the most common heat exchangers that use a PCM as a heat storage medium. The PCM melting in this spherical capsule is divided into constrained or unconstrained melting. The applications for this type are quite broad, such as thermal reservoirs, clothing, and cooling of electronic equipment, etc. [23]

Khodadadi and Zhang [24] studied computationally the constrained melting of PCM in a spherical vessel using the finite volume enthalpy formulation. The results revealed that the heat conduction transfer is dominated at the beginning of the PCM melting. Then, with the expansion of the melt zone, the buoyancy-driven convection is strengthened. Consequently, the melting in the upper part of the sphere is accelerated significantly more than in the lower part as indicated in Fig. (2.9). It is also observed that buoyancy convection does not affect the melting process when the Rayleigh number is small.

Tan et al. [25] experimentally and computationally studied the constrained melting of paraffin wax (n-octadecane) encapsulated in a

spherical container. A single-domain enthalpy formulation and finite volume numerical were used to simulate the governing equations. The results revealed that conduction is dominant in the early period and melting is faster for the PCM layer in contact with the wall of the sphere. The influence of convection grows and be dominated by the progress of time. An unstable molten layer at the lower part causes chaotic fluctuations, and it is responsible for the waviness occurring at the bottom of the PCM. The discrepancy between the predicted results and experimental findings was reasoned by staying the bottom of the container unheated due to the use of a support structure to hold the sphere.

Khot et al. [26] carried out an experimental study to evaluate the constrained and unconstrained melting of PCM inside a spherical container as shown in Fig. (2.10). The spherical container was exposed to different HTF (water) temperatures. It was found that as Stefan number increases, the melting rate increases in both constrained and unconstrained melting. The unconstrained melting takes the shorter melting time because the solid part of PCM in the bottom is in the direct thermal contact with the wall. While, the solid part of the PCM melts by convection only in the constrained melting from both upper and lower parts.

Hosseinizadeh et al. [27] carried out an experimental and numerical study on unconstrained melting using n-octadecane as PCM in a spherical container. Enthalpy-porosity method and volume of fluid were used to simulate the PCM melting. The PCM close to the wall melts at the beginning of the melting process with a high rate. Then, as time travels, melting rate decreases because of the formation of a liquid layer of the PCM between the wall and the solid PCM. Also, it is noticed that the melting rate is faster in the upper part due to the effect of natural convection.

Faistauer et al. [23] carried out a numerical study on PCM unconstrained melting in a spherical container. The enthalpy porosity method was used numerically to solve the PCM phenomena. Three types of PCM are involved namely; RT 35, RT 55 and RT 82. Also, four sizes of spheres and three temperature differences between the wall and the melting point were considered. The spheres were filled with 85% of their volumes by PCM while the rest space is occupied by the air. It was found that the melting time is increased with the increase in radius and/or with the reduction of temperature difference. Also, it was observed that the three types of PCM consumes approximately the same melting time as long as they have the same size and they exposed to the same temperature difference.

Sattari et al. [28] numerically presented the study of constrained melting of PCM in a spherical capsule. Enthalpy porosity method was adopted to solve the melting PCM problem. At the beginning of the melting process, the solid PCM closed to the inner wall of the container melts by conduction. With the progress of time, the liquid PCM expands and a molten grows due to convection domination. The results revealed that the initial temperature has a little effect on the melting rate. Also, the surface temperature has a more significant effect on the melting rate if it is compared with the effect of the geometrical and other operating conditions. In addition, it was found that the melting rate becomes faster when used higher surface temperature and a smaller diameter of a sphere container. Moreover, it is noticed that the waviness at the bottom of PCM is obtained as a result of the unstable liquid layer at the bottom of this region.

Li et al. [29] numerically investigated the effect of the geometrical and operating parameters on constrained melting in a spherical capsule. These parameters include the radius of the sphere, the temperature of the spherical surface, the thermal conductivity of PCM, and the material

of the sphere wall. To solve the PCM melting problem the enthalpy method was used by ANSYS/FLUENT software. The results showed that the melting time varies positively and inversely with the spherical size and wall temperature, respectively. Moreover, increasing the thermal conductivity of PCM and the shell of the sphere leads to an acceleration in the melting process. Also, it was found that the radius of the sphere has a more pronounced effect on melting rate among other parameters.

Junior et al. [30] presented a numerical study on the melting of Erythritol PCM filled with about 94% of a spherical container (6% occupied by air) subjected to the external airflow. The thermal storage system contains a pebble bed with spheres containing PCM as shown in Fig. (2.11). Enthalpy porosity method and ANSYS/FLUENT were used to simulate the phase change phenomenon of the PCM. The numerical investigation was considered the following parameters; the difference in temperature between the external flow and PCM melting point, Reynolds number as well as the sphere position in the array. It was found that the position of the sphere that is nearer to the airflow inlet reaches to the complete melting faster than that which far from the airflow inlet. However, the effect of position decreases when the Reynolds number increases.

Gao et al. [31] experimentally investigated the unconstrained melting of RT-27 PCM inside a spherical container. The study included the effect of various factors such as diameter, PCM filling ratio, heating temperature and initial temperature on the melting process. In the beginning, the melting process PCM is uniform inside the spherical container. The solid PCM floats because the buoyancy force is larger than solid PCM weight. With the progress of time, the solid PCM sunk in the bottom of the container and become in contact with the hot wall. The results revealed that with the increase in the diameter of the sphere and

ratio of PCM filling, the total melting time increase. In addition, the increase of the heating and initial temperatures, the melting time is decreased. It is worthy to mention that the floating melting mode (Fig. (2.12a)) occurs firstly as the solid PCM floats above the liquid PCM. After that, the solid part sinks as the liquid ascends to the voids in the upper region and the close-contact is occurred as shown in Fig. (2.12b).

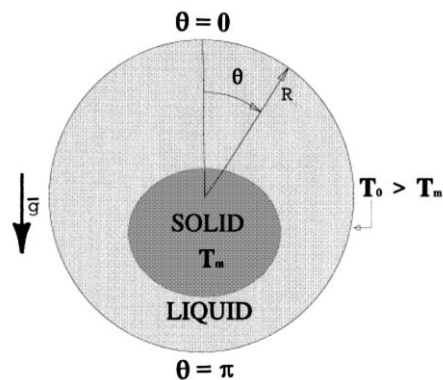


Fig. (2.9) diagram of melting Spherical container. (Khodadadi and Zhang [24])

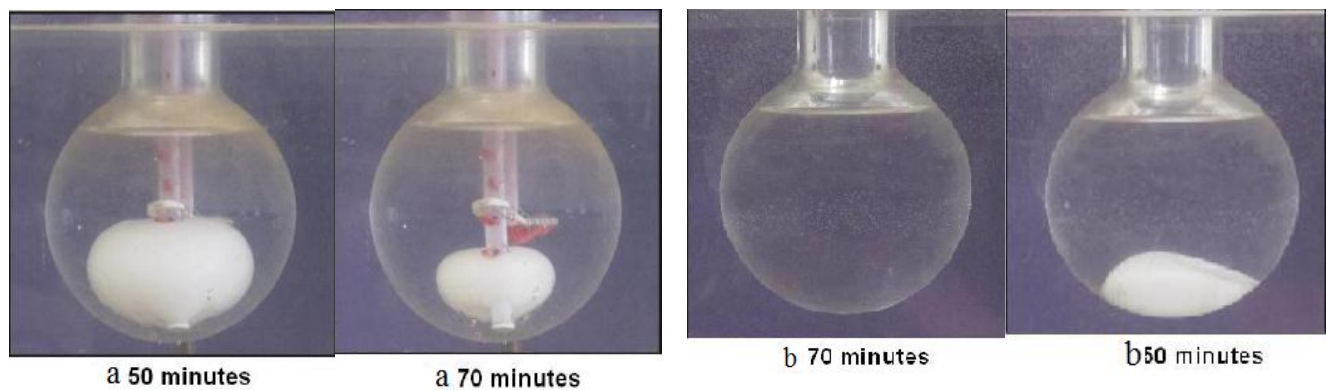


Fig. (2.10) a- Constrained melting, (b) unconstrained melting (Khot et al. [26]).

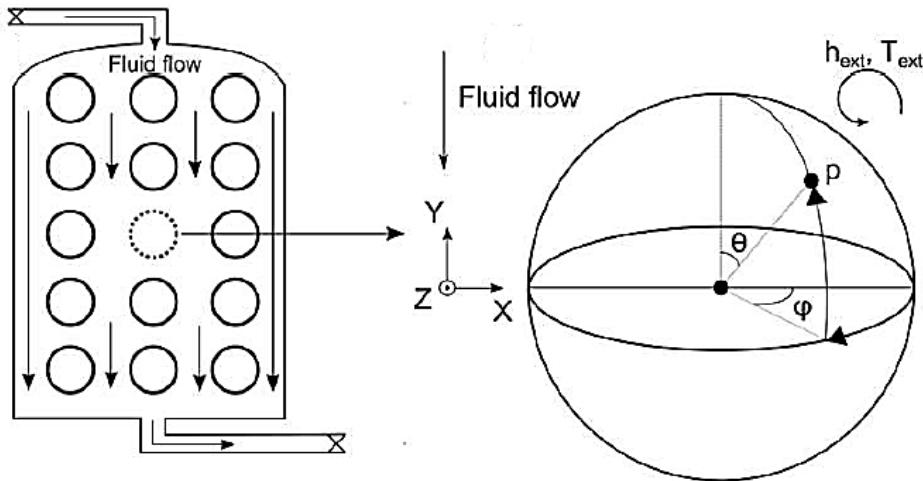


Fig. (2.11) The pebble bed storage (Junior et al. [30]).



Fig. (2.12) a- The solid heat PCM floats, b- the Sinks (Gao et al. [31]).

#### 2.4- PCM melting in the annular heat exchanger.

This type of heat exchanger is wide-used in engineering application. The PCM is contained in annular space between the inner pipe and the outer shell in most cases. The melting behavior is influenced by the orientation of heat exchanger, the shape of the outer shell and inner pipe and the dimensions of the heat exchanger. There are two orientations of annular-PCM heat exchanger which are either; horizontal or vertical.

Ng et al. [32] numerically studied the melting of PCM (n-octadecane) in a horizontal annulus heated isothermally from the inner tube while the outer pipe was adiabatic. The melting problem was solved numerically by adopting Streamline Upwind/Petrov Galerkin finite element method. The results revealed that the increase in Rayleigh number causes an earlier initiation of the natural convection and expediting of the process of melting. However, the melting rate is higher at the top of the

container, while it is small at the bottom region. Also, the temperature gradient and the heat flux decrease significantly in the upper part of the liquid region where the thermal stratification is dominated.

Khillarkar et al. [33] presented a numerical study of PCM encapsulated in concentric horizontal annuli of two configurations as described in Fig. (2.13). The study included observing the effects of heating the inside, outside, and both walls on melting. A Streamline Upwind/Petrov Galerkin finite element method was adopted to solve the convection-dominated melting problem. It was observed that the increase of Rayleigh number, the natural convection starts earlier causing an increase in melting rate. It was noticed that the effect of heating of both walls equals the effect of heating the inside and outside walls separately. Thermal stratification was observed at the top of the liquid melting part. The temperature gradient showed a significant decrease in the upper part of heat exchanger which results in smaller expected heat flux.

Ettouney et al. [34] experimentally investigated the latent heat energy storage of PCM during energy charging and discharging. The paraffin wax PCM was contained in a vertical annular space formed between the outer insulated shell and inside the tube where the heat transfer fluid (HTF) flows. It can be noticed that the melting process was controlled by natural convection whereas conduction was dominant in the solidification process. As a result PCM liquid temperature at the top of the tube is higher than in the bottom of the tube. In addition, increasing the system temperature results in enhancing the Nusselt number due to developing the role of natural convection.

Wei et al. [35] performed a numerical study to simulate the melting process of paraffin wax filled the horizontal annulus between a hot tube and insulated shell as shown in Fig. (2.14). The transient problem of



melting was solved numerically by adopting the two-dimensional governing equations and finite volume approach. The predicted results revealed that the melting starts on the surface of the tube then ascends to the upper part of the PCM container by natural convection currents. Therefore, the melting in the upper part was faster than the lower part. They reported that the convection is dominant in the upper part, while the lower part is subjected to conduction effect. In addition, the melting at both sides of the cavity is under the conduction and convection control.

Adine and El Qarnia [36] numerically studied the melting of two PCMs P116 and n-octadecane filled the annular cavity which is formed between shell and tube as illustrated in Fig. (2.15). Water was used as a heat transfer fluid inside the tube with a temperature higher than the melting point of PCMs. A control volume approach based enthalpy-porosity method was used numerically to solve the problem of PCM melting. It can be noticed that the melting of n-octadecane was faster than P116 since the former has a lower melting point than later. Moreover, the HTF inlet temperature does no influence on the maximum thermal storage efficiency of the two latent heat storage units.

Dutta et al. [37] experimentally and numerically studied heat transfer associated melting of paraffin wax as filled the horizontal annular of double pipes. The inner pipe was heated isothermally while the outer one is adiabatic. The finite volume method was used to solve the melting problem of PCM numerically. At the beginning of the melting process, a molten layer of paraffin was formed around the inner tube due to conduction. Then the layer grows upward with the progress of time as a result of natural convection. The computational results showed that eccentricity and the inclination angle of the inner pipe have a great influence on the melting of PCM. Also, the heat flux increased with the inclination angle and eccentricity.

Hosseini et al. [38] presented an experimental and computational study on the behavior of PCM (RT-50) melting inside horizontal annular space formed between inner isothermal tube and outer insulated shell. The finite volume and enthalpy-porosity methods numerically used to solve the PCM melting problem. It can be noticed that the PCM in the upper part have a higher temperature than that in the lower part due to convection role. The melting rate was affected by the inlet temperature, where the melting rate increases directly with the increase in the inlet temperature.

Darzi et al. [39] carried out a numerical study of melting of n-eicosane inside a horizontal annular cavity between a hot inner tube and outer shell for both concentric and eccentric configurations as presented in Fig. (2.16). The enthalpy-porosity method was numerically used to simulate the phase-change problem. It was reported that at the first 15 minutes, the melting rate was nearly the same for the concentric and eccentric array. After this time, the melting rate was higher for the eccentric position due to the domination of convection between the hot tube and solid PCM.

Azad et al. [40] experimentally and numerically studied the behavior of PCM (n-octadecane) melting process inside a horizontal cylindrical annular container. The HTF (water) passes through a steel pipe fixed in the center of the cylinder with different temperatures. Enthalpy porosity method was adopted to solve the PCM melting problem. The study concentrated on the effect of inlet temperature on both the melting process and the start of natural convection. Initially the heat conduction predomination on PCM melting. Then, the natural convection becomes dominant. The increase of the liquid PCM temperature causes its movement upward at the same time the cold liquid PCM moves downward. The result also shows that convection begins early as the inlet temperature increases.

Kurnia et al. [41] investigated numerically the charging and discharging of rotating latent heat energy storage where PCM is contained in the vertical and horizontal annulus between shell and tube. The finite volume and enthalpy-porosity methods were used numerically to solve the problem of PCM melting. It was noticed that the melting rate increased in vertical orientation regardless of the direction of heat transfer fluid inlet. Also, it was showed that utilizing the rotating latent heat storage unit enhances the heat transfer and expediting the melting process. The slow rotating speed of latent heat storage results in a higher improvement in heat transfer and melting rate compared with the faster-rotating speed of storage.

Faghani et al. [42] studied the melting process of PCM (RT25) in annular spaces formed between different elliptical and cylindrical tubes and shells as shown in Fig. (2.17) for vertical and horizontal orientations. To solve the PCM melting problem, an enthalpy-porosity method was used. The results revealed that the shape of the shell was more effective than the tube shape. Moreover, it appeared that the elliptical horizontal shell was the best for enhancing heat transfer and reducing the melting time. While, the vertical elliptical tube leads to higher melting rate.

Cao et al. [43] experimentally and numerically investigated the effect of natural convection during melting of PCM in eccentric horizontal shell and tube as exhibited in Fig. (2.18). The enthalpy-porosity method was adopted to solve the PCM melting problem. The results revealed that in the upper part melting occur as a result of bouncy-driven convective heat transfer between the hot tube and the liquid PCM. At the same time, natural convection occurs between the liquid PCM and the solid PCM interface, thus melting rate is higher in the upper part. Furthermore, when the tube moves downward melting rate increases due to the convective heat transfer domination.

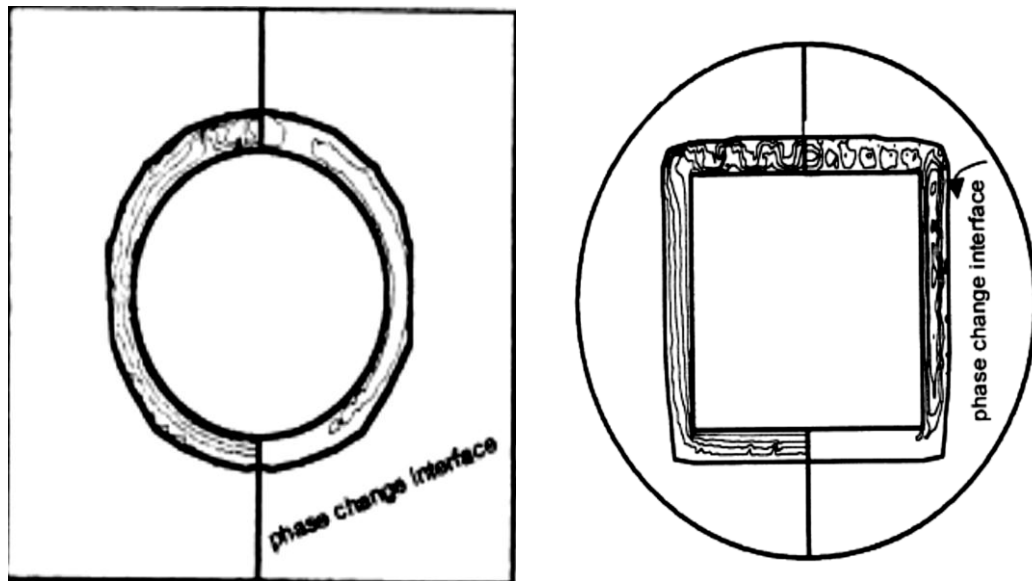


Fig. (2.13) Schematic diagram of models (Khillarkar et al.[33]).

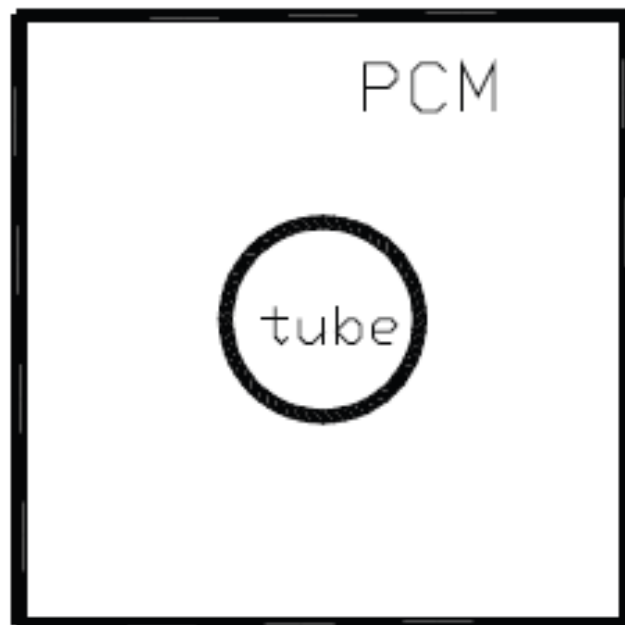


Fig. (2.14) Schematic digram of LHSU (Wei et al. [35]).

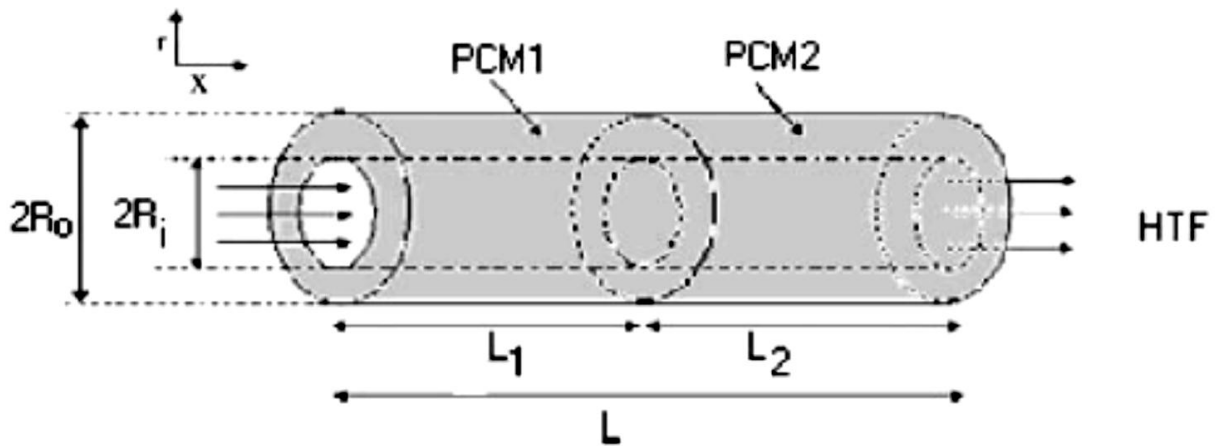


Fig. (2.15) Schematic of LHSU used two PCMs (Adine and El Qarnia[36]).

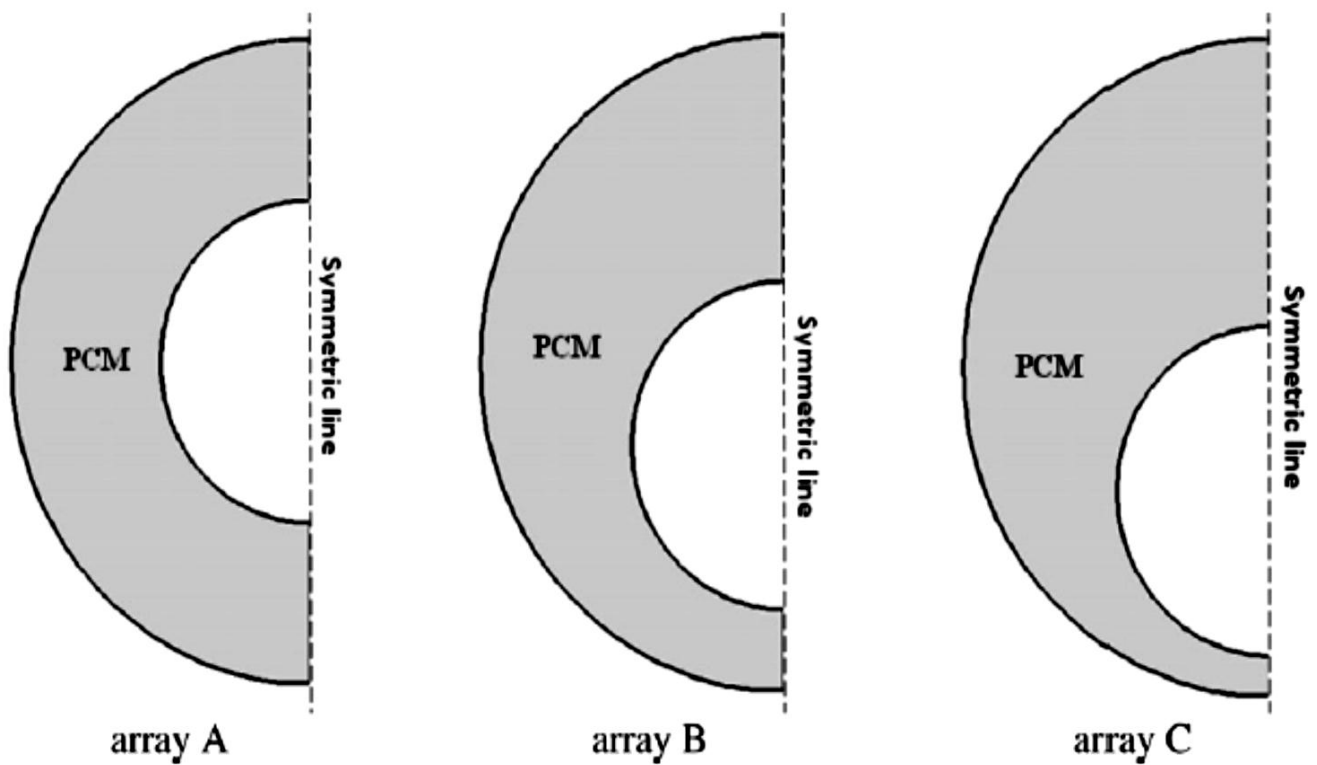


Fig. (2.16) Schematic of computational domain (Darzi et al. [39]).

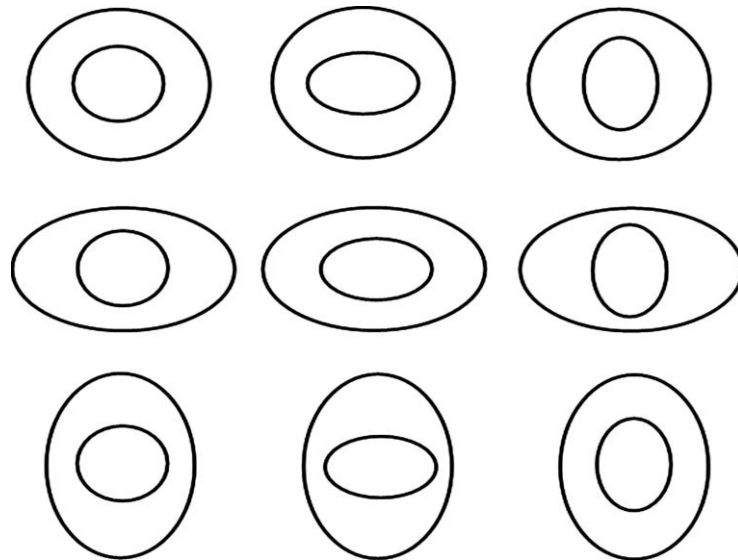


Fig. (2.17) Nine configuration of a annular between two elliptic cylinders (Faghani et al.[42]).

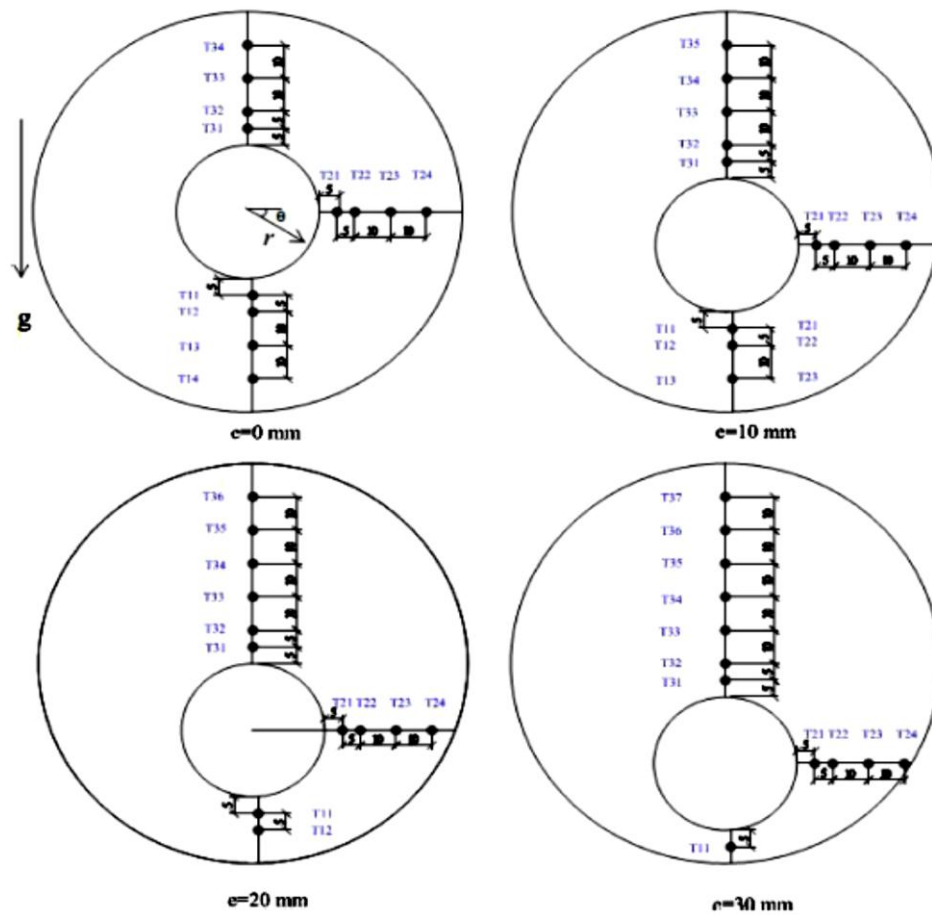


Fig. (2.18) Localtion of thermocuoples with change position of tube (Cao et al. [43])

## 2.5 The Scope of present study

The study includes an experimental and numerical investigation of the thermal performance of the melting process of PCM contained in a double pipe heat exchanger. In the other words, the paraffin wax RT-42 Rubitherm was placed inside the annular cavity between the inner copper pipe of 25 mm inner diameter and the isolated external shell of a diameter of 75 mm. In the experimental work, some thermocouples probes are inserted inside the annular enclosure to measure the temperature distribution of the PCM during charging process. Also, the photos are captured to monitor the time-progress of the melting process. The numerical solution is performed by adopting the enthalpy-porosity method and finite volume technique with the assistance of ANSYS/FLUENT package software. The study includes the inspection of the effect of different temperatures (60,70 and 80°C) of the water as HTF which is passing through the inner pipe. Also, the influence of orientation of heat exchanger (horizontal and vertical) on the thermal performance is was evaluated.

**CHAPTER THREE**  
**NUMERICAL STUDY**



## ***CHAPTER THREE: NUMERICAL STUDY***

The melting of PCM inside the annular cavity of a two-orientation heat exchangers is presented physically and numerically in the current work. The governing equations are specified with described initial and boundary conditions.

### **3.1 Physical Model**

The schematic descriptions of a PCM melting process inside the annular cavity of both horizontal and vertical heat exchangers are introduced in Fig. (3.1) and Fig. (3.2), respectively. The PCM-heat exchanger consists of the double-concentric pipes. The inner one is a copper pipe with 25 mm diameter and 0.1 mm wall thickness, and the outer one is acrylic pipe with 75 mm diameter and 2.5 mm wall thickness. The length of the heat exchanger equals 500 mm. The annular space between two pipes is filled completely with PCM (RT-42 Rubitherm) which its melting temperature ranges from 38 to 42 °C. The thermophysical properties of the used PCM are listed in Table (3.1). The heat source of the storage cell is a hot water passing through the inner pipe causing the melting of PCM RT-42. Melting starts around the inner pipe and grows toward the outer pipe.

Table (3.1) Thermo-physical properties of RT-42 PCM.

Solidus Temperature, $T_s$	38°C
Liquidus Temperature, $T_l$	43°C
Latent heat of melting, $\Delta H$	174 kJ/kg
Density, $\rho$	880 kg/m <sup>3</sup> (solid) 760 kg/m <sup>3</sup> (liquid)
Dynamic viscosity, $\mu$	0.02728 kg/m s
Thermal Expansion coefficient, $\beta$	0.0008 1/k
Specific heat capacity, $C_p$	2 kJ/kg K
Thermal conductivity, $k$	0.2 W/m <sup>2</sup> °K

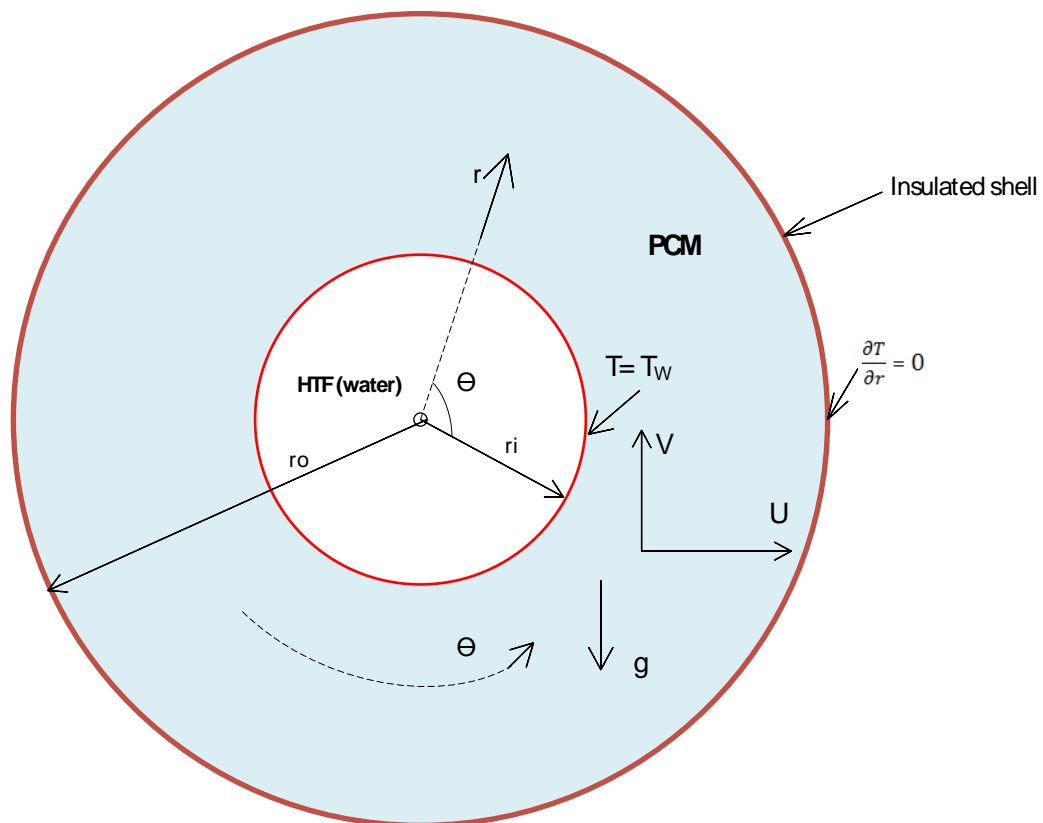


Fig. (3.1). Schematic representation of the horizontal annular-cavity heat exchanger.

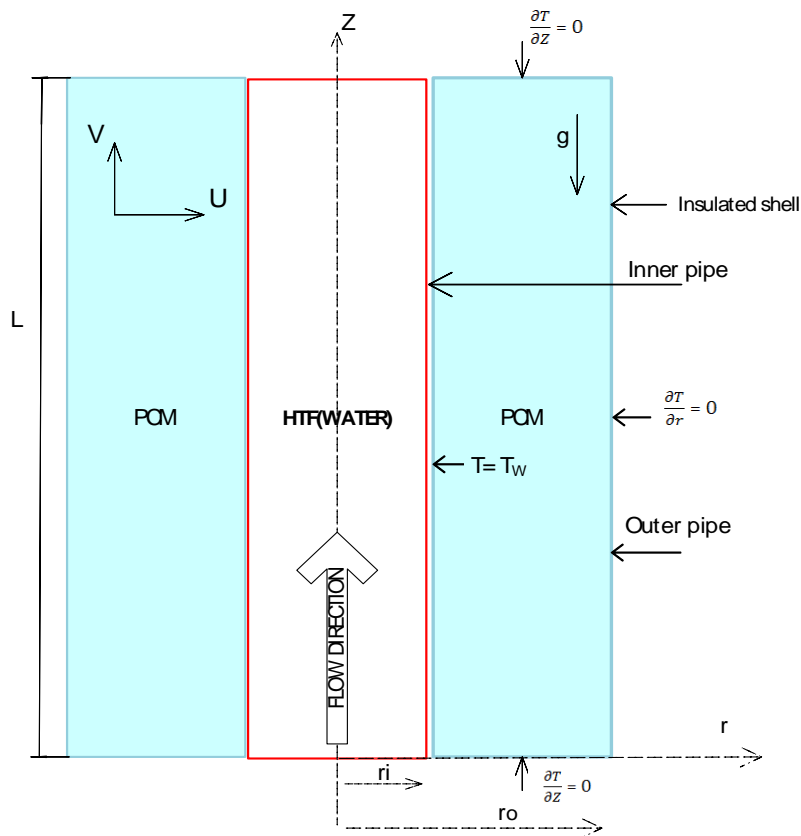


Fig. (3.2). Schematic diagram of the vertical annular-cavity heat exchanger.

### 3.2 Mathematical formulation of the problem

The PCM is contained between the inner tube of radius  $r_i$  and outer insulated shell of radius  $r_o$ . The melting process in the annular cavity is a two-dimensional problem. The radial and angular coordinates  $(r, \theta)$  are required to define the melting process inside the horizontal-annular heat exchanger. Whilst, the radial and axial coordinates  $(r, z)$  are used to define the melting of PCM in the vertical annular heat exchanger. The initial temperature of the solid PCM is  $T_{ini}$ . The HTF enters the inner tube with a temperature of  $T_w$  and a uniform velocity of  $U_{in}$ , while it exists at a pressure of the atmosphere. No-slip conditions are applied for all walls. Also, the outer shell is thermally insulated.

### 3.2.1 Model assumptions

The problem of melting of PCM inside cavities is transient, non-linear with moving boundaries. To facilitate the melting problem, the following assumptions are applied:

- 1- The annular domain is filled completely with PCM (RT-42).
- 2- The melt of PCM is homogenous, incompressible and Newtonian fluid. Also, the melt flow is considered laminar.
- 3- The melting process is assumed two-dimensional in both orientations of the heat exchanger.
- 4- The properties of PCM are supposed to remain constant excluding the density variation with the temperature where the buoyancy forces is based the Boussinesq approximation.
- 5- There is no gain or loss of heat.
- 6- Ignoring the viscous dissipation, radiation and end effects.
- 7- The volume change during the phase-change is neglected.

### 3.2.2 The Governing Equations

The governing equations of continuity, momentum, and energy used to simulate the melting process of PCM in a concentric annular cell are:

$$\frac{\partial \rho}{\partial t} + \nabla \cdot (\rho V) = 0 \quad (3-1)$$

$$\frac{\partial (\rho V)}{\partial t} + \nabla \cdot (\rho V V) = +\mu \nabla^2 V - \nabla P + S_u \quad (3-2)$$

$$\frac{\partial}{\partial t} (\rho H) + \nabla \cdot (\rho V H) = \nabla \cdot (K \nabla T) \quad (3-3)$$

Where  $\rho$ ,  $\mu$  and  $k$  are the density, viscosity and thermal conductivity of PCM, respectively.

The body force term in momentum equation is modeled by considering the Boussinesq approximation based on a reference density ( $\rho_{ref}$ ) and temperature ( $T_{ref}$ ), and the thermal expansion coefficient ( $\beta$ ).

$$\text{Where } S_u = S_D + S_g \quad (3-3a)$$

$$\text{and } S_g = \rho_{ref} g \beta (T - T_{ref}) \quad (3-3b)$$

$$\text{also } = - \frac{1}{\rho} \left( \frac{\partial \rho}{\partial T} \right)_P \quad (3-3c)$$

The natural convection influenced the melting appears due to the change of PCM density and gravitational acceleration.

### 3.2.3 Enthalpy–porosity method

To solve the PCM melting problem, the enthalpy- porosity method was used. This method depends on the liquid fraction which represents the liquid volume to the total volume in the storage unit. The domain of storage unit will be divided computationally for three regions; solid, liquid and mushy zone. The enthalpy-porosity method treats the mushy region (partially solidified region) as a porous medium. The porosity in each cell is set equal one to the liquid fraction in that cell. In fully solidified regions, the porosity is equal to zero. The region of solid-liquid contact is known as the mushy zone which represents the barrier between two phases. The porosity is represented by a liquid fraction  $f$  which is defined as ([44], [45]).

$$f = \begin{cases} 0 & \text{if } T \leq T_s \\ \frac{T-T_s}{T_l-T_s} & \text{if } T_s \leq T \leq T_l \\ 1 & \text{if } T \geq T_l \end{cases} \quad (3-4)$$

where,  $T_s$  and  $T_l$  refer to solidus and liquidus temperatures of PCM, respectively. The local temperature is denoted by  $T$ .

The total enthalpy  $H$  represents the summation of the sensible enthalpy  $h$  and latent enthalpy  $\Delta H$  and can be described by equation (3-5);

$$H = h + \Delta H \quad (3-5)$$

Where,

$$h = h_{ref} + \int_{T_{ref}}^T C_p dT \quad (3-6)$$

$$\Delta H = fL \quad (3-7)$$

where,  $h_{ref}$  is the sensible enthalpy of PCM at  $T_{ref}$ ,  $C_p$  is the specific heat at constant pressure and  $L$  represent latent heat of PCM.

It is worthy to mention that the source term or Darcy term  $S$  in momentum equation (3-2) is an important treatment technique for the mushy zone,

$$S_D = \frac{(1-f)^2}{f^{3+\varepsilon}} VA_{mush} \quad (3-8)$$

The constant  $\varepsilon$  is used as a small number of 0.001 to avoid division by zero. Also, the mushy zone constant  $A_{mush}$  is a constant number which it ranges from  $10^4$  to  $10^7$  [46] which refers to the morphology of the melting front.

### 3.2.4 Boundary and Initial Condition

In the two orientation of heat exchanger the melting behavior of PCM is symmetrical. The wall of inner pipe remain approximately constant temperature while the outer pipe and the ends of heat exchanger is adiabatic. Also, the HTF (water) enters the inner pipe from the bottom to the top. As presented in figures (3.1 and 3.2). The boundary condition of the domain are:

At time,  $t=0$ , Temperature of water and PCM equals  $T_{ini}$

At time,  $t > 0$

For horizontal heat exchanger

The outer surface of inner pipe.  $r=r_i$ ,  $U=V=0$  and  $T=T_w$ .

The outer surface of outer pipe.  $r=r_o$ ,  $U=V=0$  and  $\frac{\partial T}{\partial r}=0$ .

For vertical heat exchanger

At  $r_i \leq r \leq r_o$  and  $Z=0$ ,  $U=V=0$ ,  $\frac{\partial T}{\partial z} = 0$

At  $r_i \leq r \leq r_o$  and  $Z=L$ ,  $U=V=0$ ,  $\frac{\partial T}{\partial z} = 0$

At  $r = r_i$  and  $0 \leq Z \leq L$ ,  $U=V=0$ ,  $T = T_w$

At  $r = r_o$  and  $0 \leq Z \leq L$ ,  $U=V=0$ ,  $\frac{\partial T}{\partial r} = 0$

### 3.3 Computational model

The simulation of PCM melting in annular cavity PCM-heat exchanger of two orientations was carried out using the ANSYS FLUENT 17.2 software package. The computational procedure can be illustrated by a flowchart as shown in Fig. (3.3).

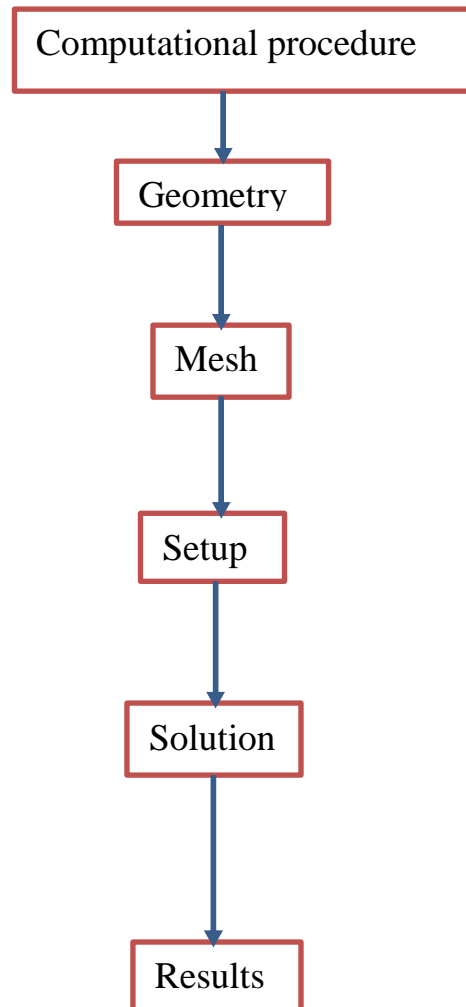


Fig. (3.3). Flow chart of computational procedure.



The geometry is represented as a 2D model by design mold of software. It consists of two domains; PCM inside annular cavity of heat exchanger and water flowing through the inner copper pipe. The domains are discretized by quadrilateral elements where they are concentrated on the boundaries of the computational domain. The purpose of the spatial discretization is to achieve a numerical solution. Thus, the gradient is set as Least Squares Cell-Based while pressure, momentum and energy set as Second-Order Upwind technique. A relationship between velocity and pressure corrections is used in the SIMPLE algorithm in order to enforce mass conservation and to calculate the pressure field. The pressure-based solver uses under-relaxation of equations to control the update of computed variables at each iteration. The relaxation-factors for pressure, density, body force, momentum, and Liquid fraction of 0.3, 1, 1, 0.7 and 0.9, respectively are used to accelerate the convergence of pressure-velocity iteration methods. At the end of each solver iteration, the residual sum for each of the conserved variables is computed and stored. The convergence criteria of  $10^{-6}$  for continuity, velocity and energy are applied.

### 3.4 Validation of the Numerical model

For the purpose of validation, the current result must be compared with the experimental or numerical results of other researchers taking into consideration the similarity in melting problem and the operating condition. Accordingly, the predicted results were compared with the experimental findings of Tan et al. [25] of constrained melting of n-octadecane PCM ( $T_m=28.2$  °C) inside a spherical cell of diameter 101.66mm with 1.5mm thickness. The spherical storage cell was immersed in a hot water tank of temperature 40 °C. A reasonable agreement was achieved between the numerical results of the present work and experimental findings of Tan et al. [25] as presented in Fig. (3.4). The maximum difference between the two results is about 14.2%. This difference can be reasoned by the heat

loses in experimental work and the assumptions required to obtain the numerical solution. Furthermore, the present numerical achieves more accurate results than that numerical model of Tan et al. [25].

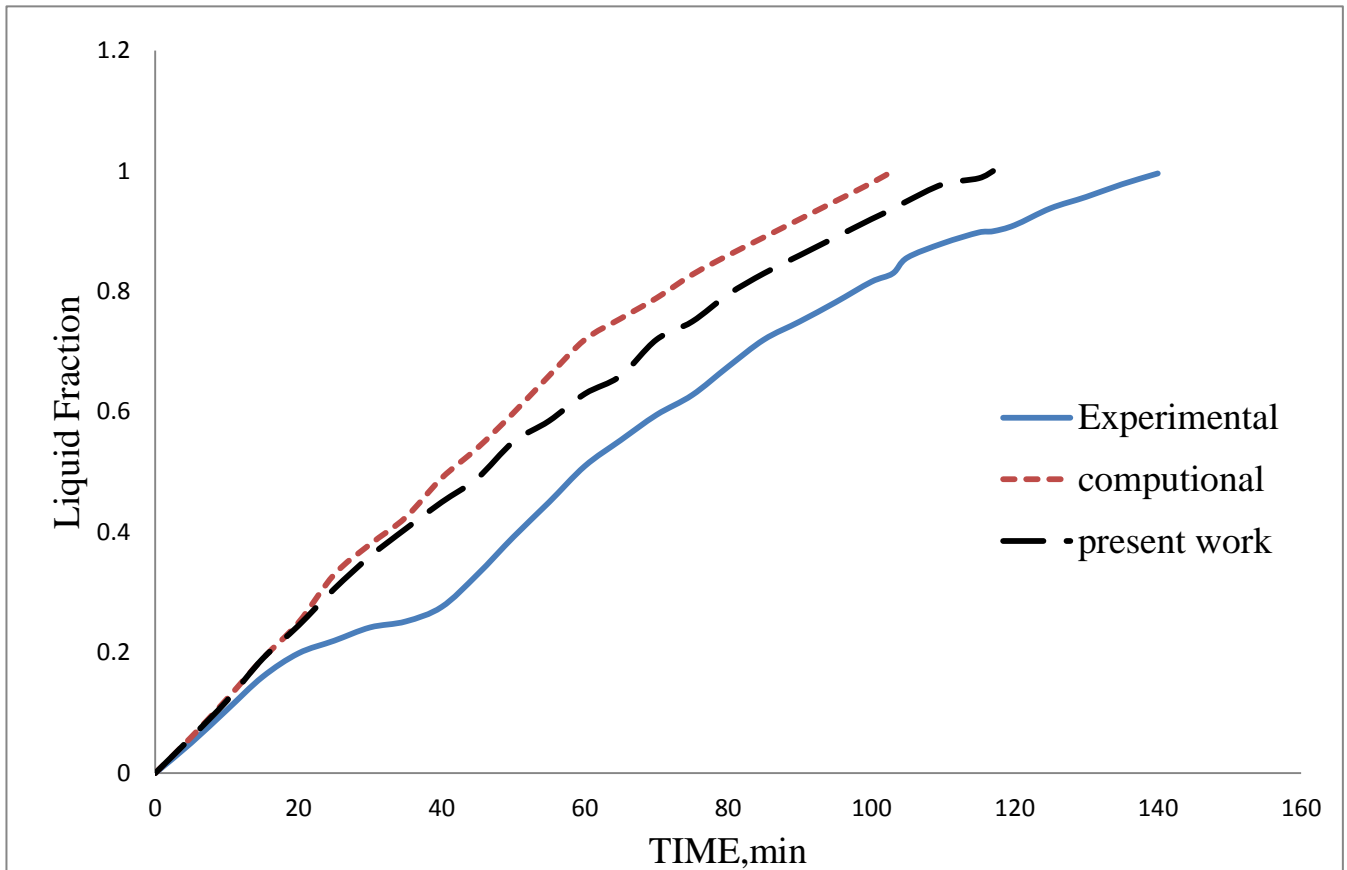


Fig. (3.4). Comparison of melt fraction between the present work and results of Tan et al. [25].

### 3.5 Grid- independence test

The grid independence test was carried out in order to find the optimum number of grid-elements that compromise between the accuracy of the solution and the cost and time of implementation of the computational model. The results of variation of the melt fraction are considered for determining the suitable grid-size system as shown in Figs. (3.5a) and (3.5b) for horizontal and vertical heat exchangers, respectively. The initial temperature of PCM is 17 °C, the inlet temperature and flow rate of water are 70 °C and 6 l/min, respectively. The computational domain of

horizontal annular cavity PCM-heat exchanger is discretized by three meshing sizes of 2221, 5001 and 7653 elements. The results of the variation of a liquid fraction indicate that the melting times are 184, 190 and 192 min for three sizes of elements. Therefore, the meshing of 5001 is adopted throughout the numerical study. On the other hand, the meshing of 1500, 2196 and 4342 was tested for vertical orientation of heat exchanger and the registered melting times are; 125, 130 and 133 min, respectively. The discretization of 2196 grids was adopted for vertical orientation of heat exchanger throughout the study.

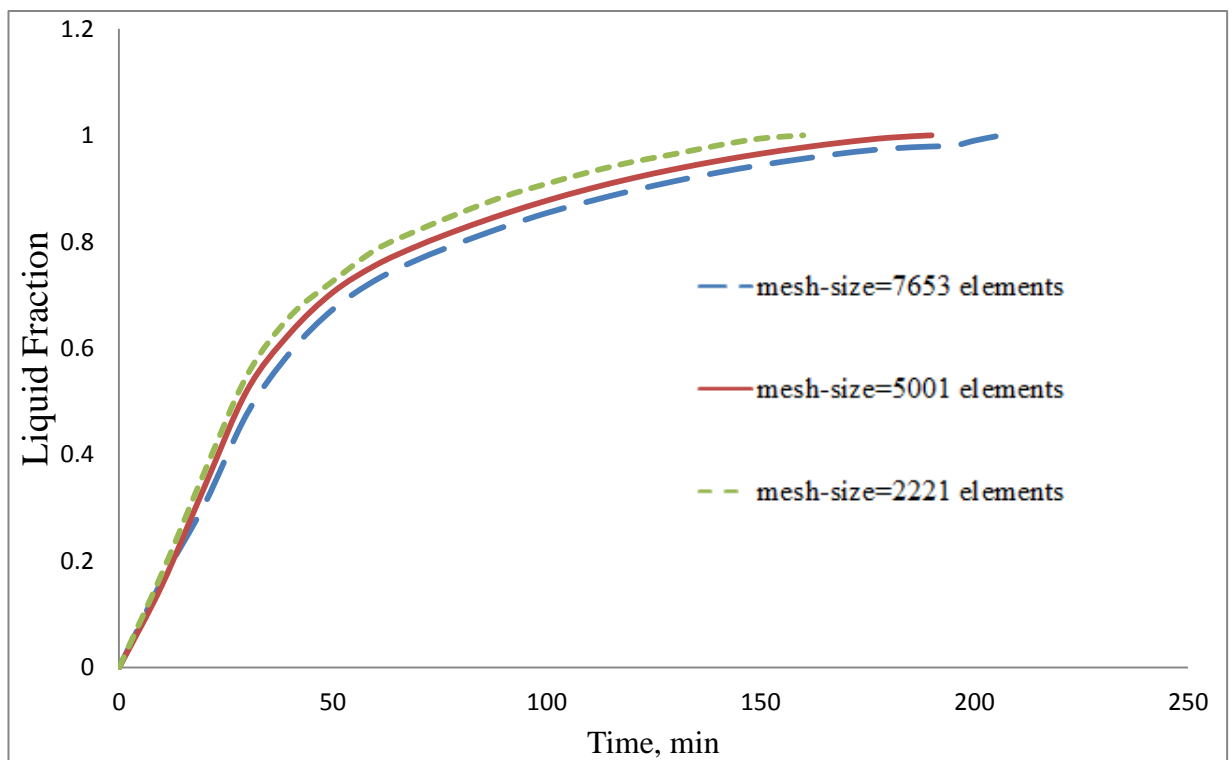


Fig. (3.5 a). Grid-independence test for a horizontal heat exchanger.

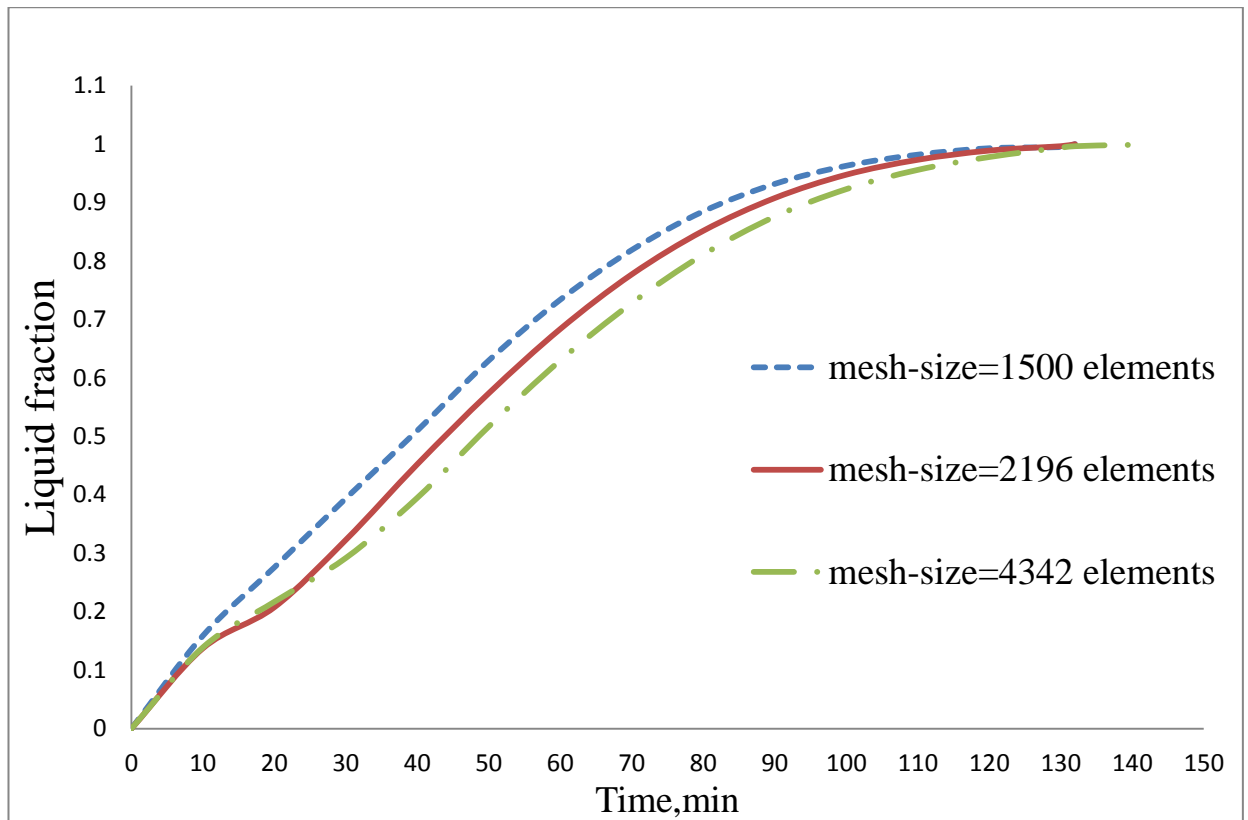


Fig. (3.5 b). Grid-independence test for a vertical heat exchanger.

### 3.6 Time-step independence test

The time-independence test is also carried out to examine the influence of the time-step in each iteration on the accuracy and convergence of the numerical results. Three different values of time step are tested; 0.5, 0.1 and 0.01s. The influence of time-step on the melt fraction is revealed in Figs. (3.6a) and (3.6b) for horizontal and vertical heat exchangers and for  $T_{ini}=17\text{ }^{\circ}\text{C}$ ,  $T_w=70\text{ }^{\circ}\text{C}$  and water flow rate of 6 l/min. The results revealed that the insignificant effect of time-step on the melt fraction. Also, the melting time values are; 187, 190 and 191.5 min in the horizontal heat exchanger and 127, 130 and 132 min for vertical one for each time-step. Therefore, a time-step of 0.1 s was selected throughout the numerical study.

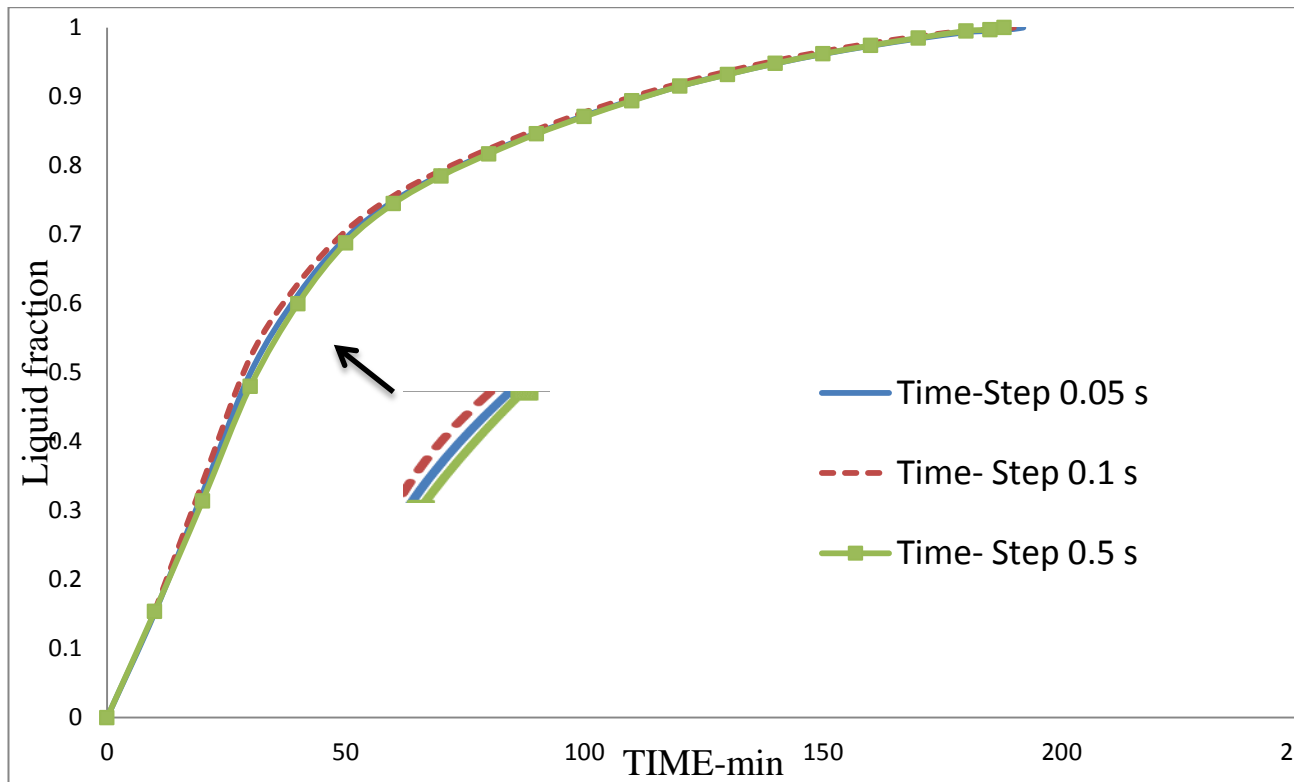


Fig. (3.6a). Effect of time-step on the melt fraction inside the horizontal heat exchanger.

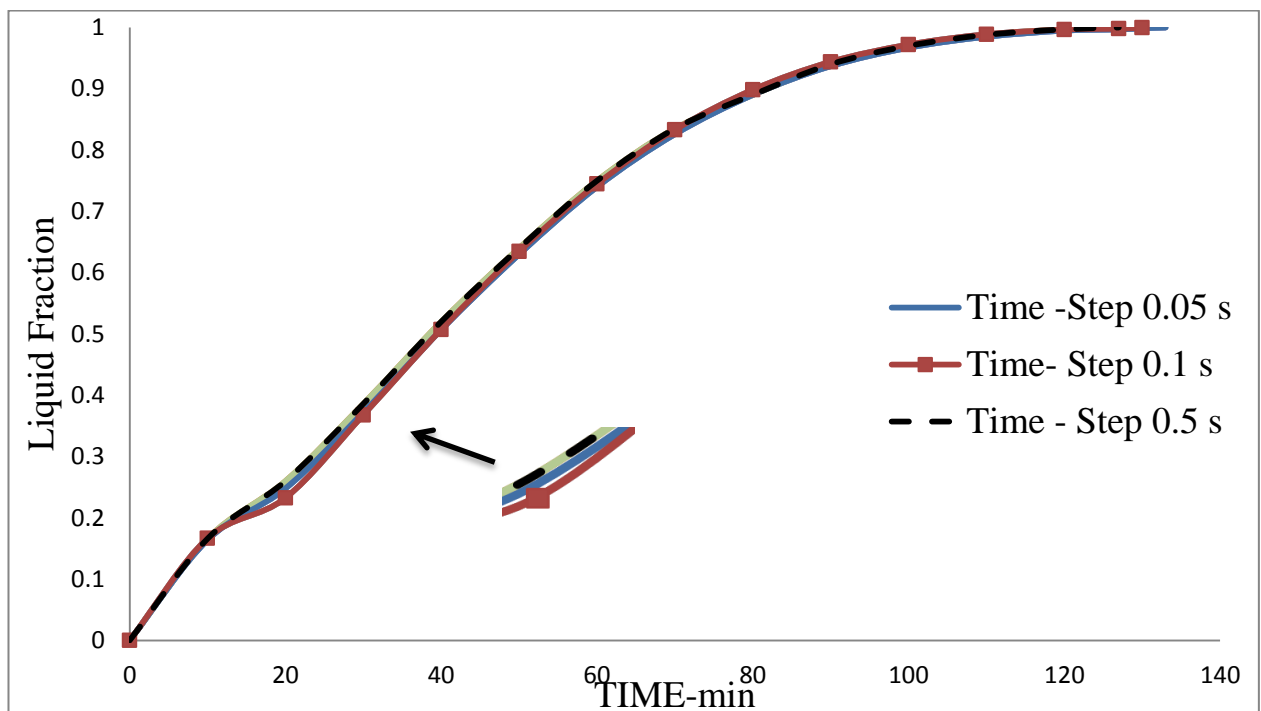


Fig. (3.6b). Effect of time-step on the melt fraction inside the vertical heat exchanger.

### 3.7 The influence of the mushy zone constant

In the literature, it was observed that the values of the mushy zone constant ( $A_{mush}$ ) affect the heat transfer of PCM. Thus when the constant of mushy zone increases, the resistance of heat transfer increases too [47]. The influence of the three values of mushy zone constant ( $10^5$ ,  $10^6$  and  $10^7$ ) on the melt fraction of PCM inside horizontal and vertical heat exchangers is illustrated in Fig. (3.7a) and Fig. (3.7b), respectively at  $T_{ini}=17$  °C,  $T_w=70$  °C and water flow rate of 6 l/min. The results showed a clear effect of the mushy zone constant on melting time. The increase in mushy zone value leads to an increase in melting time. The melting time values are 190, 205 and 212 min in the horizontal heat exchanger for mushy zone constant of  $10^5$ ,  $10^6$  and  $10^7$ , respectively. For the same values of mushy zone constant, the melting process requires 130, 142 and 150 min for complete melting in the vertical heat exchanger, respectively. According to these results, the value of  $10^6$  is adopted for the mushy zone constant.

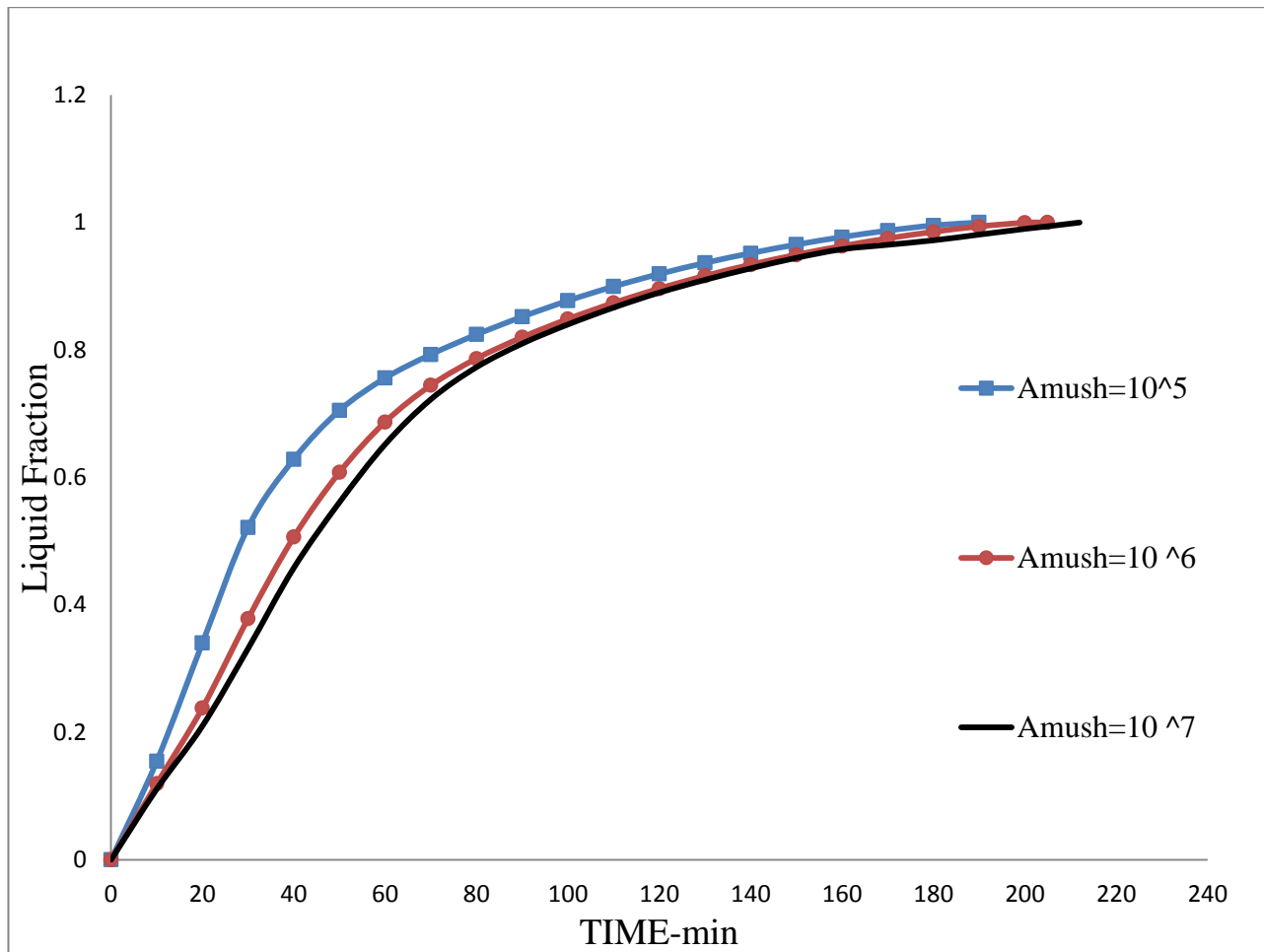


Fig. (3.7a) independence test of mushy zone for horizontal position.

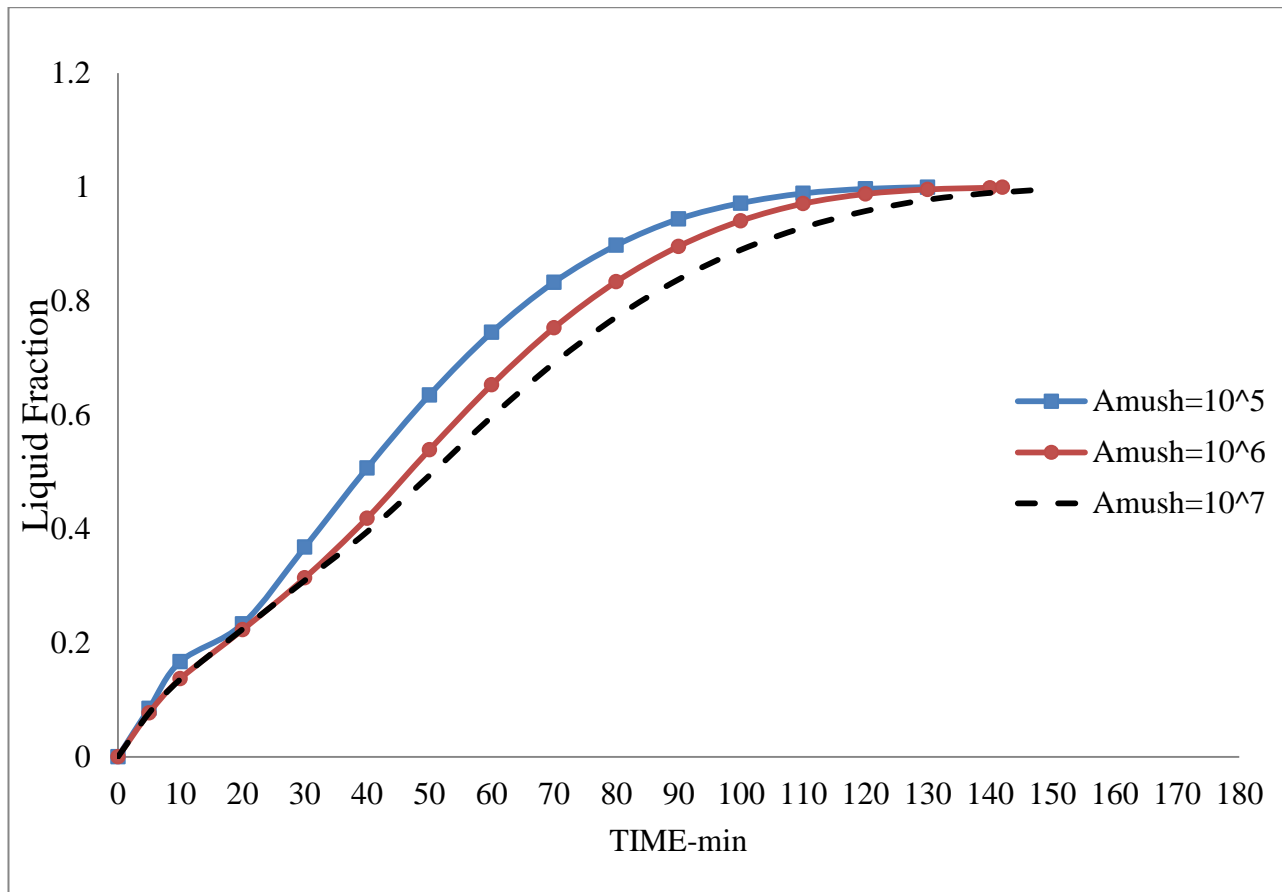


Fig. (3.7 b) independence test of mushy zone for vertical position.



**CHAPTER FOUR**  
**EXPERIMENTAL**  
**WORK**

## Chapter Four: Experimental Work

This chapter presents a detailed description of the experimental work related to the examination of the thermal behavior of PCM melting inside circular annular cavity of two orientations of the heat exchanger. The rig test was configured in the Heat Transfer Laboratory of the Chemical Engineering Department in the College of Engineering, Babylon University, Babylon, Iraq.

### 4.1 Experimental setup

A schematic diagram and a photograph of the experimental apparatus are shown in Fig. (4.1) and Fig. (4.2), respectively for horizontal and vertical heat exchangers.

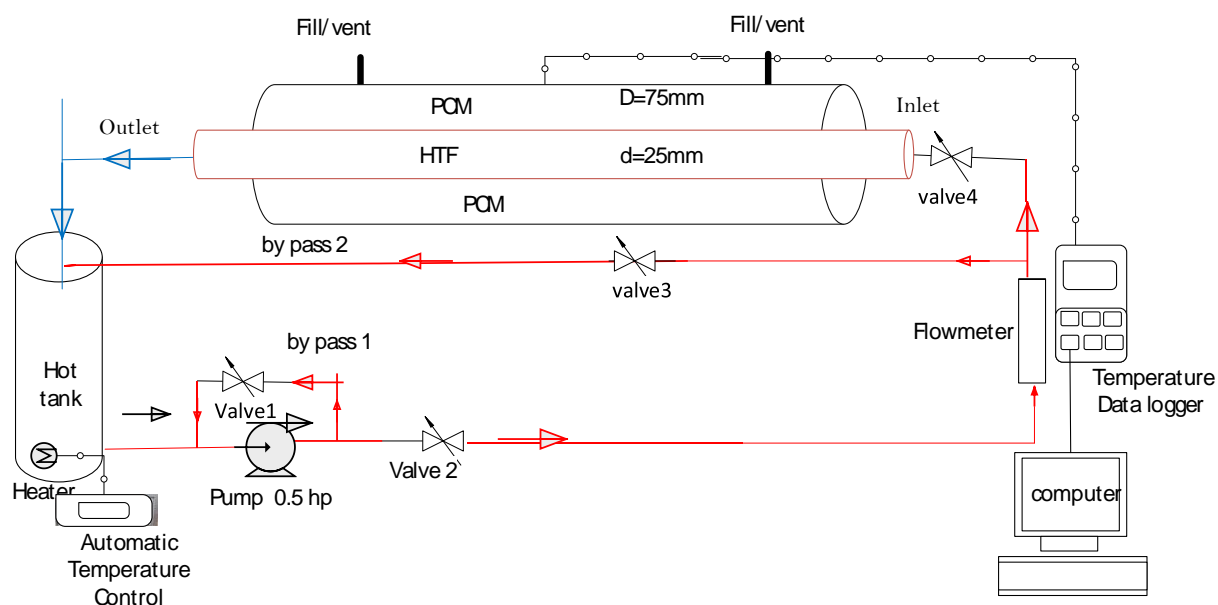


Figure (4.1) Schematic diagram of the experimental setup.

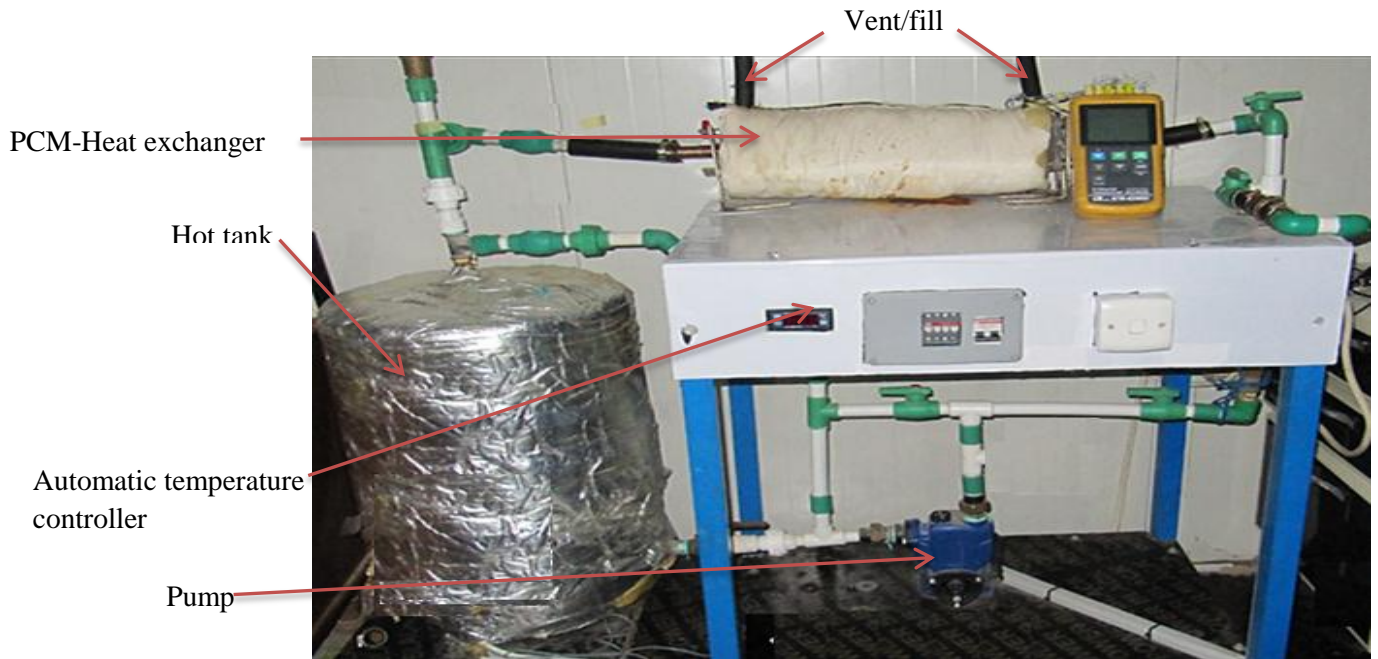


Fig. (4.2a) Photographical representation of the horizontal PCM annular cavity heat exchanger.



Fig. (4.2b) Photographical representation of the vertical PCM annular cavity heat exchanger.

## **4.2 The components of the experimental setup**

The experimental setup was composed of the following components and measuring devices:

- 1-Hot water tank with an electric heater.
- 2- Automatic Temperature Controller.
- 3- Water pump.
- 4- Water flowmeter.
- 5- Thermocouples and temperature data logger.
- 6- Annular thermal heat storage cell.
- 7- Control valves.

### **4.2.1 Hot water tank with an electric heater**

A cylindrical tank with a capacity of 80 liters is made of stainless steel and thermally-insulated by using glass wool. The tank is equipped with an electric heater with a power consumption of 1000 W to heat up the water and raise the temperature of water to the required level.

### **4.2.2 Automatic temperature controller**

Automatic Temperature Controller was used to control the temperature of the water entering the inner tube of the test rig. This device has a digital screen that is set for the required temperature. It is also provided with a temperature sensor that is incorporated inside the electric heater.

### **4.2.3 Water pump**

Centrifugal pump was used to deliver the heat transfer fluid HTF (water) from the tank into the copper inner tube and then return back to the tank. The pump has a maximum flow rate 50 liters/min, head of 9 m and with power 0.5 hp.

#### 4.2.4 Water flowmeter

The flowmeter (rotameter) was used to measure the flow rate of water passing through the inner tube with the measuring range of 2-18 liters/min as described in Fig. (4.3).

Direct calibration of the flow meter has been done by using a scalar vessel as well as a stopwatch. The time required to fill the scalar vessel is recorded. The process is repeated for several times and the calculated flow rates and measured values of the flow rates are represented in Fig. (4.4).

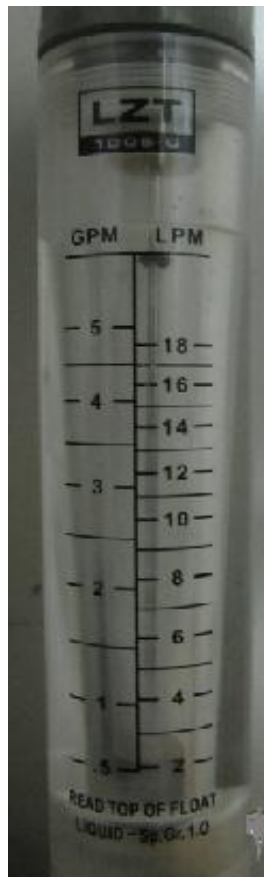


Fig. (4.3) Photo of flowmeter (rotameter).

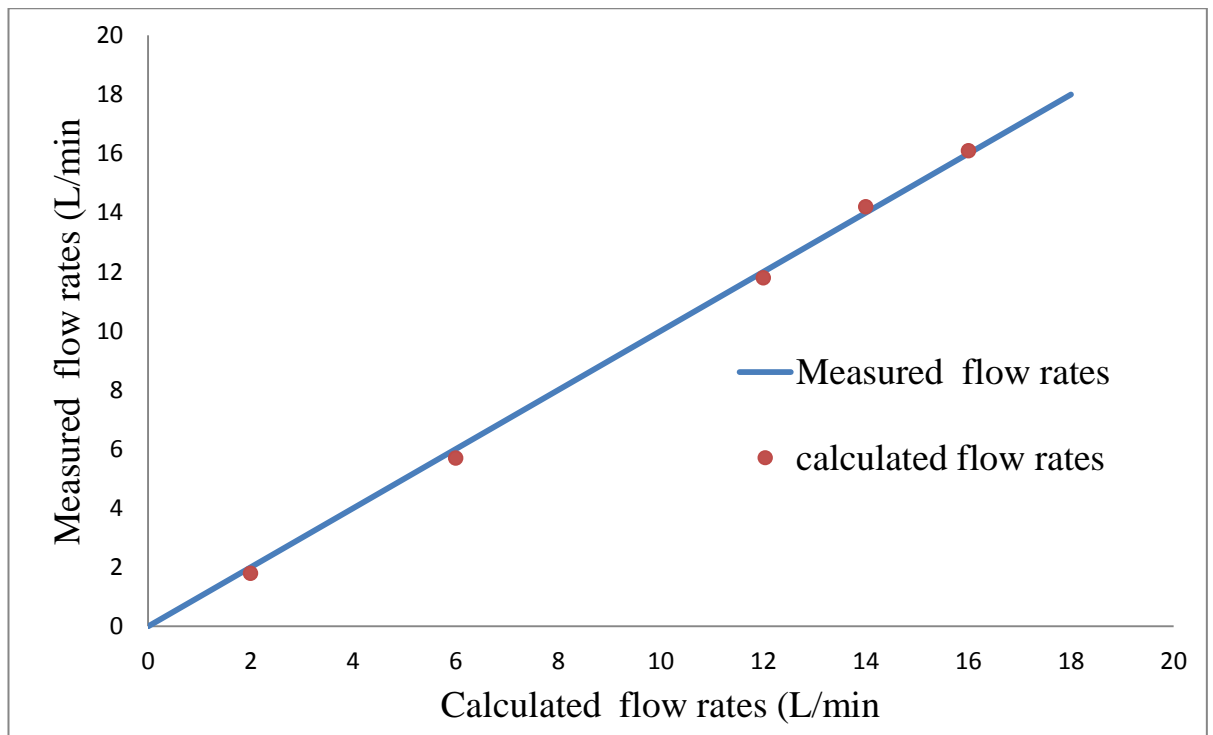


Fig. (4.4). Calibration of the flowmeter.

#### 4.2.5 Thermocouples and temperature data logger

The transient thermal behavior of the PCM melting inside the test rig was monitored by fifteen K-type thermocouples (TCs). Two of them were used to measure the inlet and outlet temperatures of water. Also, one thermocouple was used for monitoring the temperature of by-passing water. The other twelve thermocouples were placed inside the test rig to record the transient temperature distribution of the PCM in different locations during the melting process. To record the temperatures, two temperature data loggers (Lutron-BTM-42085SD) which have 12 channels for each were used. Calibration of thermocouples is presented in Appendix (A). The positions of TCs were decided according to preliminary numerical examination to compromise between the number of available TCs and temperature variations within PCM. Also, the thermocouples are fixed accurately at their locations by using a plastic rake.

In the horizontal heat exchanger, twelve thermocouples are placed in the middle of the acrylic tube and distributed in certain locations as presented in Fig. (4.5). The radial and angular positions ( $r$ ,  $\theta$ ) of TCs are specified in Table (4.1). Also, the fill/vent tube was fixed on the top side of the insulated acrylic tube.

In the vertical orientation of heat exchanger, the temperatures vary in axial and radial positions ( $r$ ,  $z$ ) as depicted in Fig. (4.6) and Table (4.2). On the other hand, the fill/vent tube was placed at the top of the acrylic tube.

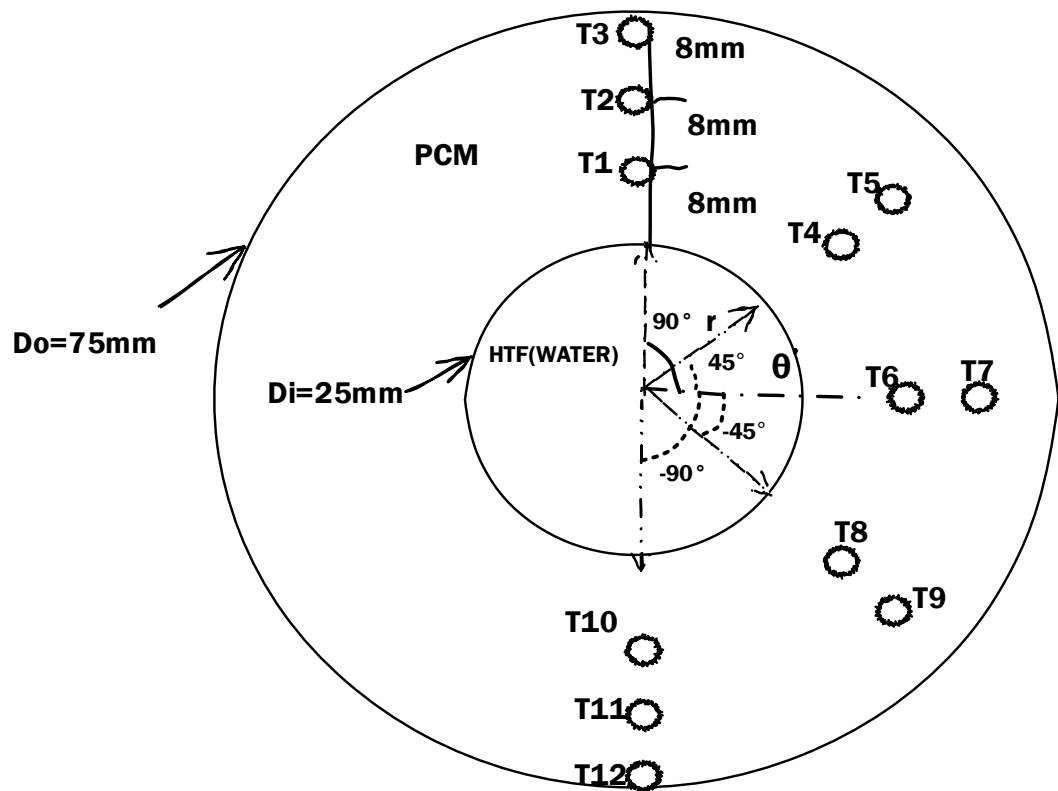


Fig. (4.5) The thermocouples distribution inside the horizontal annular cavity.

Table (4.1) The radial and angular positions of thermocouples inside the horizontal annular cavity.

<i>TC no.</i>	<i>T1</i>	<i>T2</i>	<i>T3</i>	<i>T4</i>	<i>T5</i>	<i>T6</i>	<i>T7</i>	<i>T8</i>	<i>T9</i>	<i>T10</i>	<i>T11</i>	<i>T12</i>
<i>r, mm</i>	20.5	28.5	37.5	20.5	28.5	20.5	28.5	20.5	28.5	20.5	28.5	37.5
$\theta$ , degree	90	90	90	45	45	0	0	-45	-45	-90	-90	-90

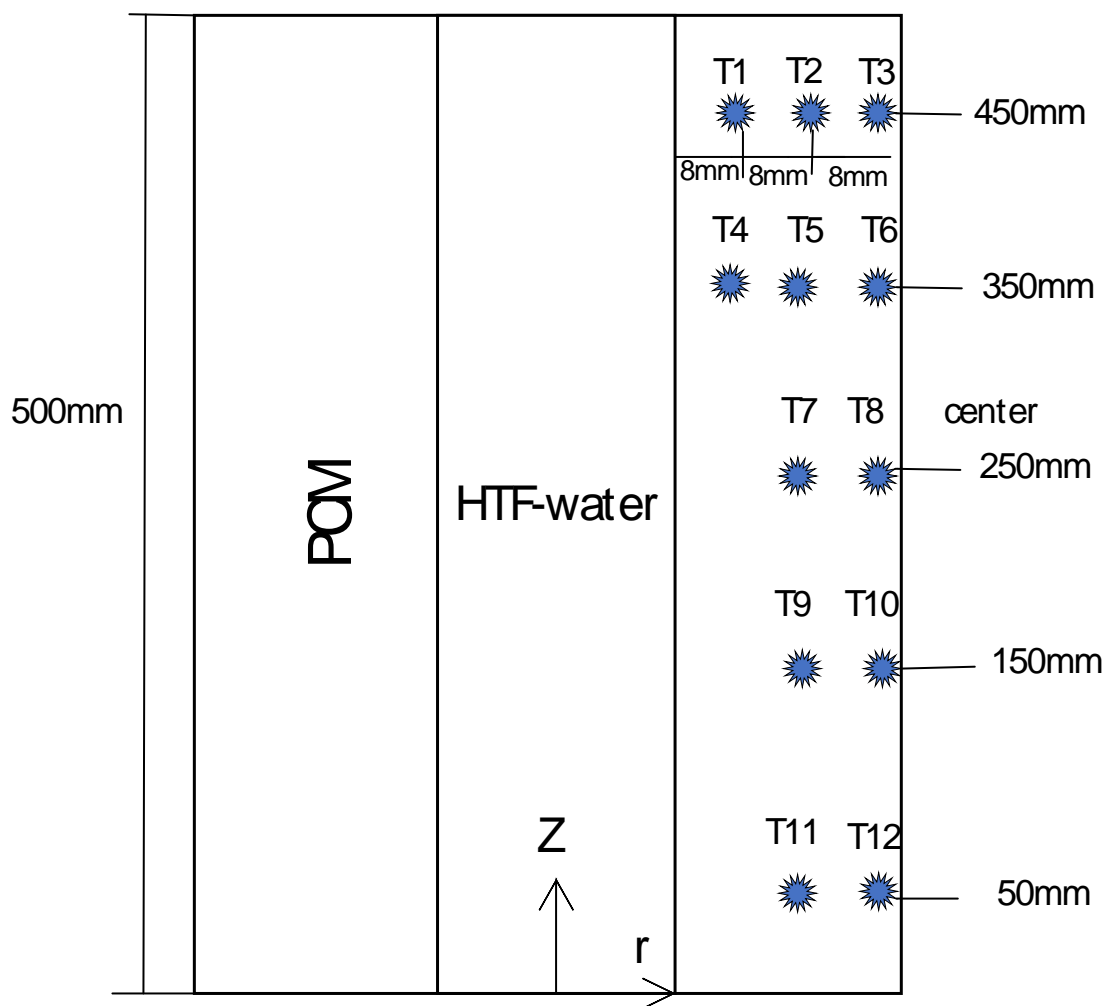


Fig. (4.6) The thermocouples distribution inside the vertical annular cavity.



Table (4.2) The radial and axial positions of thermocouples inside the vertical annular cavity.

TC no.	T1	T2	T3	T4	T5	T6	T7	T8	T9	T10	T11	T12
r (mm)	20.	28.	37.	20.	28.	37.	20.	28.	20.	28.	20.	28.
z(mm)	450	450	450	350	350	350	250	250	150	150	50	50

#### 4.2.6 Thermal storage unit

The PCM was contained in an annular space between an inner copper tube and outer thermally insulated acrylic shell. The inner tube is 25 mm outside diameter, 1 mm thickness and 700 mm length. The hot water as heat transfer fluid HTF flows inside the inner tube to transmit the thermal energy into the PCM. The outer shell has inside diameter of 75 mm, the thickness of 2.5 mm and a length of 500 mm. Transparency of acrylic provides visual access for the melting behavior of PCM. Also, an insulator of 40 mm glass-wool layer thickness is used to reduce the heat losses. The acrylic shell has two vents for filling liquid PCM and accommodating any volume change of PCM during the melting process. In addition, two square acrylic sheets with 10 mm thickness were used to support and grantee the symmetrical concentric configuration of double tubes. A rubber ring is used between the copper pipe and the square sheets to prevent leakage of liquid PCM outside thermal storage unit as shown in Fig. (4.7).

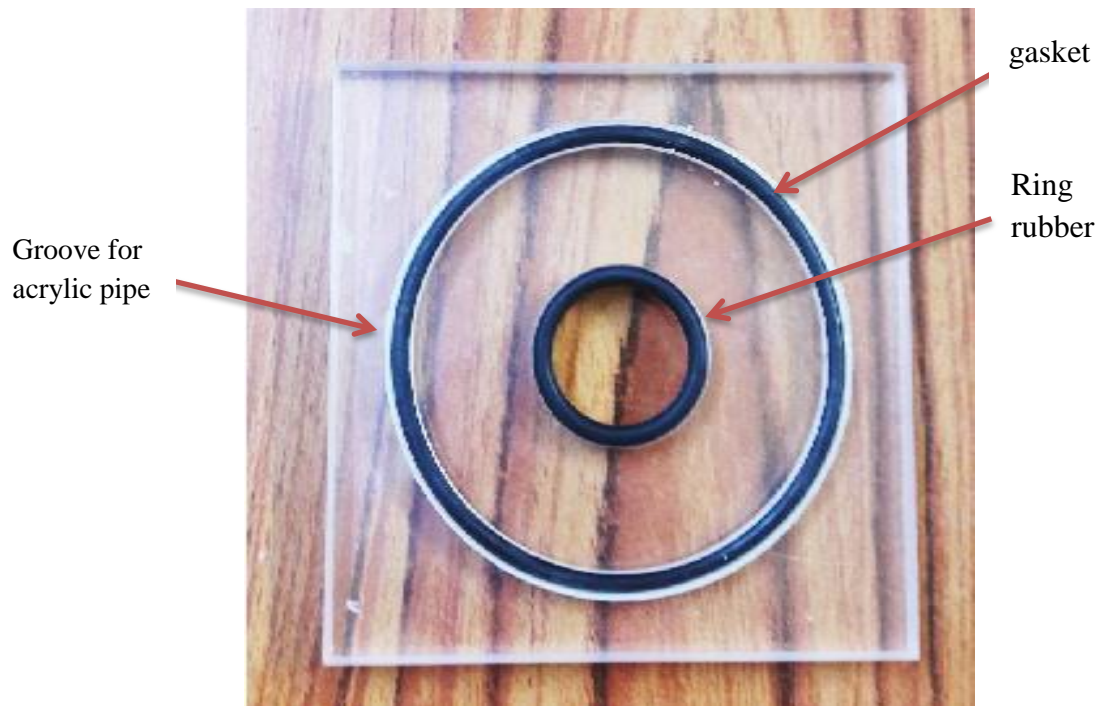


Fig. (4.7) Acrylic square sheet.

#### 4.2.7 Ball Valves and PVC piping system

Four valves are used to control flow direction the flow rate of water inside the copper pipe. The PVC piping system was used to transmit the HTF between the tank and the test rig.

#### 4.3 Phase change material (RT-42)

The paraffin wax RT-42 (Fig. (4.8)) was used as a PCM in the experiment. This paraffin was manufactured by Rebitherm company, Germany. The thermo-physical properties of RT-42. The wax is white-colored in the solid phase and transparent in the liquid phase. The selection of this type of wax due to its melting range which can be used in many applications besides its high latent heat of melting.



Fig. (4.8) Paraffin wax RT-42.

#### 4.4 Experimental Procedure

The liquid PCM was filled gradually inside the annular through the vent to avoid air gaps. The filling process was achieved in several stages where the liquid PCM was left to solidify layer by layer in each stage.

In each test, the water was heated inside the tank to above-required temperature to accommodate the heat losses in the piping system before entering the test rig. The temperature of the by-pass was observed so that when it reaches the required level, the bypass valve is closed and the hot water is allowed to enter the storage unit through the inlet valve. The experiment was terminated when the solid PCM was fully melted. The readings of all thermocouples were recorded and the images of the solid-

liquid front were captured by a digital camera. Three different temperatures 60, 70 and 80 °C of HTF were considered to show their influence on the melting process. Each experiment was repeated three times to confirm the reproducibility of the measured data.

#### 4.5 Dimensionless parameters and data reduction

The melting of PCM inside enclosures was governed by dimensionless parameters such as the Rayleigh number and Stefan Number.

The Rayleigh number is the buoyant force divided by the viscous force,

$$Ra = \frac{\rho^2 c_p \beta g D^3 (T_w - T_m)}{\mu k} \dots \dots (4.1)$$

The Stefan number represents the ratio of heat sensible amount to the latent heat of the material. It can be described as:

$$Ste = \frac{c_p (T_w - T_m)}{L} \dots (4.2)$$

Where  $c_p$ ,  $\rho$ ,  $\mu$ ,  $L$ ,  $\beta$  and  $D$  represent specific heat, density, dynamic viscosity, latent heat of phase change, thermal coefficient expansion and the characteristic length, respectively.

The average Nusselt number is defined as:

$$Nu = \frac{h D}{k} \dots (4.3)$$

where,  $h$  represents the heat transfer coefficient and obtain from

$$h = \frac{q_w}{(T_w - T_m)} \dots (4.4)$$

$$Nu = \frac{D(T_w - T_c)}{\Delta X(T_w - T_m)} \dots (4.5)$$

where,  $k$  represents the thermal conductivity of PCM respectively and  $\Delta X$  represents the distance between wall and thermocouples.

The thermal energy stored in the PCM equals the sensible heat absorbed by solid and liquid phases and latent heat absorbed during the phase-change process. The stored energy can be estimated by the equation:

$$Q_s = m_{pcm} [Cp_s(T_{avs} - T_i)(1 - f) + f L + f Cp_l(T_{avl} - T_l)] \dots(4.6)$$

Where  $T_{avs}$ ,  $T_{avl}$ , and  $T_i$  represents the average temperature of solid and liquid phase and initial temperature respectively. While  $f$  represent the liquid fraction can be defined as

$$f = \frac{V_L}{V_s + V_L} \dots(4.7)$$

where  $V_s, V_L$  represent the volume of solid PCM and volume of melted PCM respectively.

#### 4.6 Error Analysis and Uncertainty

All measurements of physical quantities are subject to uncertainties in measurements. Variations in the results appear during repeated measurements, even after controlling the surrounding conditions. Therefore, it is impossible to keep the variables constant. In addition, the devices are manufactured with certain accuracy and method of reading the scale with fractional estimates increases the uncertainties. Thus, steps can be taken to reduce the error by calibrating the measuring devices as well as reducing the uncertainty. In order to correctly calculate the uncertainty, reference must be indicated and sources of uncertainty identified for each source. The estimation of errors has an extreme significance in each experimental study. The following procedure described by **(Holman)** [48] was used to evaluate the uncertainty in each calculated variables.

Assume the dependent variable  $R$  relates with many independent variables;  $x_1, x_2 \dots x_n$ . The uncertainty  $w_R$  in the result is;

$$w_R = \left[ \left( \frac{\partial R}{\partial x_1} w_1 \right)^2 + \left( \frac{\partial R}{\partial x_2} w_2 \right)^2 + \dots + \left( \frac{\partial R}{\partial x_n} w_n \right)^2 \right]^{\frac{1}{2}} \quad \dots\dots\dots (4-8)$$

where,  $w_1, w_2, \dots, w_n$  be the uncertainties in the independent variables.

For example, the uncertainty in calculating the Nusselt number (Eq. (4.5)) depends on the experimental errors that maybe happening in the independent parameters as given in in Table (4.4).

Table (4.4) Uncertainties of independent parameters

Independent parameter, $e$	Uncertainty ( $w$ )
Temperature difference	$\pm 0.3^{\circ} \text{C}$
Different diameters of the cell	$\pm 0.001\text{m}$
Distance between wall and thermocouples	$\pm 0.0005 \text{ m}$

The experimental error in the Nusselt number calculation can be explained in the following way:

$$w_{Nu} = \left[ \left( \frac{\partial Nu}{\partial \Delta T} w_{\Delta T} \right)^2 + \left( \frac{\partial Nu}{\partial D} w_D \right)^2 + \left( \frac{\partial Nu}{\partial \Delta x} w_{\Delta x} \right)^2 + \left( \frac{\partial Nu}{\partial \Delta T_w} w_{\Delta T_w} \right)^2 \right]^{\frac{1}{2}} \quad (4-9)$$

$$\frac{\partial Nu}{\partial \Delta T} = - \frac{\Delta T_w D}{\Delta X (\Delta T)^2} = \frac{Nu}{\Delta T} \quad \dots(4-9 \text{ a})$$

$$\frac{\partial Nu}{\partial D} = \frac{\Delta T_w}{\Delta X (T_w - T_m)} = \frac{Nu}{D} \quad \dots(4-9 \text{ b})$$

$$\frac{\partial Nu}{\partial \Delta X} = \frac{\Delta T_w D}{\Delta X^2 (T_w - T_m)} = \frac{Nu}{\Delta X} \quad \dots(4-9 \text{ c})$$

$$\frac{\partial Nu}{\partial \Delta T_w} = \frac{D}{\Delta X (T_w - T_m)} = \frac{Nu}{\Delta T_w} \quad \dots(4-9 \text{ d})$$

$$w_{Nu} = \left[ \left( \frac{\partial Nu}{\partial \Delta T} w_{\Delta T} \right)^2 + \left( \frac{\partial Nu}{\partial D} w_D \right)^2 + \left( \frac{\partial Nu}{\partial \Delta x} w_{\Delta x} \right)^2 + \left( \frac{\partial Nu}{\partial \Delta T_w} w_{\Delta T_w} \right)^2 \right]^{\frac{1}{2}}$$

$$w_{Nu}/Nu = \left[ \left( \frac{w_{\Delta T}}{\Delta T} \right)^2 + \left( \frac{w_D}{D} \right)^2 + \left( \frac{w_{\Delta x}}{\Delta x} \right)^2 + \left( \frac{w_{\Delta T_w}}{\Delta T_w} \right)^2 \right]^{\frac{1}{2}}$$

$$w_{Nu}/Nu = \left[ \left( \frac{0.39}{18.5} \right)^2 + \left( \frac{0.001}{0.005} \right)^2 + \left( \frac{0.0005}{0.008} \right)^2 + \left( \frac{0.39}{27} \right)^2 \right]^{\frac{1}{2}}$$

$$\frac{w_{Nu}}{Nu} = \pm 0.0445 = \pm 4.45\%.$$

#### 4.7 Repeatability Check

Repeatability or test-retest reliability is the nearness of the agreement between the results of successive measurements of the same parameter carried out under the same conditions of measurement. The measurements are taken by a single person or instrument on the same item, under the same conditions, and within a specified period time. In the experimental work, the test was conducted in several days and at different times of the day, some tests start from early morning and end to midday and some start from midday to midnight. To check the repeatability in a certain case, TC7 was selected in the vertical heat exchanger for an inlet temperature of 70 °C and 6 liters/min of water flow rate. The readings of TC7 are shown in Fig. (4.9). There are small differences of results between three tests. However, each test is repeated three times and the mean values of the measured data are considered.

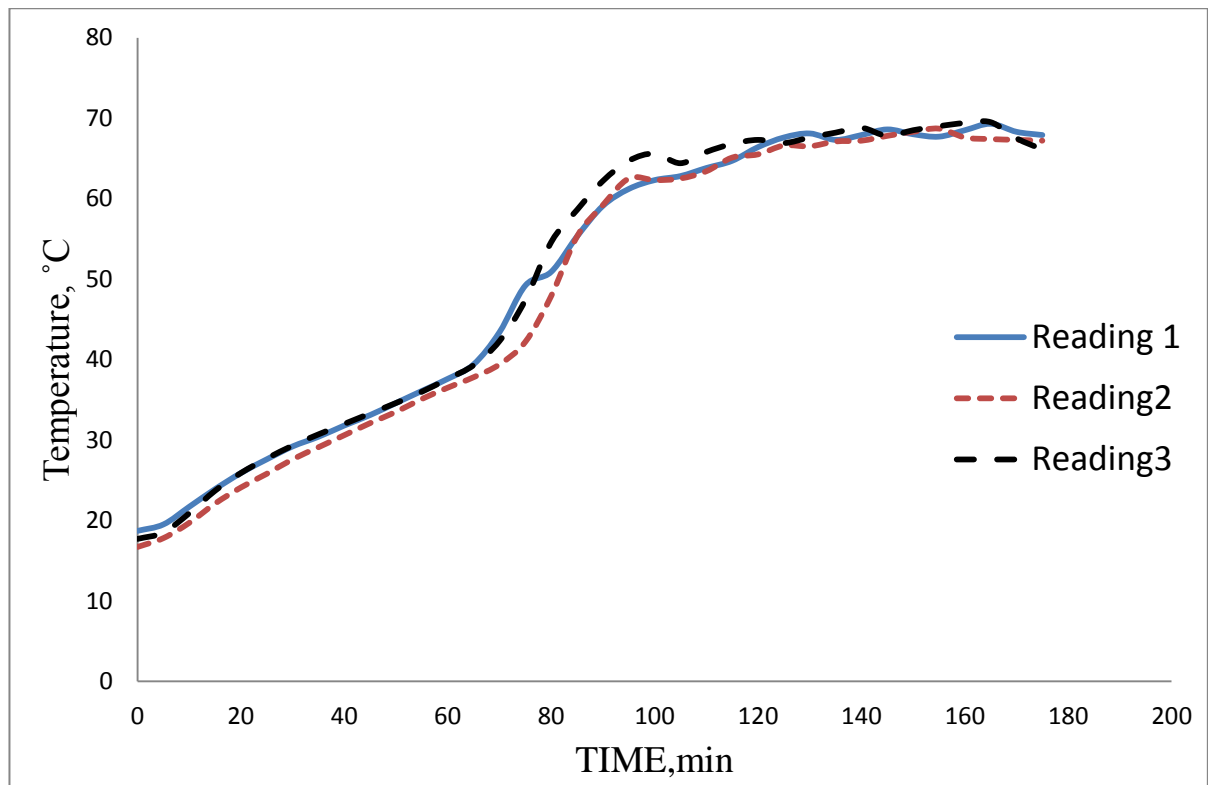


Fig. (4.9) Repeatability of temperature reading of TC<sup>v</sup>.



**CHAPTER FIVE**  
**RESULTS AND DISCUSSION**

## *Chapter Five: Results and Discussion*

The experimental and numerical results of the melting process of PCM (RT-42) inside an annular thermal heat exchanger are presented and discussed in this chapter. A shell-and-tube heat exchanger was used in current study. Its annular space between filled by a PCM, and hot water at desired temperature is passing through the inner tube to be the heat source for melting process. Two orientations of the heat exchanger are considered; horizontal and vertical. The influence of inlet water temperature (60, 70 and 80 °C) on the behavior and performance of the PCM melting within the storage unit is investigated. The effect of flow rate is insignificant effect on the melting behavior of the PCM as explained in Appendix B. The behavior and performance of PCM melting can be understood by evaluation the phase-change characteristics such as the distribution of temperature within the PCM, the growth and evolution of the melting interface, the amount of heat exchange between the wall and PCM and the stored energy. These characteristics were estimated experimentally and numerically. The dimensionless parameters that govern the melting process were the Rayleigh and Stefan numbers which are listed in Table (5.1).

Table (5.1) The calculated values of Rayleigh and Stefan numbers.

<i>Water temperature, °C</i>	<i>Ra</i>	<i>Ste</i>
60	$5.92 \times 10^5$	0.195
70	$9.40 \times 10^5$	0.310
80	$1.29 \times 10^6$	0.425

## 5.1 The Experimental Results

In this section, the experimental results of the melting of PCM inside an annular cavity are presented. The results are illustrated as readings recorded by thermocouples within PCM, the evolution of the melting front by using digital imaging, estimating the Nusselt number as well as obtaining the amount of energy stored in PCM.

### 5.1.1 PCM melting in the horizontal heat exchanger.

This section is concerned with the experimental results of the PCM melting within a horizontal annular cavity.

#### 5.1.1.1 Temperature Distribution of PCM

The temporal temperatures distribution of PCM inside the horizontal cavity is illustrated in Fig. (5.1). The readings of the thermocouples vary according to their locations inside the cell as indicated previously in Chapter 4 of this thesis (Fig. (4.5)). The readings of temperatures  $T_1$ ,  $T_2$ ,  $T_3$ ,  $T_4$ ,  $T_5$ ,  $T_6$  and  $T_7$  reach the melting point faster than the rest of thermocouples due to earlier initiation of natural convection in the upper part of the storage cell. Also, the temperatures  $T_1$ ,  $T_4$  and  $T_6$  arrive the melting point and steady-state condition before the rest locations (e.g.  $T_8$  and  $T_{10}$ ). Although those five thermocouples have the same radial positions from the center, they have different angular locations. This difference in temperatures is justified to the privilege of natural convection in the upper region of the storage unit. On the other hand, the temperature fluctuations are observed for the temperature readings of TCs in the upper portion of the unit. While the variations of the temperatures in the lower part of the cell are uniform and un-fluctuated due to the domination of conduction heat transfer at that region. It is worthy to mention that the temperature variation is low in the melting range region

between  $T_{solidus}$  and  $T_{liquidus}$  for thermocouples that do not fall under the dominant influence of natural convection.

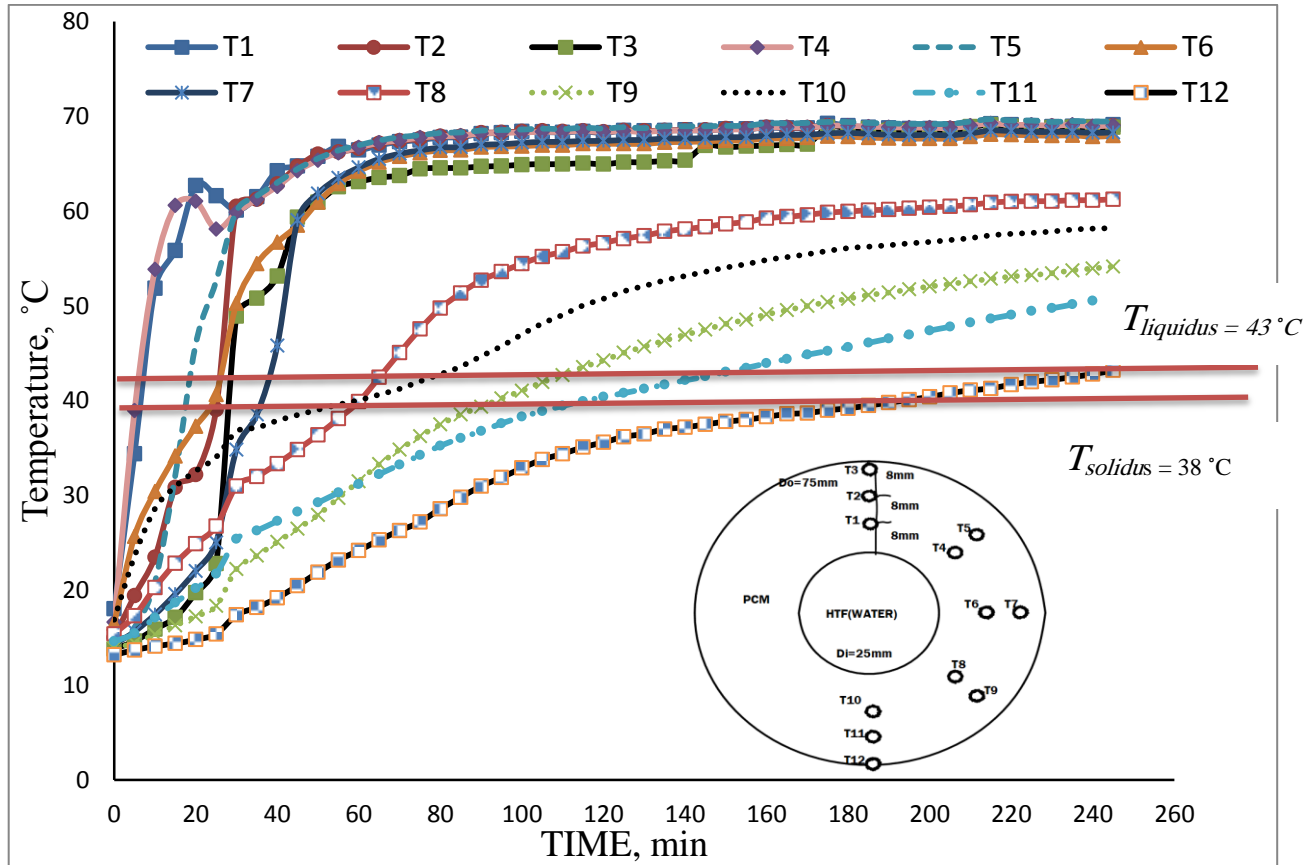


Fig. (5.1) The temperature distribution of PCM at a water temperature of 70°C.

The effect of dominated heat transfer is explained by a comparison between two temperatures  $T_1$  and  $T_{10}$  for different temperatures of hot water as presented in Fig. (5.2). The thermocouples  $TC_1$  and  $TC_{10}$  have the same radial positions but different angular locations of 90 and -90 degree, respectively. Clearly, the increase in temperature of hot water leads to an intensification of thermal energy that transferred from HTF into PCM, earlier evolution of natural convection currents and acceleration of the melting process. Thus, the temperature values are raised with the increase of temperature of hot water. On the other hand, the effect of natural convection

causes that the values of temperature  $T_1$  exceed that of  $T_{10}$ . Also, it is observed that the increase rate in temperature  $T_1$  is higher than that of temperature  $T_{10}$ .

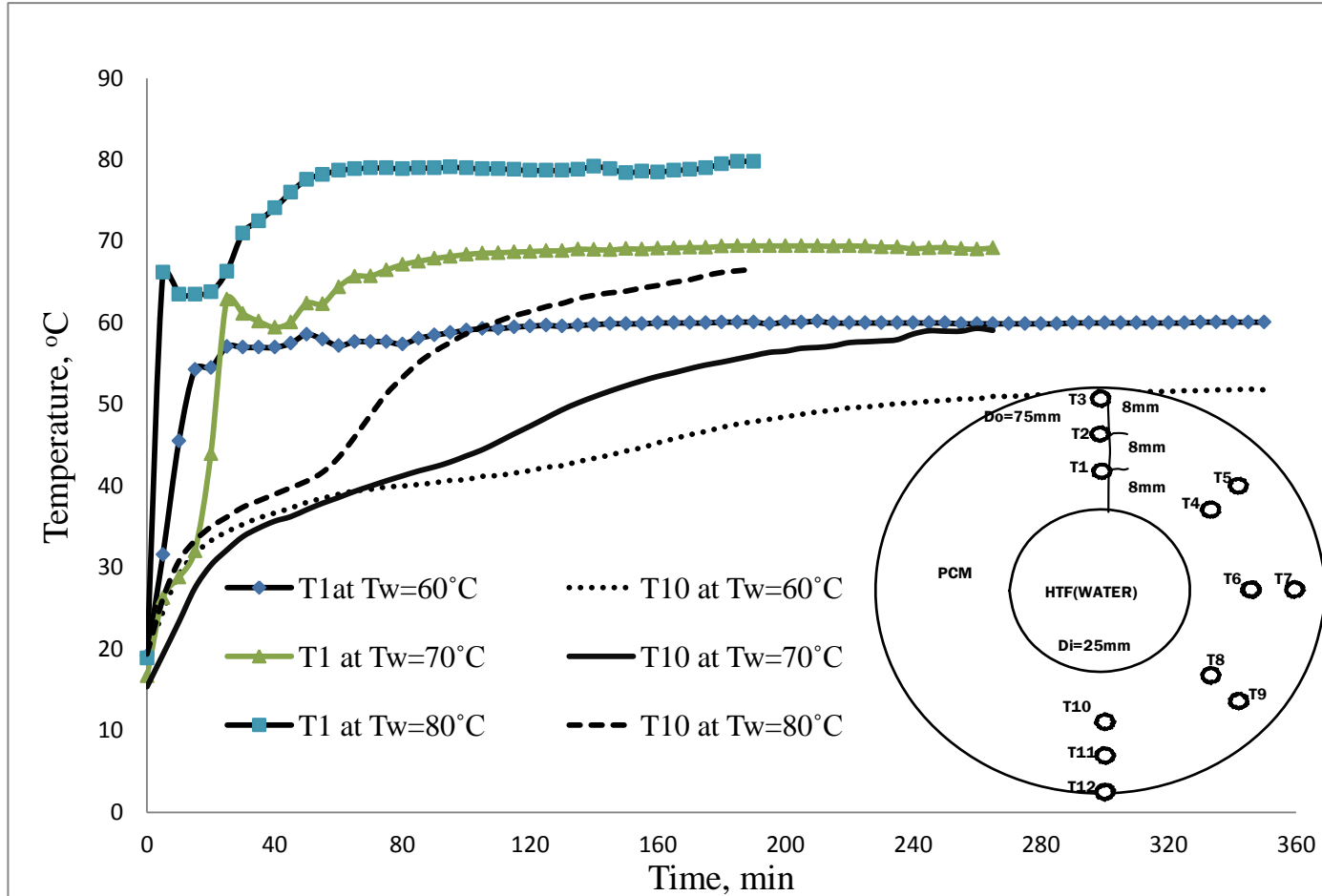


Fig. (5.2) A comparison between the temperatures  $T_1$  and  $T_{10}$  for different temperatures of HTF.

### 5.1.1.2 Transient Evolution of Solid-Liquid Interface and Melt Fraction

The photographic representation of the time-progress of melting process is illustrated in Fig. (5.3) for three different temperatures of water. It is observed that the symmetric melting front and diffusion-heat transfer is dominated at the early periods (15 min) of melting at water temperatures of 60 and 70 °C. However, for the same period of 15 min but at water temperature of 80 °C, it is noticed that the natural convection is developed, and the melting rate is faster at the upper half of the cell. After initial periods, the movement of natural convection currents strengthens the melting rate at the upper part of the cell for different water temperatures. However, as time progress the overall melting rate of the PCM inside the cell is decelerated as the transmitted thermal energy from HTF is carried from natural convection currents to the upper part of the cell rather than melting extra solid PCM at the lower part. Therefore, the overheating and thermal stratifications occur for the PCM melt at the upper part of the storage unit. On the other hand, the temperature of HTF has a positive influence on the melting rate as confirmed by Fig. (5.4). The melting time is reduced by about 27.5% and 46.3% when the HTF temperature varies from 60 to 70 °C and from 60 to 80 °C, respectively.

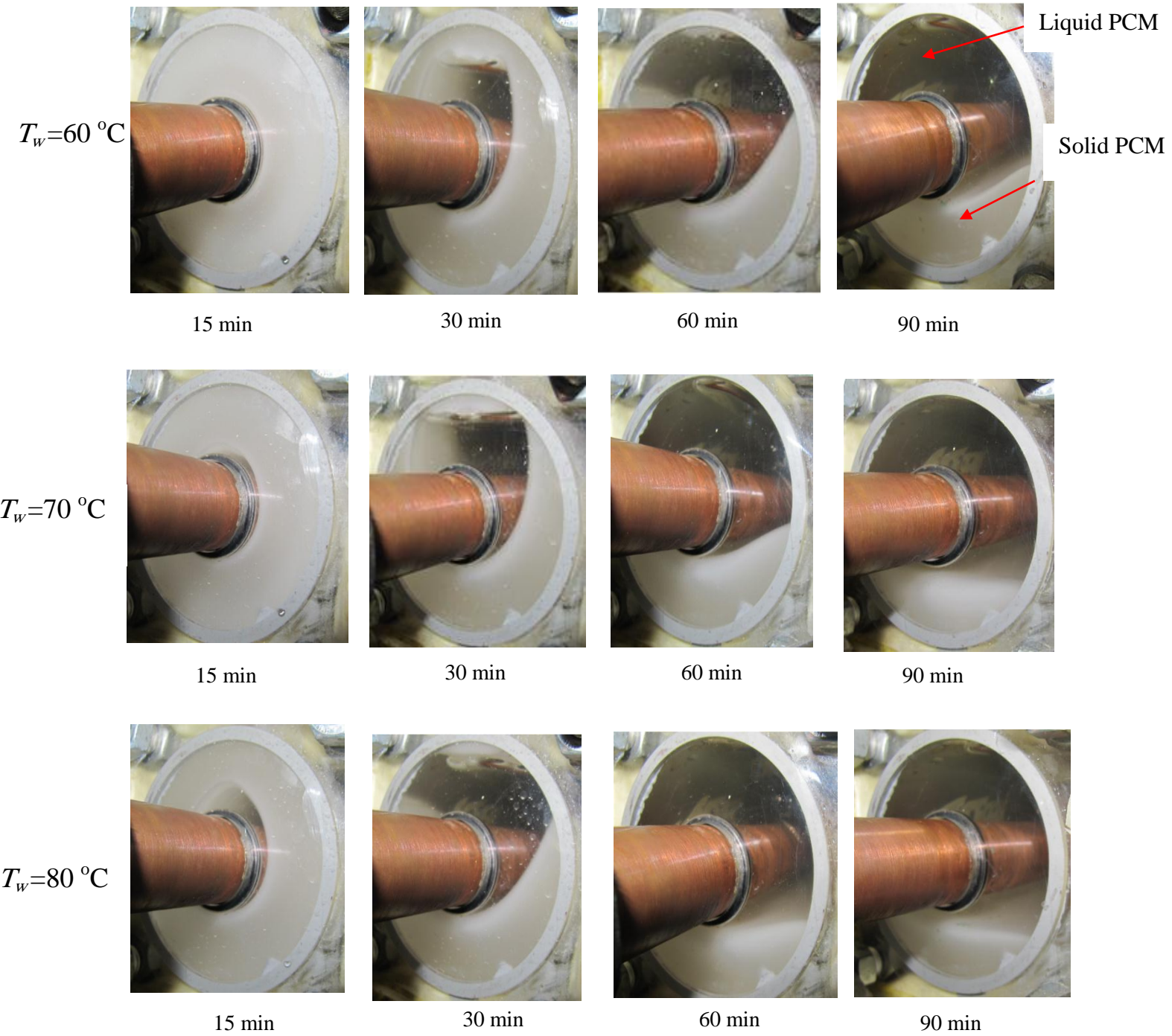


Fig. (5.3) Instantaneous photographs of the melting of RT-42 at 15, 30, 60 and 90 min for various temperatures of water.

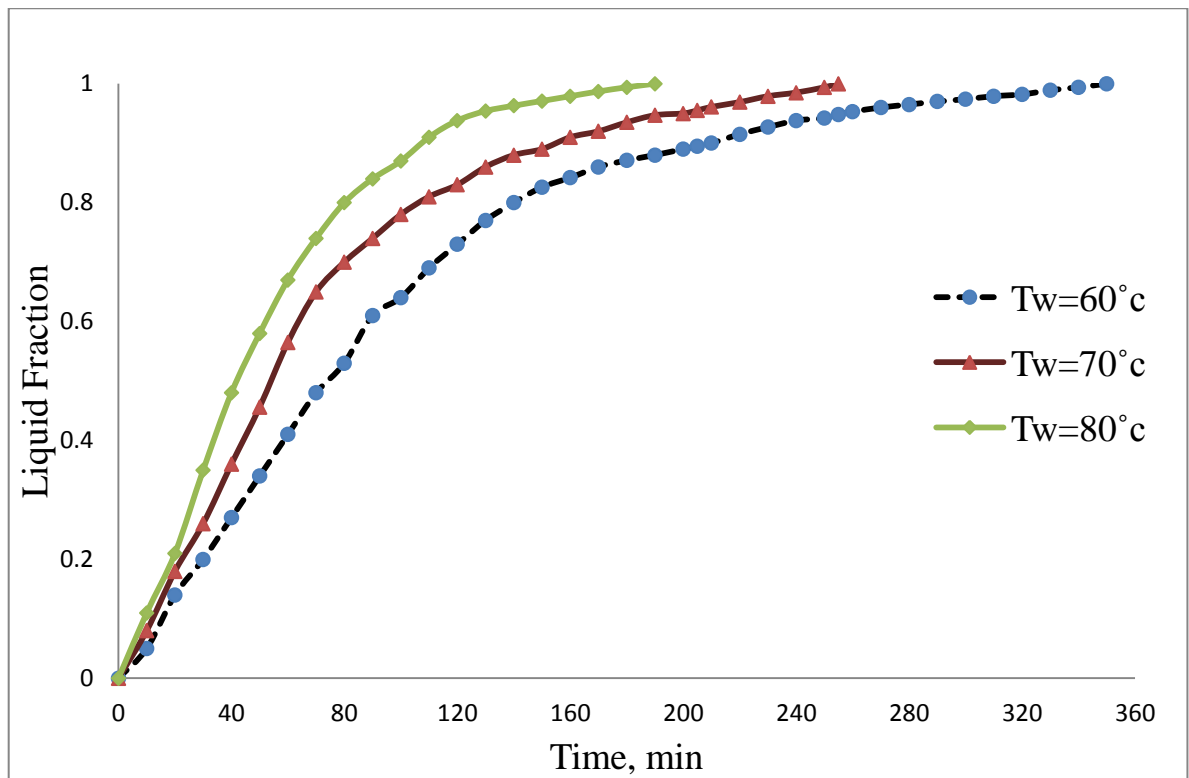


Fig. (5.4). Time-variation of the liquid fraction for different values of HTF temperatures.

### 5.1.1.3 Variations of the Nusselt number.

The transient variations of the Nusselt number for different temperatures of water are revealed in Fig. (5.5). It is obvious that for all cases, the Nusselt number increases highly at a very small initial period as the conduction is dominated and higher temperature gradient over a thin melted PCM exists. After, the Nusselt number decays dramatically as the role of conduction is decreased and the thickness of melted PCM is increased, and it causes a reduction of transmitted thermal energy from HTF into solid PCM. However, the role of natural convection is evolved and will be dominated heat transfer of the melting process.



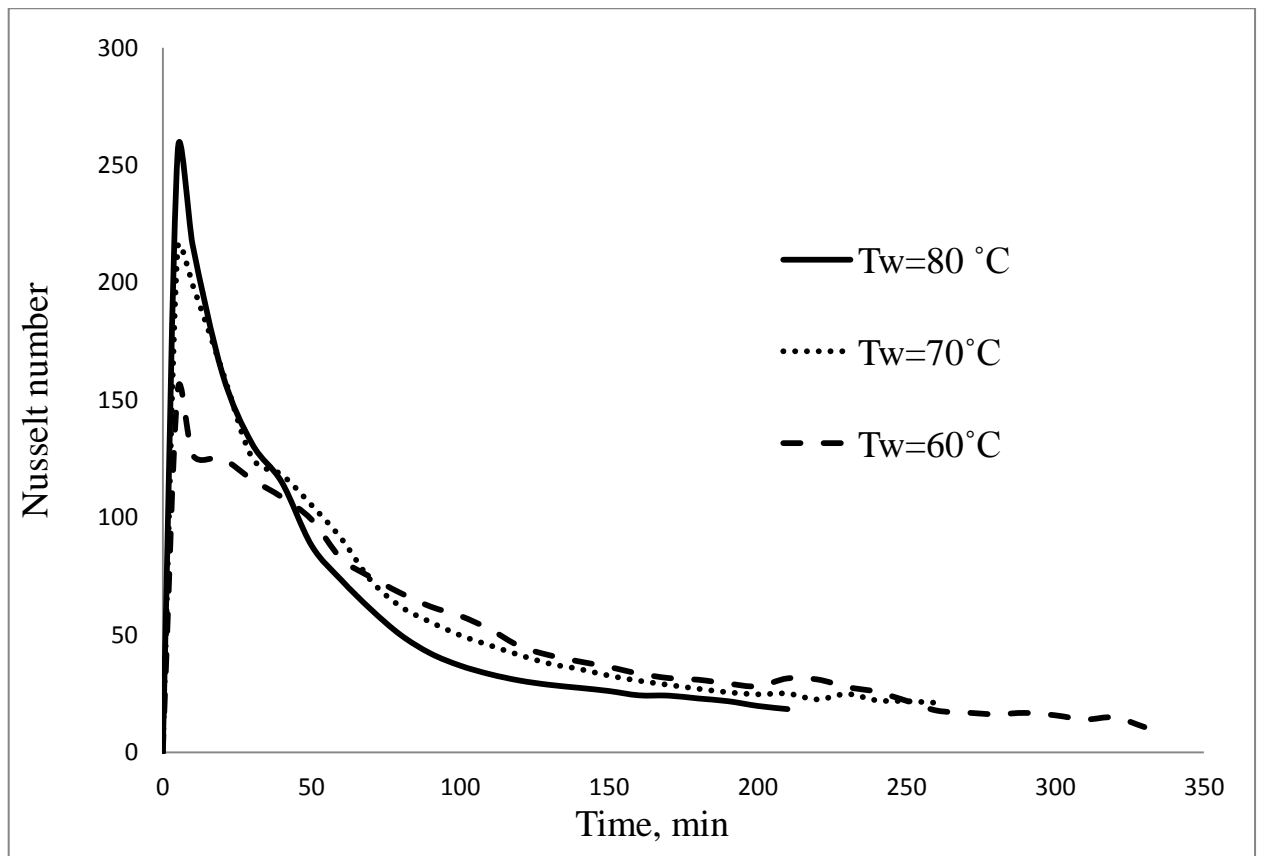


Fig. (5.5). Temporal variations of the Nusselt number.

#### 5.1.1.4 Stored energy by PCM

The time-variations of thermal energy stored inside PCM for different temperatures of water are exhibited in Fig. (5.6). The energy is stored sensibly for both phases of PCM (solid, liquid) and latently during the phase-change process. In the beginning, the transmitted energy from the hot water is absorbed sensibly by solid PCM. As the PCM starts to melt, a large part of the transmitted energy is consumed for solid-to-liquid phase change conversion. Also, the liquid melt of PCM starts to absorb energy sensibly. It is noticed that the accumulated thermal energy stored increases with time for all temperatures of HTF. When all solid PCM is melted, the increase of thermal energy storage is damped as all transmitted energy is absorbed sensibly by liquid PCM. Moreover, increasing the temperature of the water

causes higher transmitted energy and higher stored energy of PCM. The stored energy inside PCM can be retrieved when it is required as the solidification (discharging) mode is activated. The stored energy by PCM is increased by about 8.6 % and 16.8% when the HTF temperature varies from 60 to 70 °C and from 60 to 80 °C, respectively.

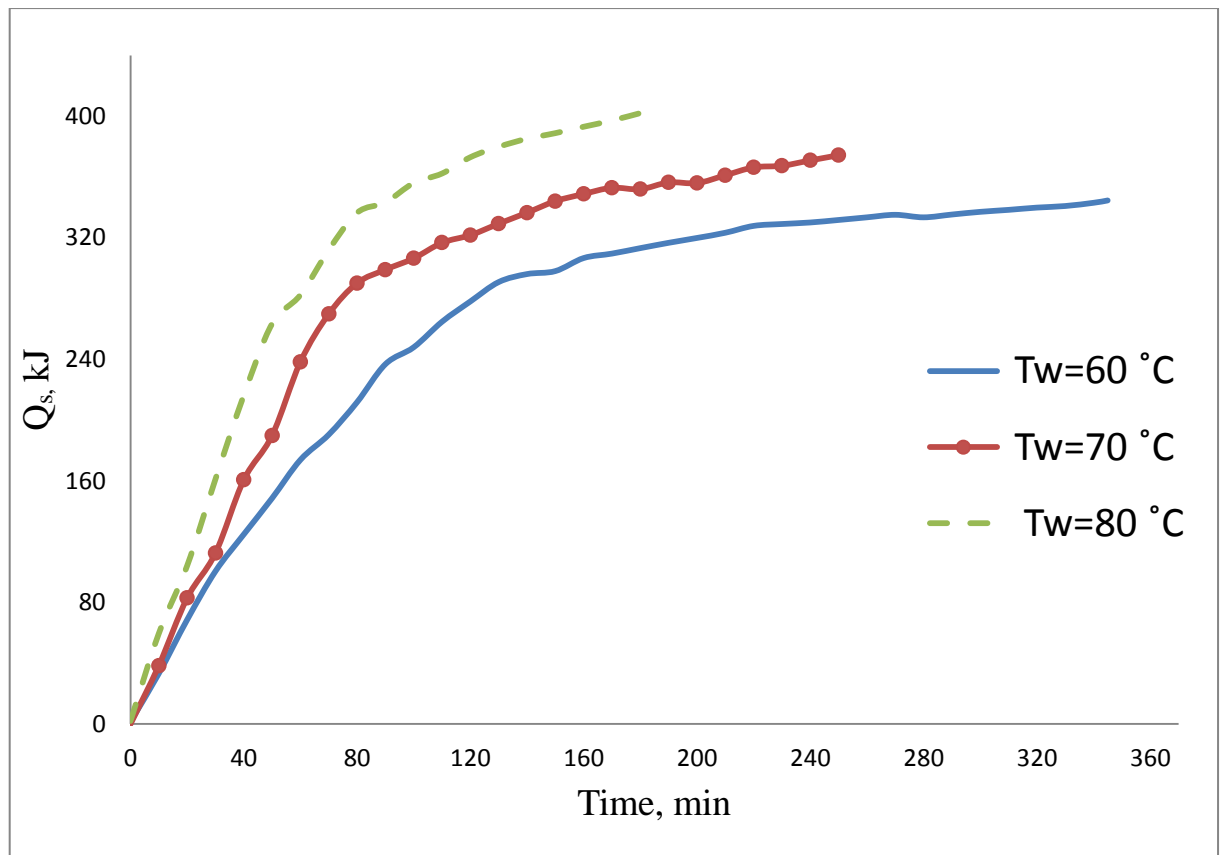


Fig. (5.6). Thermal energy stored vs. time for different temperatures of water.

### 5.1.2 PCM melting inside the vertical heat exchanger

This section is concerned with the experimental results of the PCM melting within a vertical annular cavity.

#### 5.1.2.1 Temperatures distribution of PCM.

The temperature distribution of PCM placed in a space between a hot inner pipe and an outer isolated pipe at 70 °C of inlet water temperature is shown in Fig. (5.7). Twelve thermocouples were mounted at five levels arranged from top to bottom with different distances from the inner pipe surface (See Fig. (4.6 for more details). At the initial period of the melting process, the conduction is dominated, so the variations of thermocouples readings are approximately equal except ( $T_1$  and  $T_4$ ) which are closer to the tube. The temperature  $T_1$  reaches the melting point of 42 °C earlier than the rest locations since it is closer to the tube and at a top position in the storage cell. The currents of natural convection carry the thermal energy to the upper part of the cell. In contrast, the thermocouple TC12 registers the minimum temperatures due to its location which is far away from the HTF tube and the effect of natural convection. The positions of  $T_2$ ,  $T_5$ ,  $T_7$ ,  $T_9$  and  $T_{11}$  have the same radial distance from the hot pipe but with different axial positions. It is noticed that  $T_2$  reaches melting point and steady-state faster than the others due to natural convection effect. Furthermore,  $T_4$  reaches melting point faster than  $T_3$  even though  $T_4$  is located at a lower position, but it is near to the hot pipe. Also, at the latent heat region bounded between  $T_{solidus}$  and  $T_{liquidus}$ , the slight change in temperature is observed. After that, a significant change of temperature occurs as a result of sensible heat.

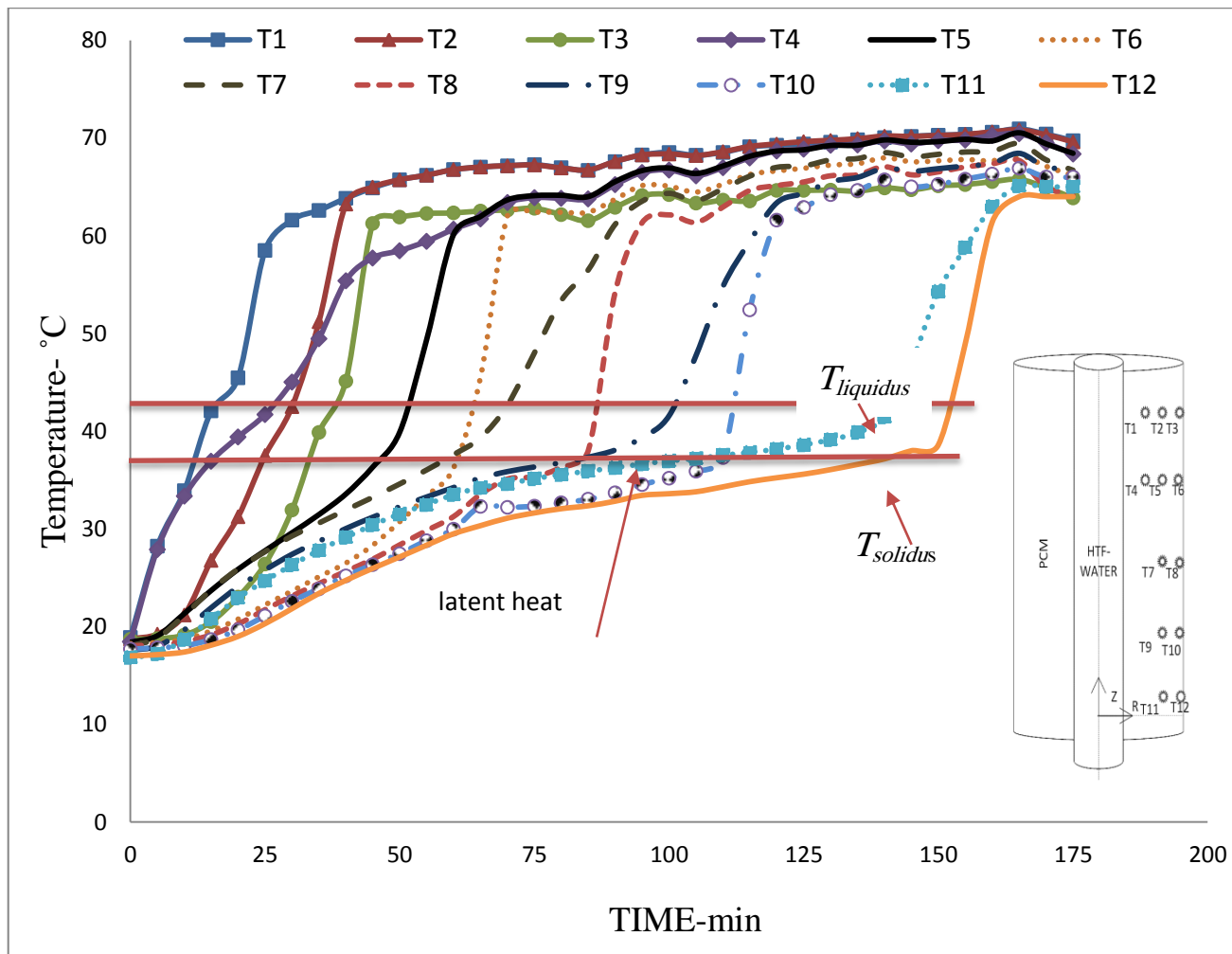


Fig. (5.7) Temperature distribution of PCM at 70 °C of water inlet temperature.

The effect of inlet temperature of the water on the temperature distribution of the PCM is explained in Fig. (5.8). The readings of thermocouples TC2 and TC11 are selected due to the same radial positions that they have but different axial positions. As the temperature of the inlet water increases, the amount of heat transferred to the PCM is increased, and the initiation of natural convection is started early. Therefore, it is clear that  $T_2$  reaches the melting point earlier compared to  $T_{11}$  for different inlet temperatures of the water as a result of the influence of natural convection.

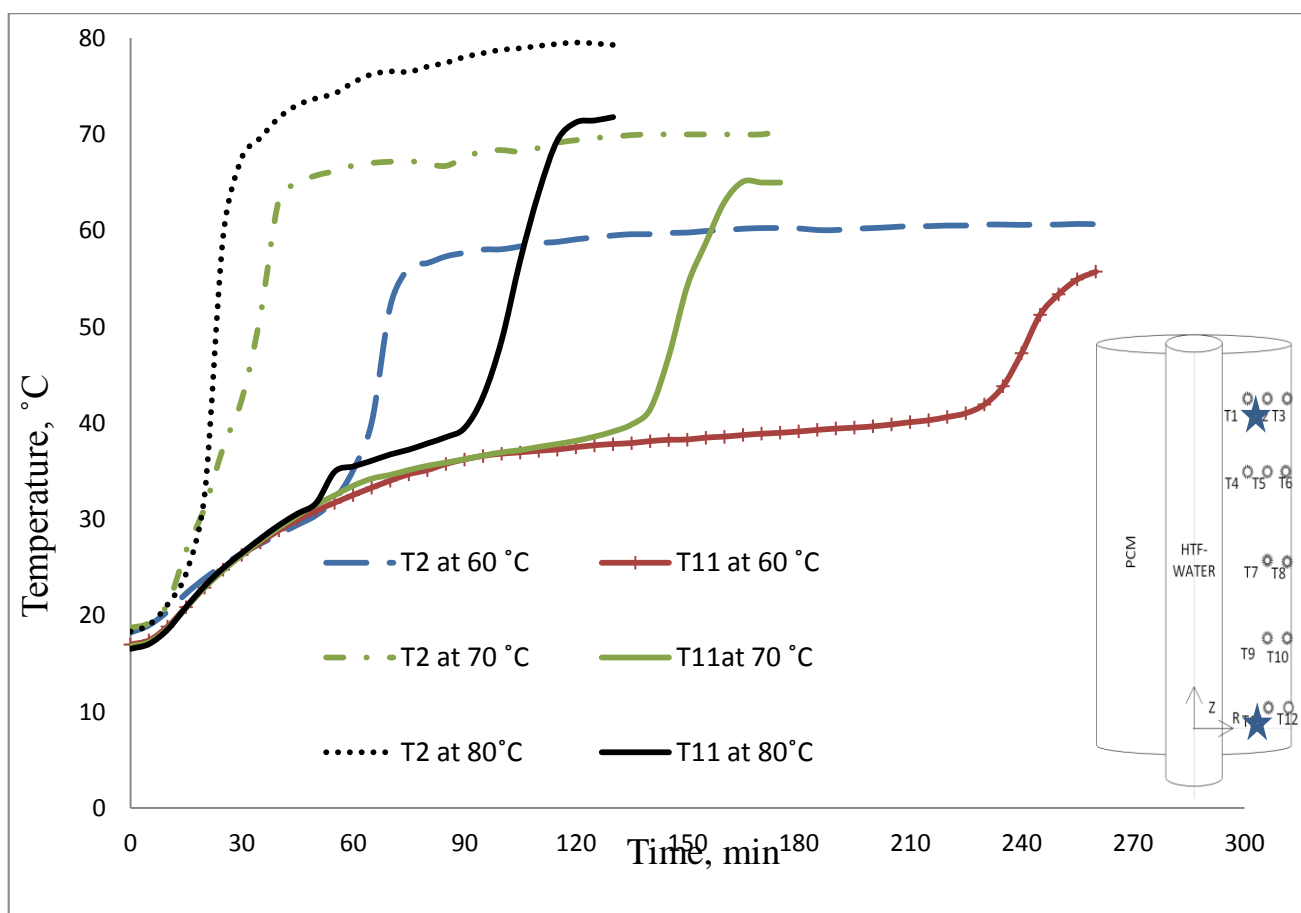


Fig. (5.8). Influence of temperature of HTF on the temperature distribution of PCM.

### 5.1.2.2 Transient Melting Front and Melt Fraction

Photographical expressions of the transient advance of PCM melting front for various water temperatures are presented in Fig. (5.9). At the first stage, the mechanism of heat transfer from the hot inner pipe to the solid PCM close to the pipe is done by conduction. A layer of liquid PCM is formed symmetrically around the inner pipe. A short time is consumed in this stage due to a quick heat absorption and a high-temperature difference between the initial temperature of solid PCM and the hot pipe surface. Later, the liquid PCM is accumulated at the top of the annular cavity due to the natural convection domination. After absorbing heat, the liquid PCM becomes lighter and moves upward while the solid-liquid melting front

moves toward the solid PCM at the bottom. This behavior is similar for all temperatures set for inlet water. In addition, the melt liquid fraction of PCM is illustrated in Fig. (5.10). It is clear that the melting rate is affected by the inlet temperature positively where heat transfer amount increases from the hot pipe to the PCM with the increase in inlet temperature. On the other hand, the melting time is reduced by about 32.6% and 50.2% when HTF temperature is changed from 60 to 70 and 80 °C, respectively. The solid-liquid interface is slightly inclined due to the uncertainty in the verticality of the heat exchanger.

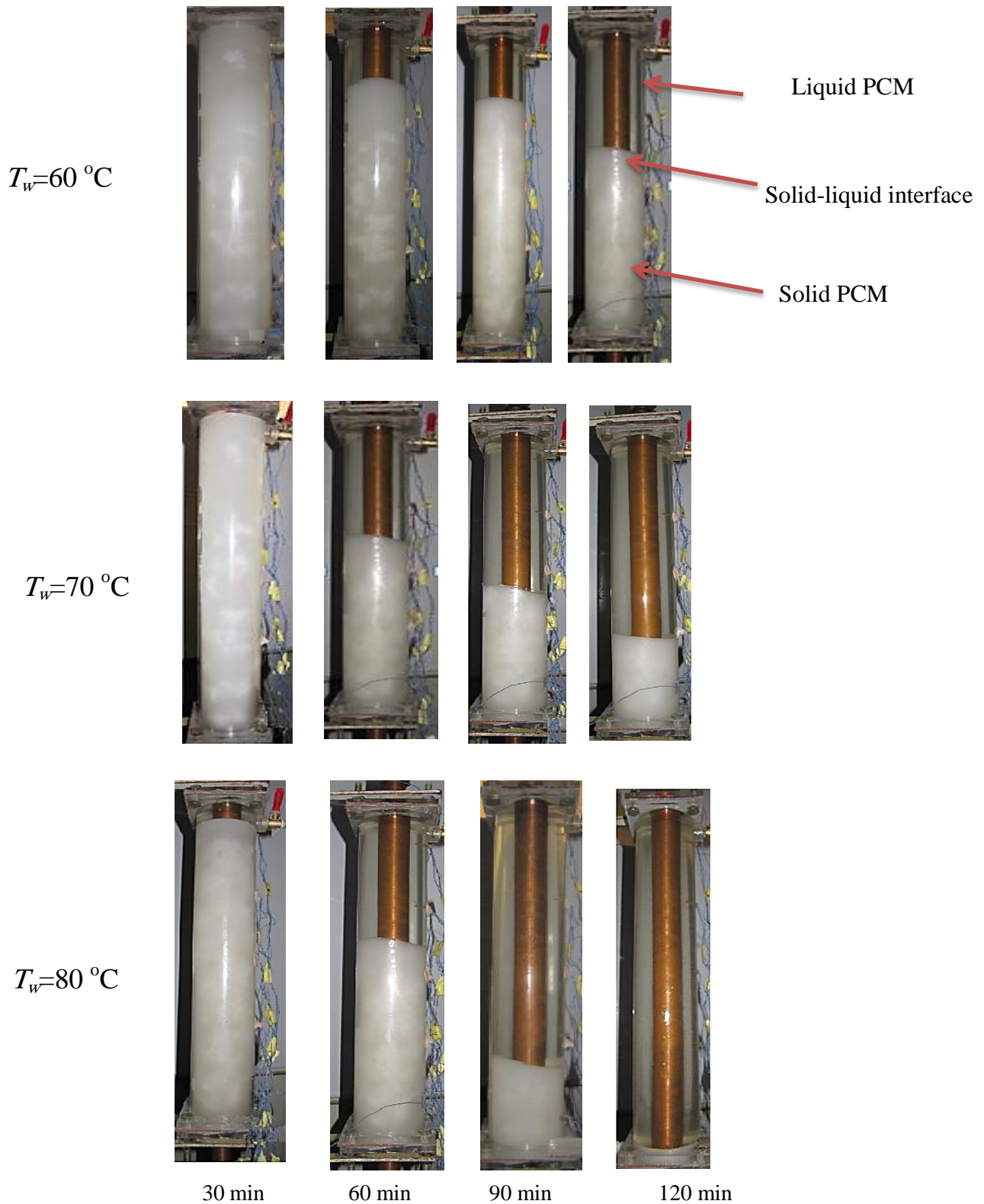


Fig. (5.9) Transient melting front progress of PCM in the vertical heat exchanger for various temperatures of water.

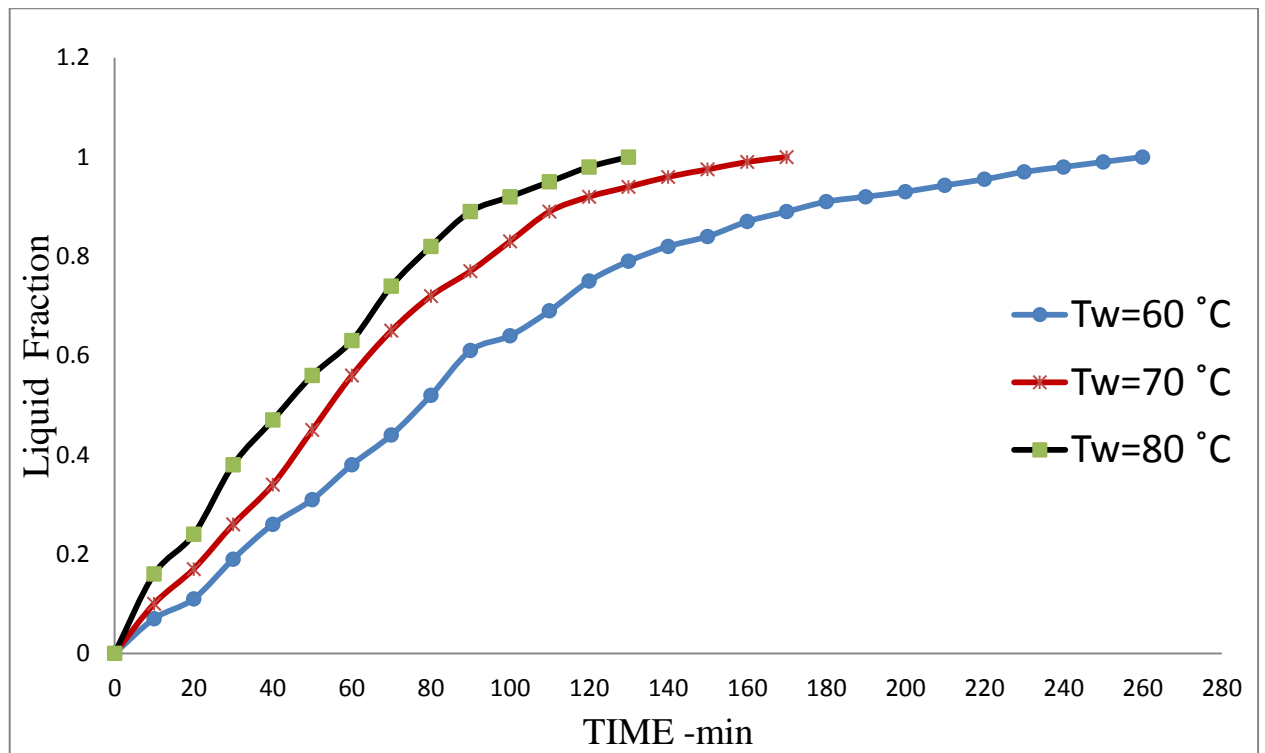


Fig. (5.10) Liquid fraction vs. time of PCM in the vertical heat exchanger for different HTF temperature.

### 5.1.2.3 The Time-Behavior of the Nusselt number

The time-wise changing of the Nusselt number for various temperatures of the HTF is illustrated in Fig. (5.1). The Nusselt number is high at the beginning of the melting process as a result of heat conduction domination, and higher temperature gradient is indicated. Later, the Nusselt number abruptly drops due to natural convection domination and temperature gradient decreases. On the other hand, the value of Nusselt number is higher and faster to drop at 80 °C inlet temperature in comparison with other inlet temperatures of 60 and 70 °C. This behavior is due to a higher temperature gradient between the 80 °C and initial temperature of PCM.



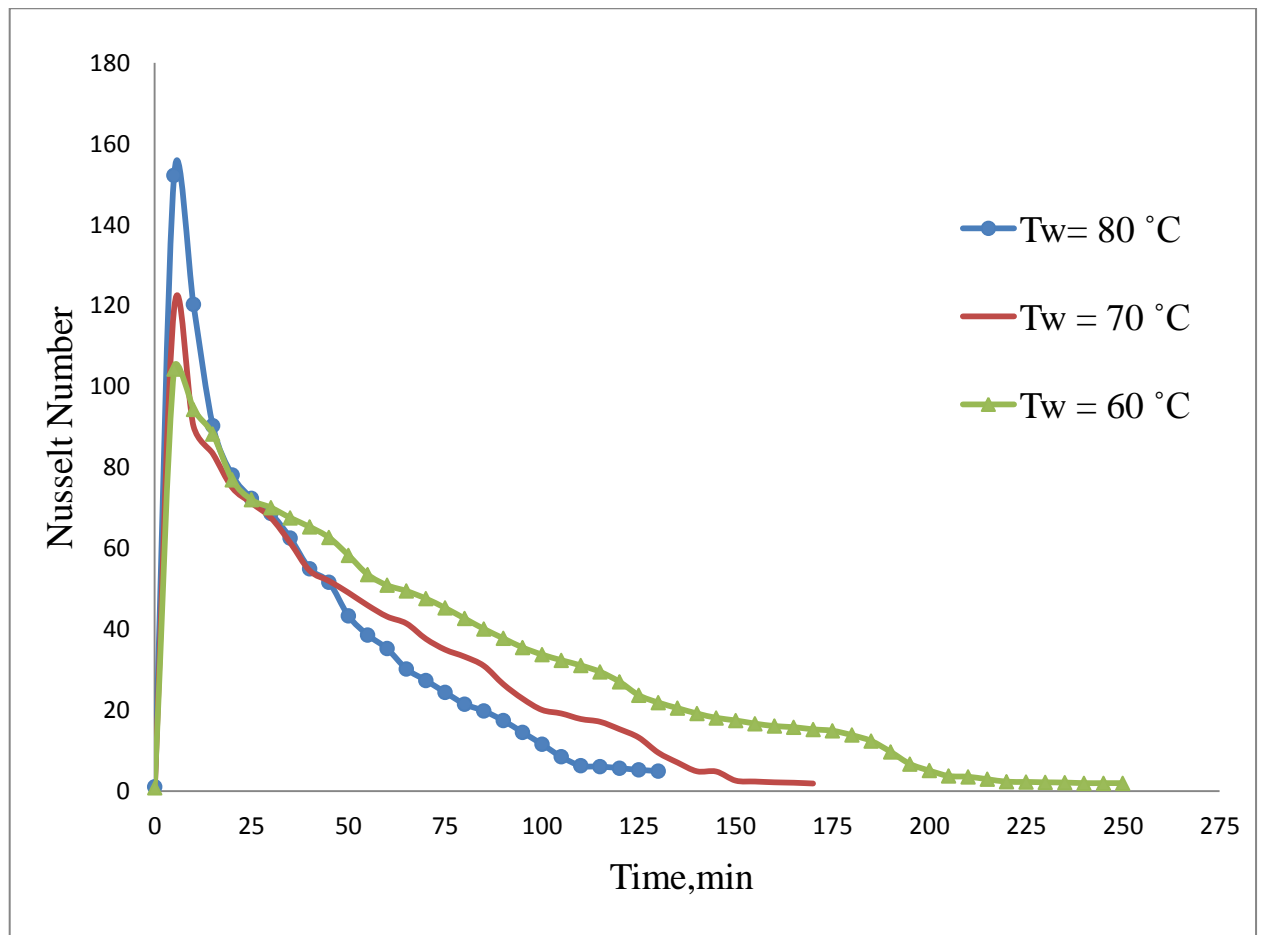


Fig (5.11) Time-variation of the Nusselt number

#### 5.1.2.4 Stored Energy

The energy stored by PCM equals the summation of sensible heat in the solid and liquid phases as well as the latent heat during the phase-change process. The stored energy changes proportionally with the inlet temperature of the water as revealed in Fig. (5.12). As time advances, the sensible energy absorbed by solid PCM decreased while the sensible energy in the liquid phase and latent energy absorbed latently during the phase-change are increased depending on the amount of the liquid fraction. It is observed that the stored energy by PCM is increased by about 8.6% and 16.8% when the HTF temperature is varied from 60 to 70 °C and from 60 to 80 °C, respectively. It is the same percentage obtained in the horizontal direction.

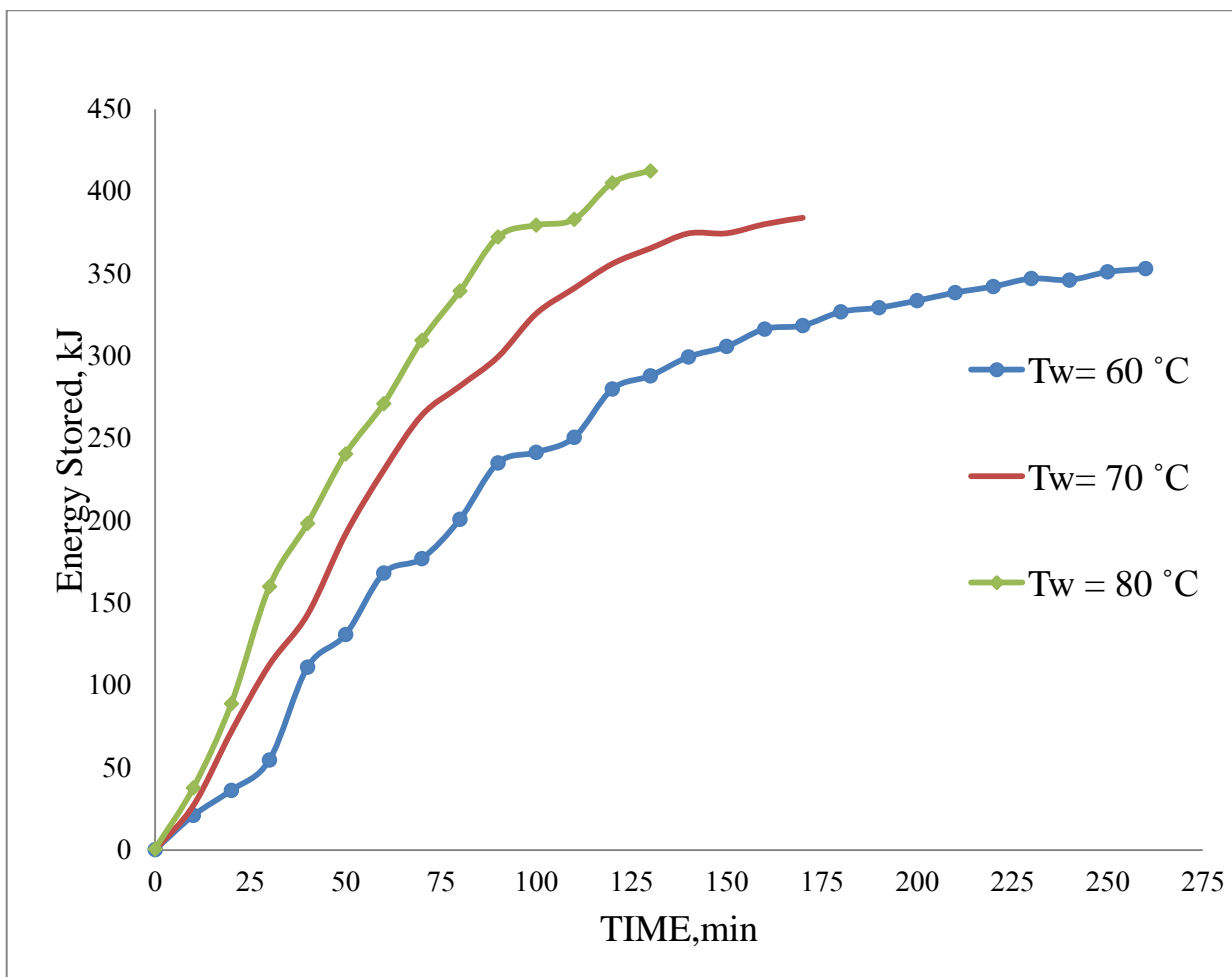


Fig. (5.12) Energy stored by PCM for different temperatures of water.

## 5.2 NUMERICAL RESULTS

Numerical simulation of the melting process of PCM contained in an annular cavity between shell and tube heat exchanger is performed using ANSYS/FLUENT 17.2 software. To achieve the most accurate numerical results, a grid-independent test is performed for all the number of elements. In addition, the time step in each iteration was also examined to compromise between the accuracy of the results and the cost and time of the computations. The effect of the mushy zone constant is also tested. Moreover, the validation of the numerical model was performed as described previously in Chapter 3.

### 5.2.1 Predicted melting front and temperature contours of PCM

The predicted results of the melting front (left) and temperature contours (right) for PCM inside horizontal annular cavity heat exchanger is presented in Fig. (5.13) for the three different inlet water temperatures. The melting begins when the PCM temperature reaches the melting point. The molten PCM formed around the hot tub due to the predominated conduction heat transfer. Then, the buoyancy-driven convection have been developed, and PCM liquid ascends upward leading to a higher melting rate at the upper part of the cavity. Moreover, the melting rate at the bottom portion of the cavity consumes a longer time in comparison with the upper part. The same behavior is shown for vertical-cavity heat exchanger as presented in Fig. (5.14).

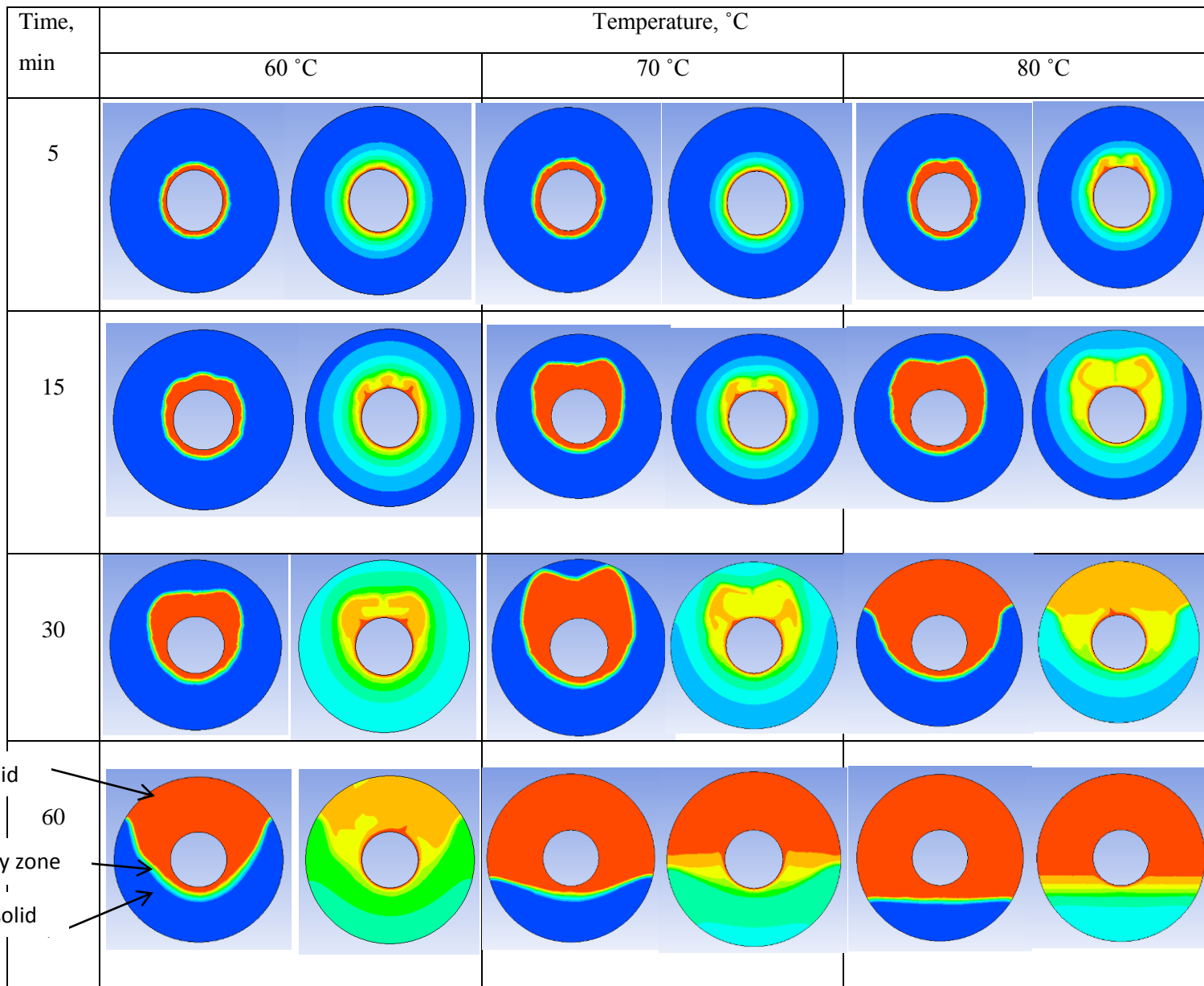
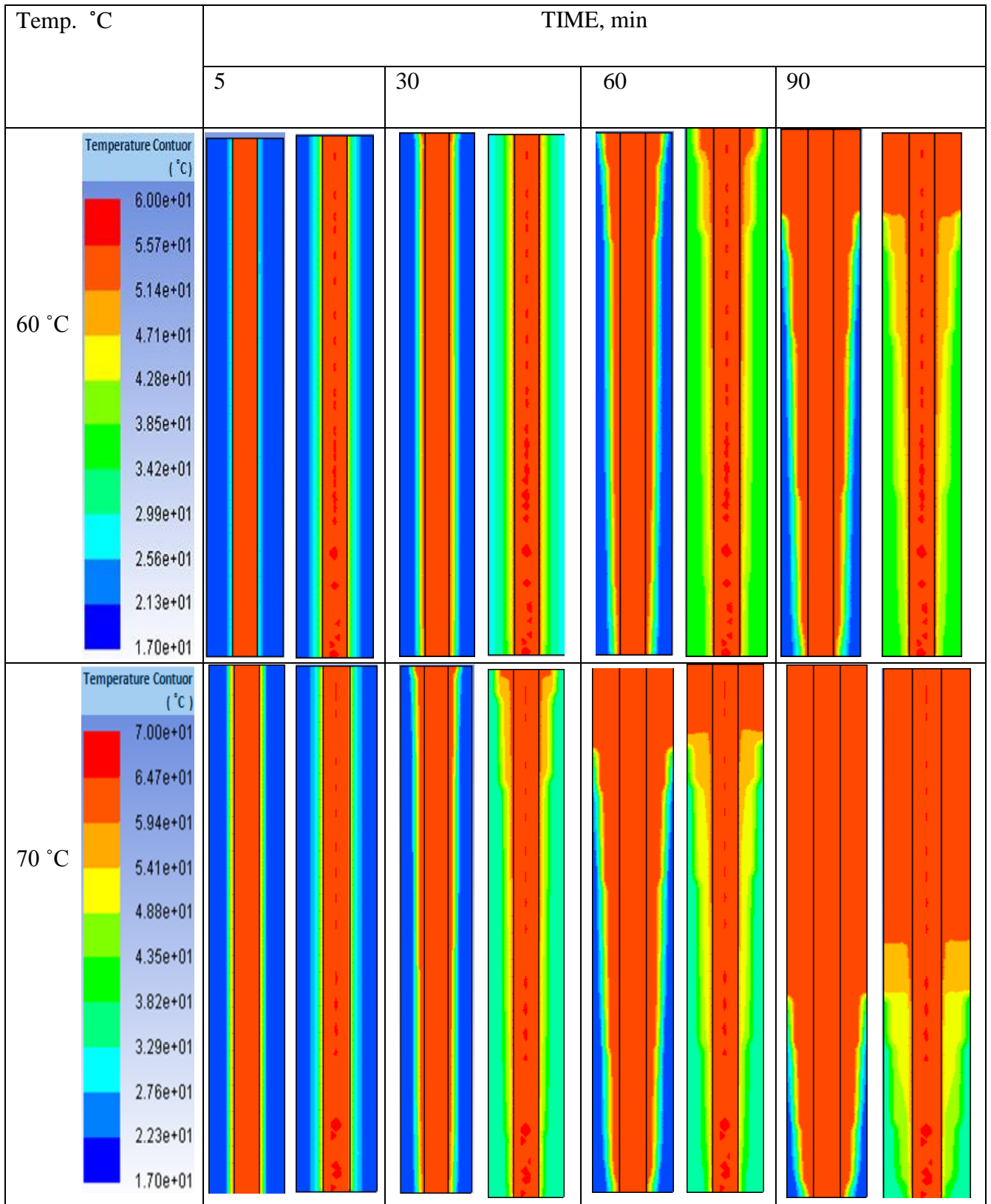


Fig. (5.13). Temporal development of the melting front and temperature



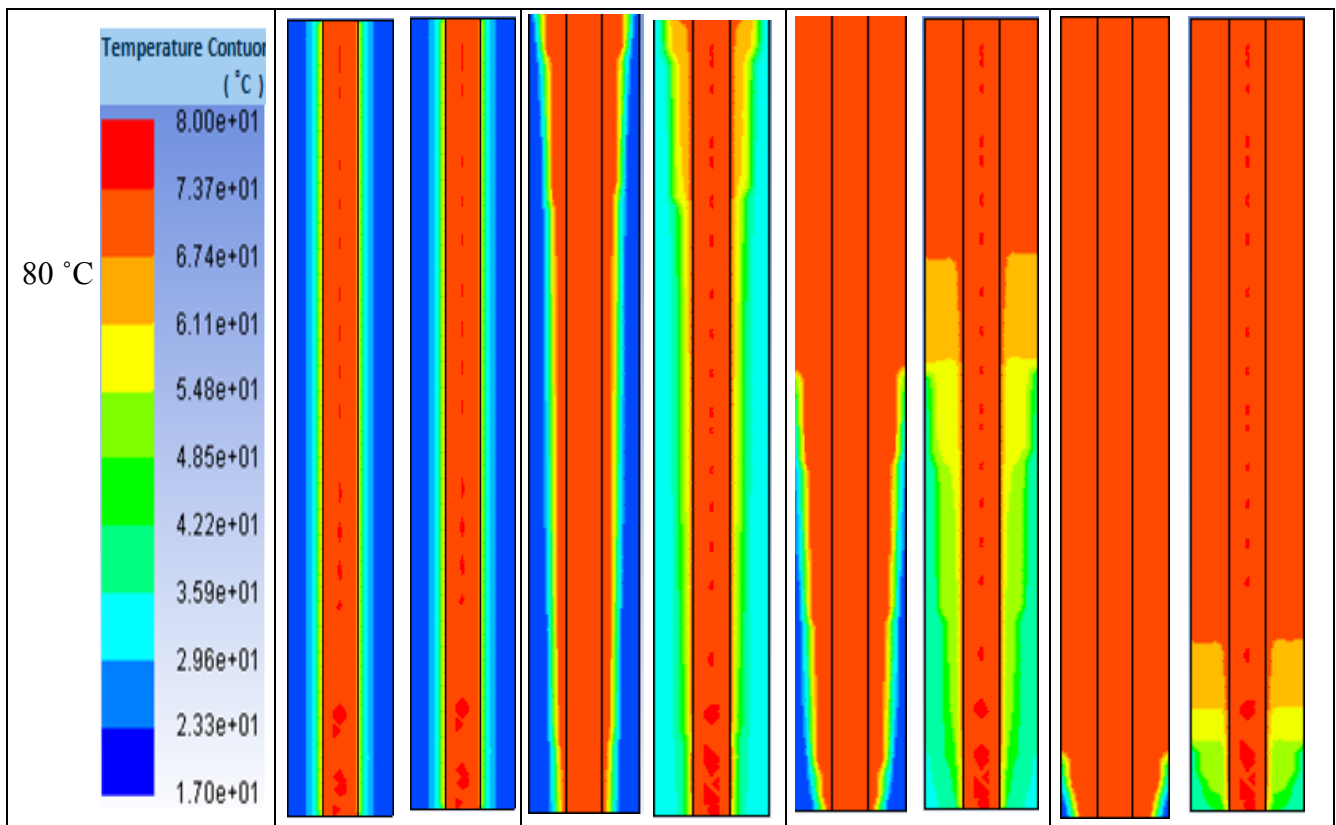


Fig. (5.14) Temporal development of the melting front and thermal with different water temperatures

### 5.2.2 Numerical results of the liquid fraction

The numerical results of the liquid fraction for both orientations of the heat exchangers and various inlet water temperatures are exhibited in Fig. (5.15). Initially, it is observed that the melting rate is high due to a large temperature gradient and conduction-dominated melting process. After that, as the temperature gradient decreased and thermal resistance increased, the effect of conduction and resulted melting rate are decreased. However, the influence of natural convection is grown especially in the upper part of the heat exchanger for both orientations. The effect of natural convection-assisted melting is higher in vertical heat exchanger than that existed in a horizontal one. Hence, the melting time of PCM is lower in the vertical orientation of heat exchanger as shown in Fig. (5.15 ). The melting periods of vertical heat exchanger are reduced by 28.7%, 30.4% and 31.2% than that time needed for complete melting in a horizontal heat exchanger for inlet

water temperatures of 60, 70 and 80 °C, respectively. Besides that, it is noticed that the melting rate is directly affected by the water inlet temperatures. Thus, PCM melting time was reduced by about 29.7% and 47% in a horizontal orientation and about 31.7% and 48.5% in a vertical orientation when the inlet temperature is changed from 60 to 70 °C, and from 60 to 80 °C, respectively.

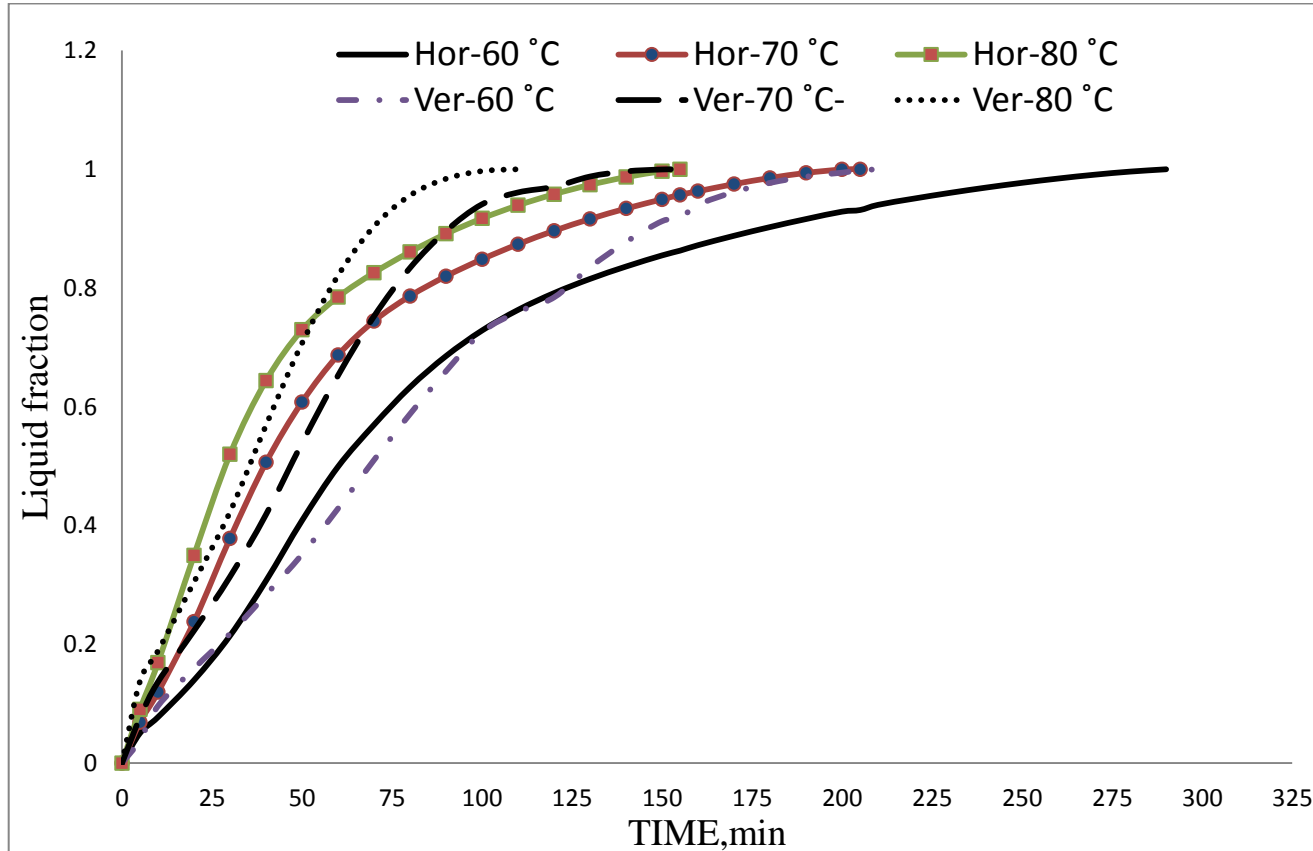


Fig. (5.15) liquid fraction vs. time for two orientations of the heat exchanger at different water temperatures.

### 5.2.3 The velocity vector of the PCM melt

The velocity vector of the melted PCM at 70 °C inlet water temperature within the horizontal and vertical annular cavities are shown in Fig. (5.16) and Fig. (5.17), respectively. At the initial times, there is no generation and movement of PCM liquid. Later, a simple movement around the inner tube is generated at the start of the melting process causing a layer of liquid PCM under the conduction control. After a while, the velocity vector of liquid PCM increases and the hot low-density liquid moves towards the top part of the cell due to buoyancy effect. The liquid velocity is slow in the lower part where the conduction is dominated. Also, it is observed that the velocities of liquid PCM are higher in the vertical heat exchanger than those shown in a horizontal one.

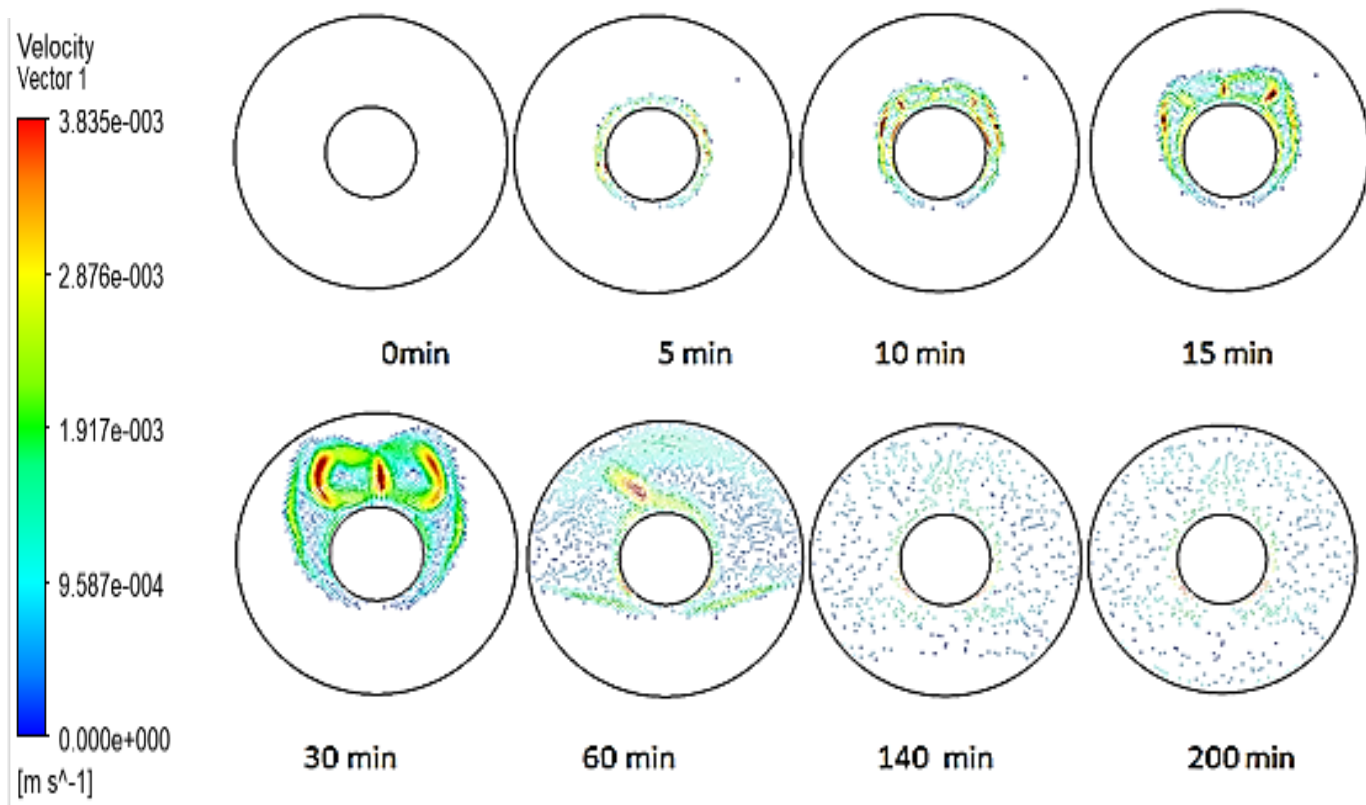


Fig. (5.16) Velocity vector of the liquid PCM for a horizontal heat exchanger at 70 °C of inlet water temperature.



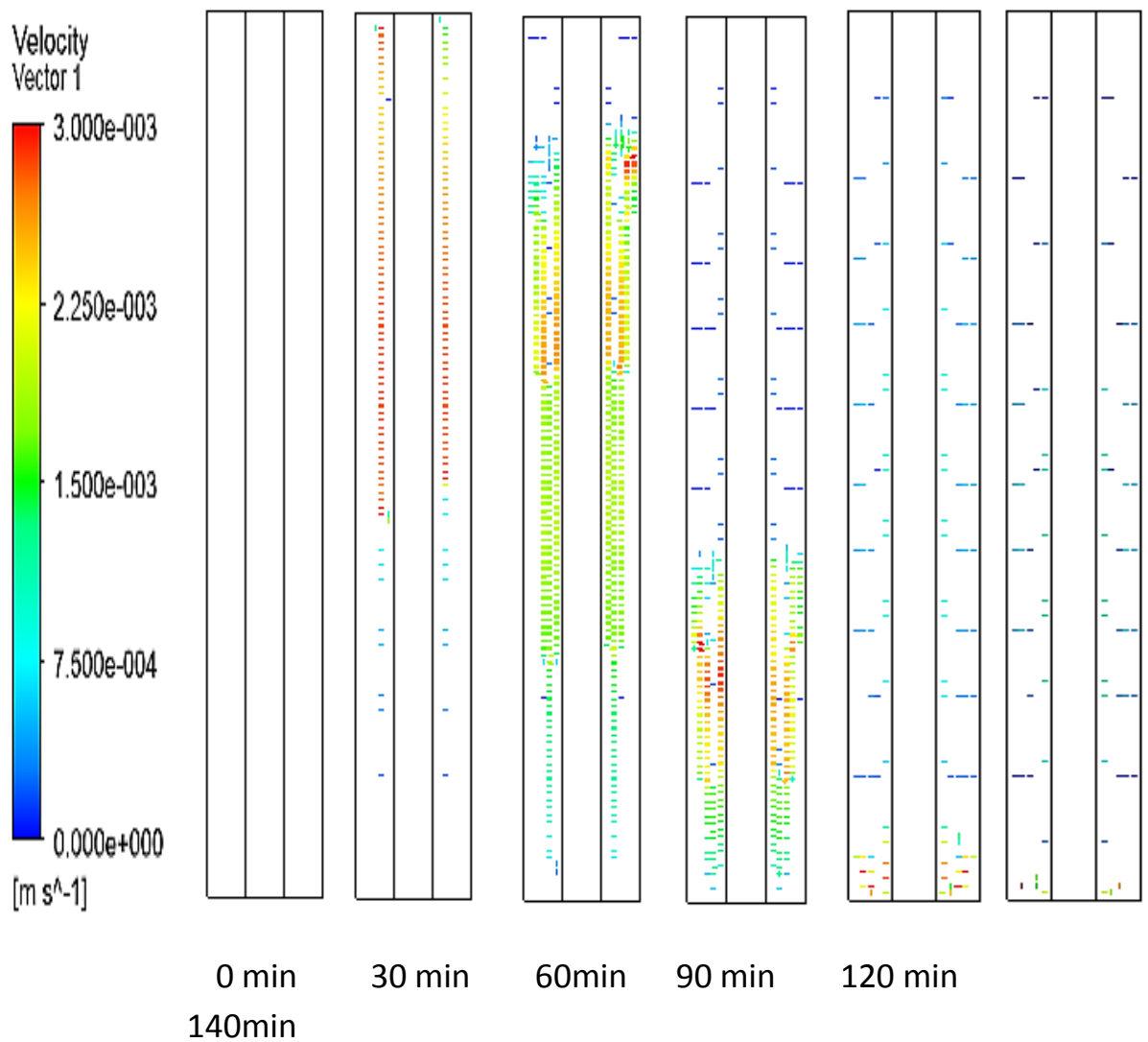


Fig. (5.17) Velocity vector of the liquid PCM for a vertical heat exchanger at 70 °C of inlet water temperature.

The influence of water temperature on the melt velocity is presented in Fig. (5.18). It is noticed that the velocity of liquid PCM increases by increasing the temperature of the inlet water. Increasing the water temperature leads to an increase in the transferred thermal energy into the PCM and excitation of rapid initiation of natural convection.

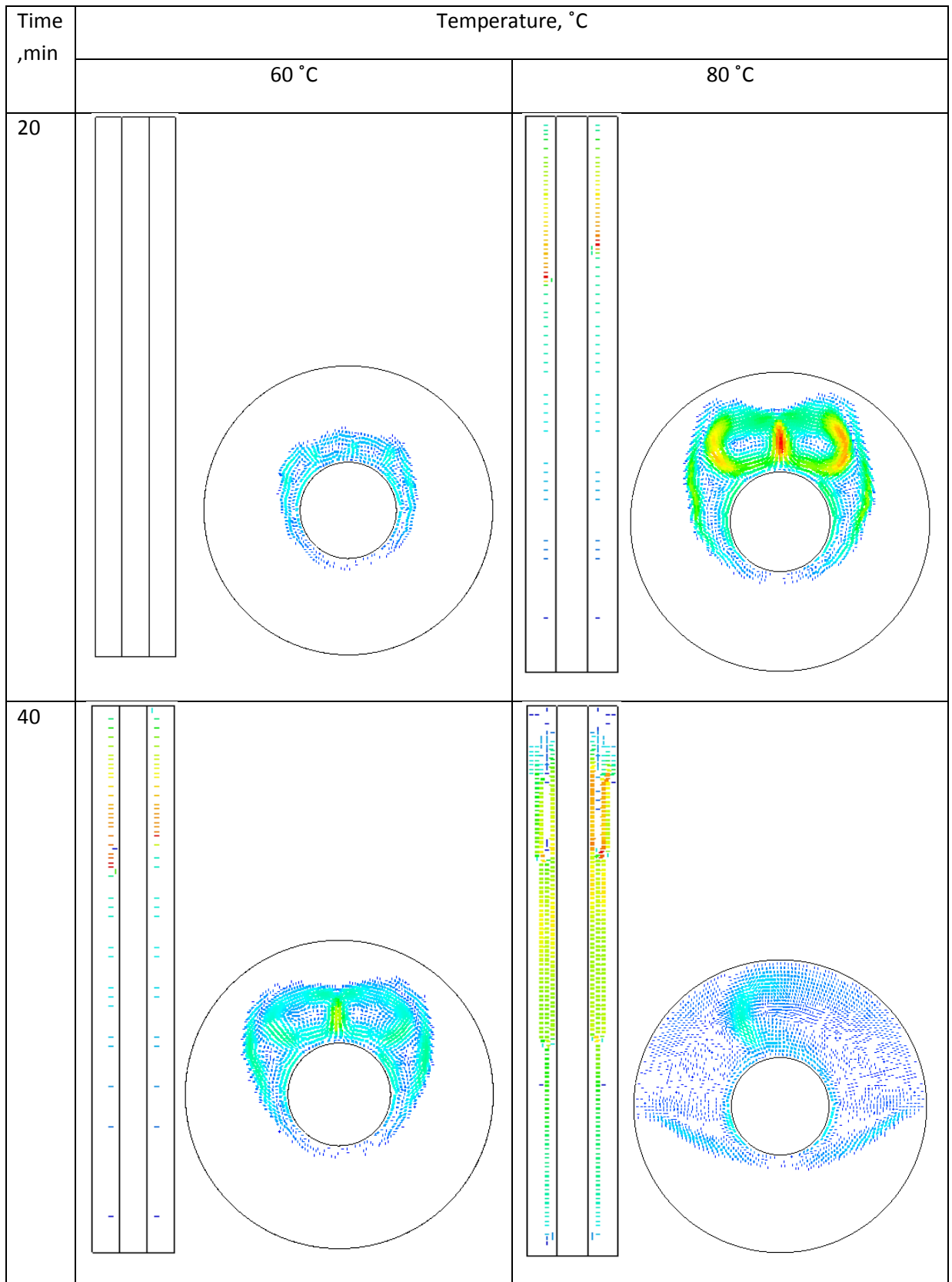


Fig. (5.18). The effect of HTF temperature on the velocity vector of liquid PCM in the horizontal and vertical heat exchanger.

#### **5.2.4 Numerical results of the Nusselt number**

The predicted values of the Nusselt number for two orientations of the heat exchanger and different inlet water temperatures are illustrated in Fig. (5.19). It is found that the transient Nusselt number has the same behavior for two orientations. There is a rapid increase in the Nusselt number at the beginning of the melting process due to the conduction-dominated between the solid (or thin layer liquid) PCM and the inner tube. Therefore, the low thermal resistance and associated high-temperature gradient cause a dramatic growth in the Nusselt number. Thereafter, the decrease of the Nusselt number is rapid for vertical heat exchanger while it has an exponential reduction for horizontal orientation of heat exchanger. In this period, the conduction role decreases, but the convection effect is developed. Later, the convection is dominated, and the melting process reaches the steady-state condition. In all cases, the Nusselt number was changed positively with the amount of transferred thermal energy from HTF which in turns varies proportionally with an inlet temperature of HTF.

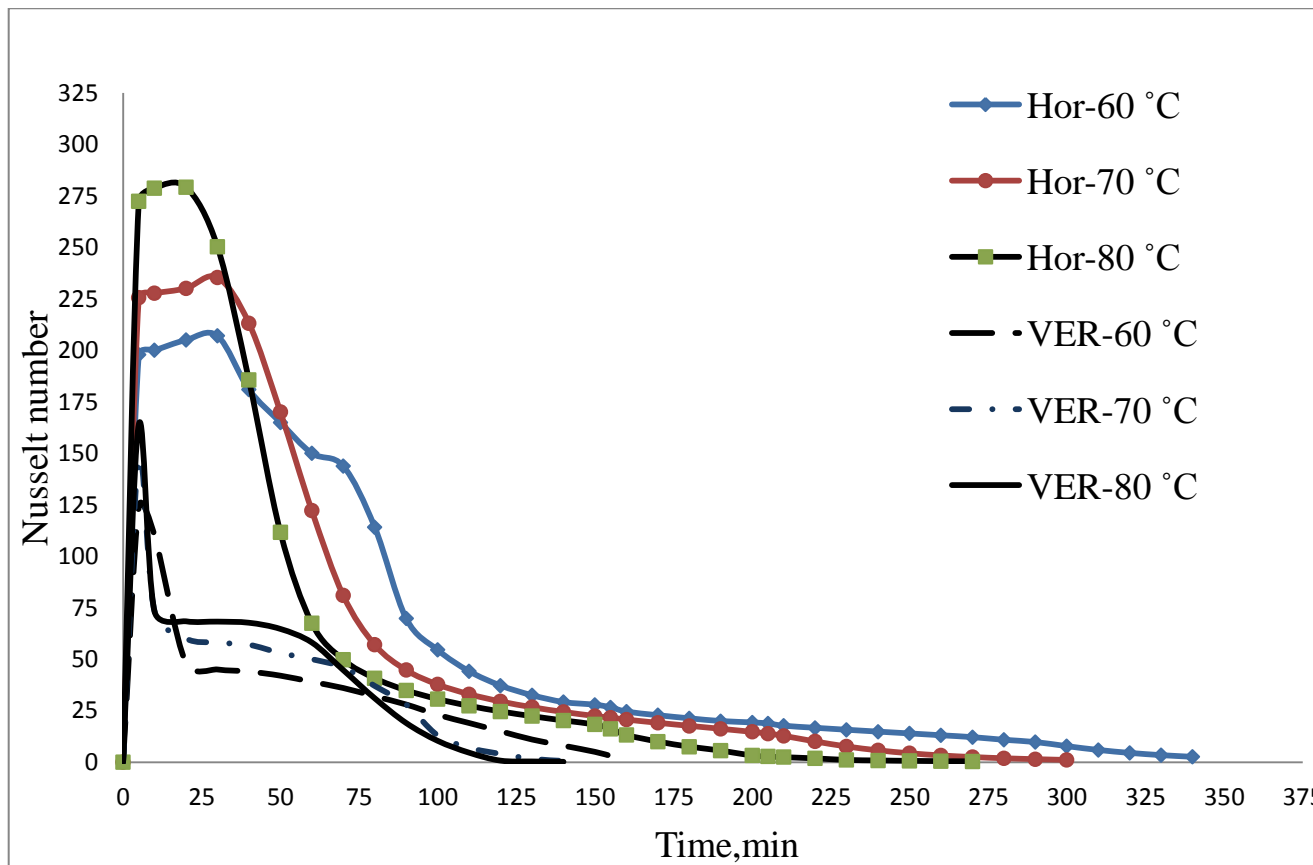


Fig (5.19). Nusselt number vs. time with different HTF temperatures for both heat exchangers.

### 5.2.5 Numerical energy stored by PCM.

The transient change of stored energy by PCM inside an annular cavity of both orientations for three different inlet water temperatures is presented in Fig. (5.20). The general trend of variation of stored energy is the same as exhibited in experimental findings. In addition, it is observed that the amount of stored energy by PCM in the vertical heat exchanger is higher than that obtained in the horizontal orientation. That happened due to the higher melt fraction in the vertical heat exchanger as discussed previously. For example, at time of 140 min, the accumulated stored energy in PCM in the vertical heat exchanger is; 375.8, 477.7 and 489.4 kJ for inlet water temperatures of (60, 70 and 80) °C, respectively. However, for the same time and inlet water temperatures, the stored energy are; 362.4, 410.8

and 460.5 kJ for horizontal heat exchanger. Furthermore, the stored energy reaches its steady-state value after completing melting as shown in the figure.

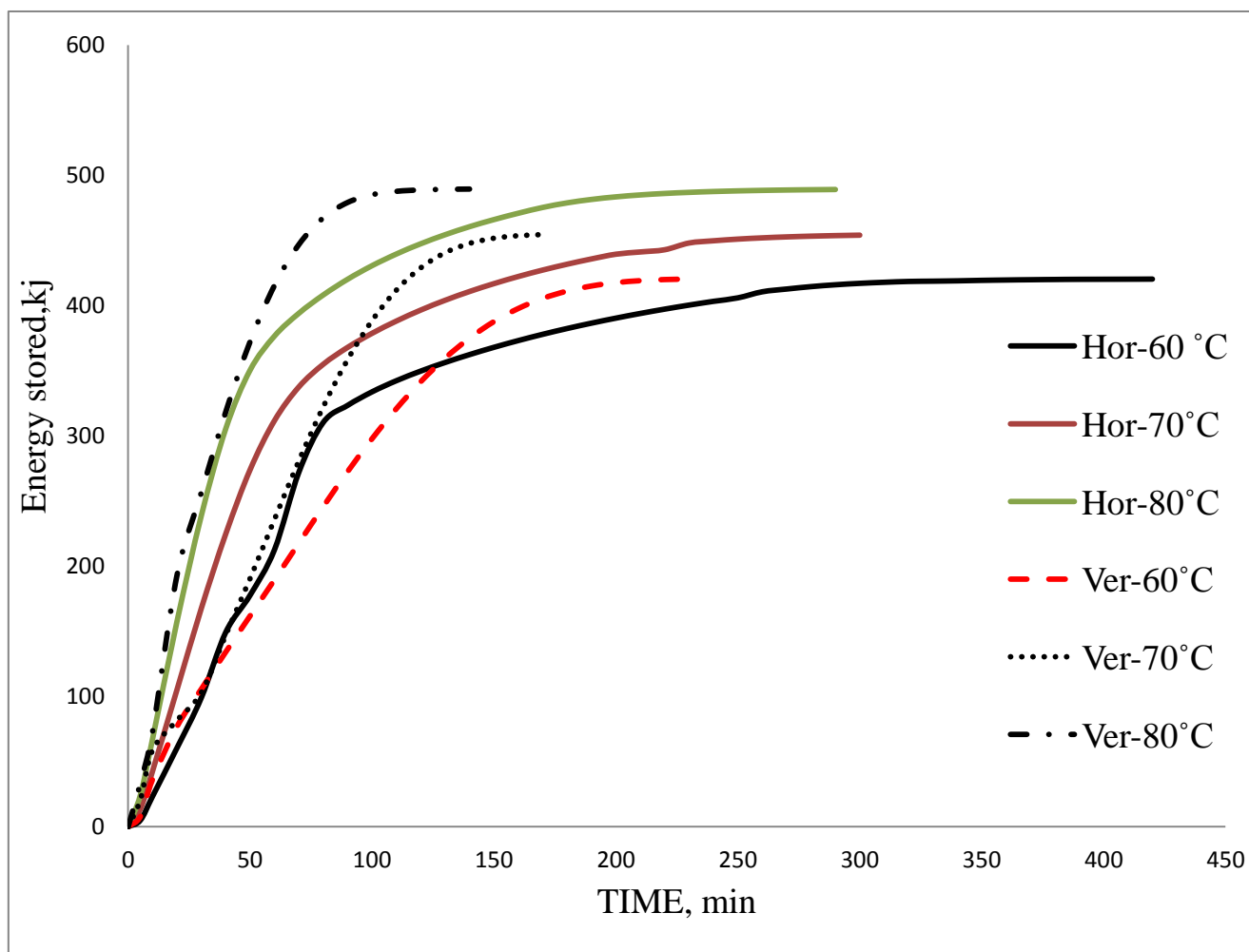


Fig. (5.20) Predicted energy stored by PCM for both orientations at different water temperatures.

### 5.3 Comparison between Experimental findings and Numerical results.

The melting characteristics such as temperature distribution of PCM, the progress of melting front, melt fraction, stored energy within PCM and the Nusselt number are evaluated experimentally and numerically for two orientations of the heat exchanger and different values of HTF temperatures. The comparison between experimental and numerical results is performed for an inlet water temperature of 70 °C. Good agreements are obtained between the experimental and numerical results. The results revealed that the numerical values of melting characteristics are higher than the experimental ones. This discrepancy between the results is justified by:

- 1- Heat losses in the experimental side.
- 2- Considering the mathematical assumption in the numerical investigation as stated in chapter 3.
- 3- Ignoring the variations of PCM thermophysical properties of PCM in the numerical model. Actually, the thermophysical properties are temperature-dependent.
- 4- The difference in the imposed boundary conditions between experimental and numerical investigation.
- 5- Uncertainty and error associated with the measurements of the devices.
- 6- The accuracy of the installation of rig test parts.

The experimental temperature readings of  $T_2$  in a horizontal heat exchanger and  $T_7$  in the vertical heat exchanger are compared with the similar corresponding numerical temperatures as described in Fig. (5.21). The maximum discrepancies between the numerical and experimental temperatures are approximately 17.4 % and 12.3% for  $T_2$  and  $T_7$ , respectively.

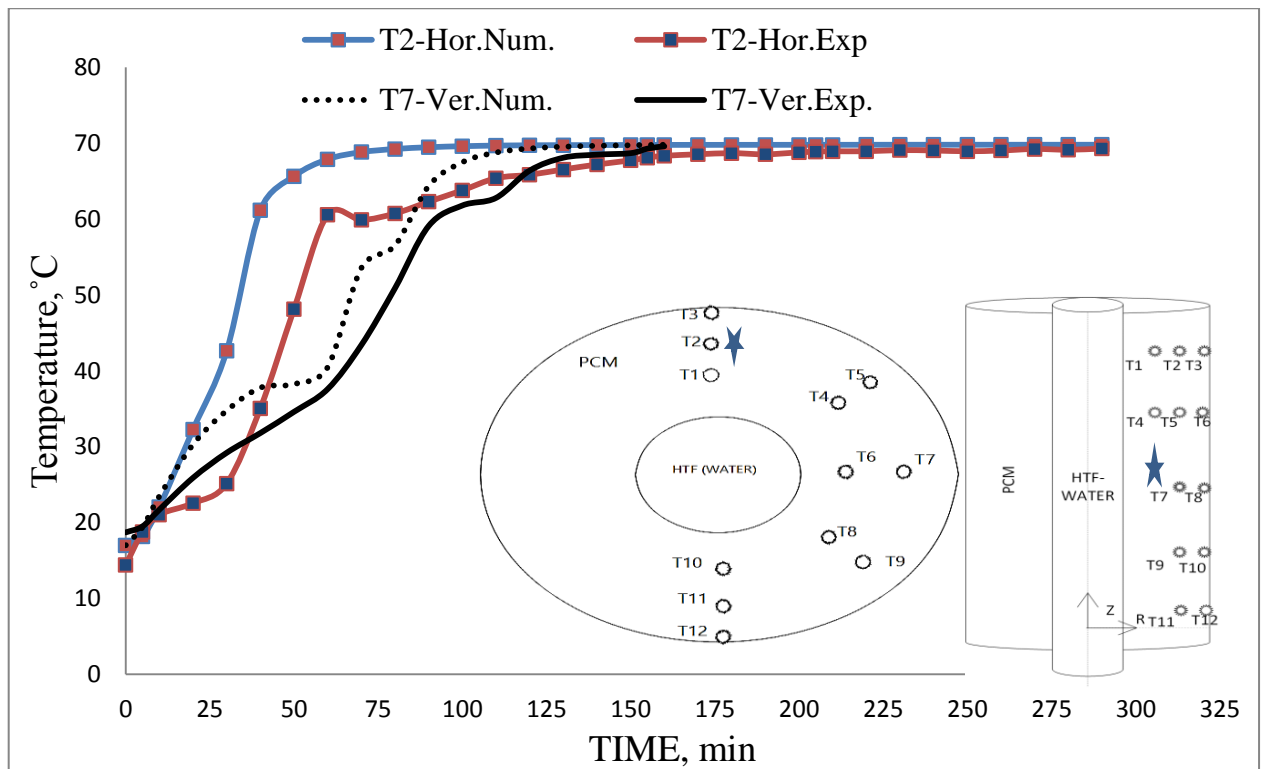


Fig. (5.21) Comparison between experimental and numerical temperatures for water inlet temperature of 70 °C.

The temporal evolution of the PCM melting front in the horizontal and vertical annular heat exchangers is depicted in Fig. (5-22). While, the experimental and numerical melt fraction is compared and presented for two orientations in Fig. (5.23). The maximum difference between experimental and numerical results of melting time is about 12.4% and 10.7% for the horizontal and vertical heat exchangers, respectively.

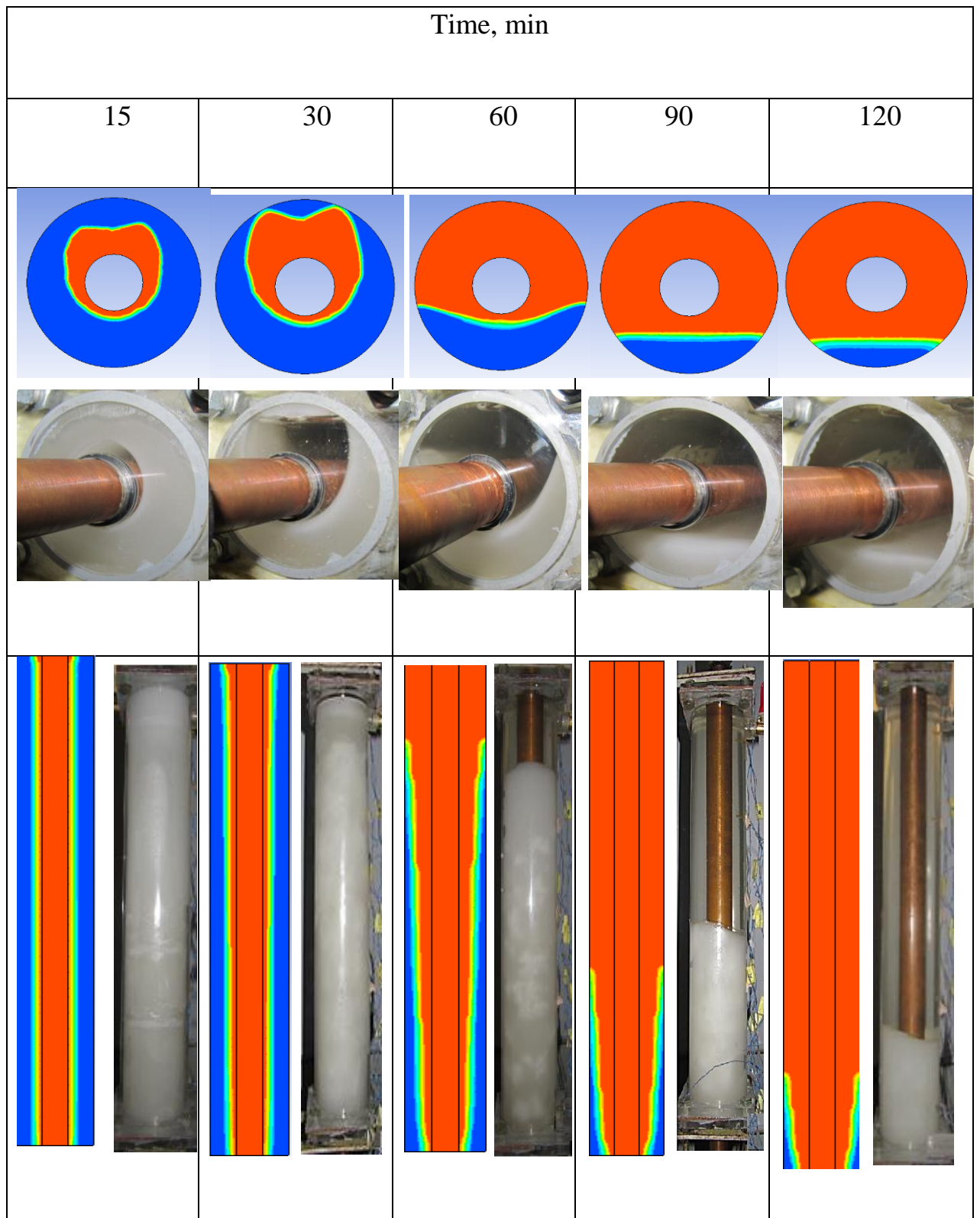


Fig. (5.22). Progress melting front in both study experimental and numerical.



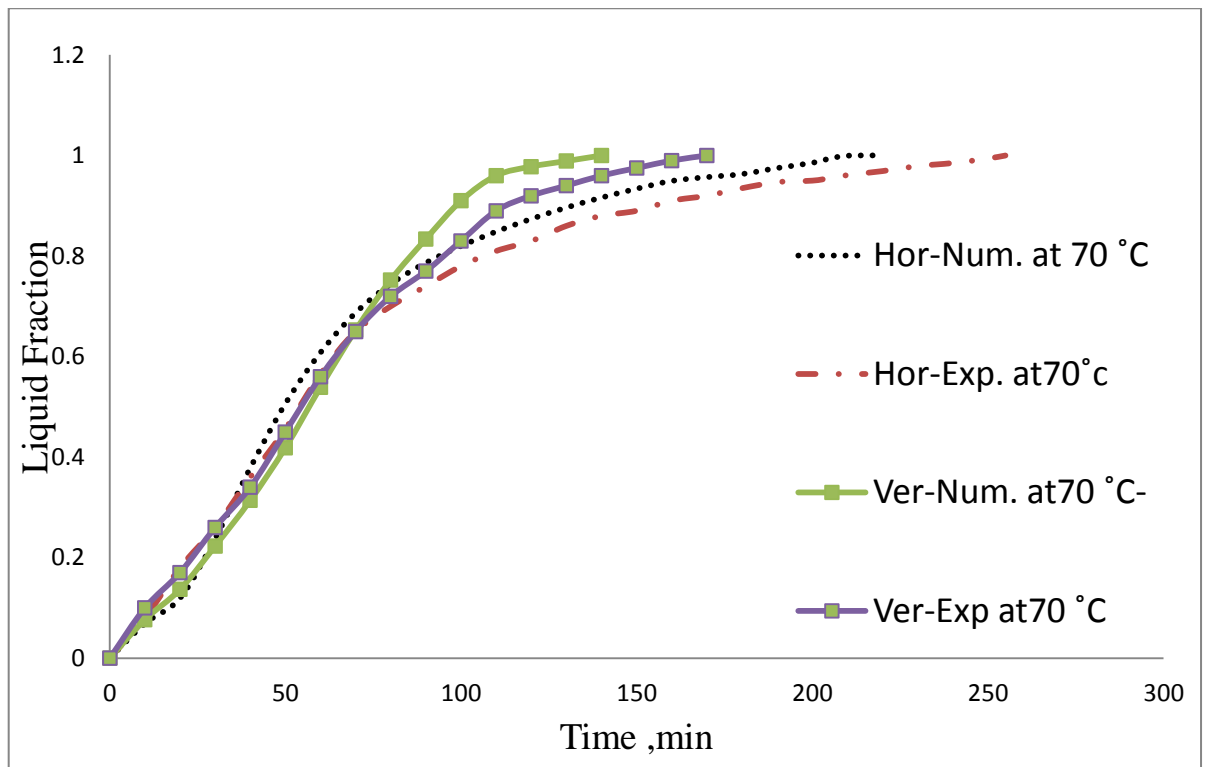


Fig. (5.23) Experimental and numerical liquid fractions for two orientations of the heat exchanger.

The experimental and numerical results of the transient variations of the Nusselt number for both orientations of the heat exchanger are illustrated in Fig. (5.24). In general, the results showed the same behavior but with a difference of 22.5% in a horizontal position while 14.96% in the vertical direction. Another reason causing differences between experimental and numerical results mentioned previously, the Nusselt number was calculated experimentally at a distance of 8 mm and 16 mm from the surface of the inner pipe in horizontal and vertical heat exchangers, respectively for practical necessity. While, the predicted Nusselt number is calculated at a distance very near to the hot wall.

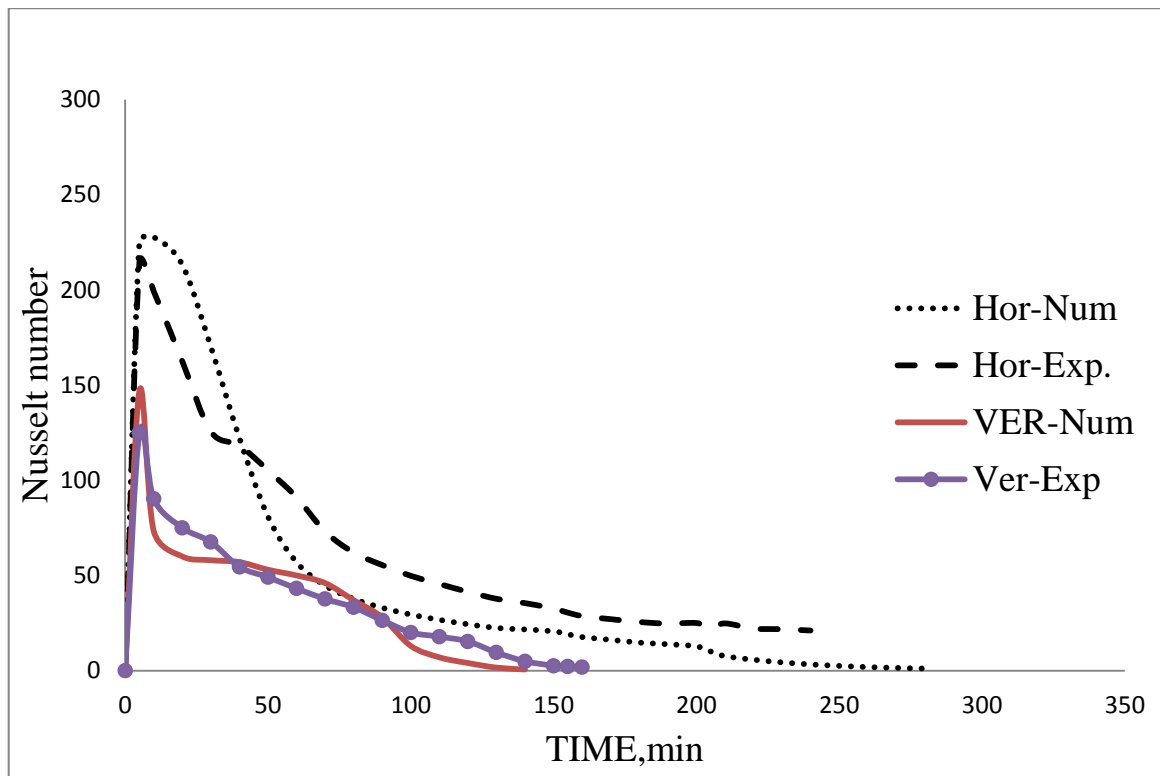


Fig. (5.24) Experimental and numerical Nusselt number for two orientations of the heat exchanger.

The experimental and numerical results of the stored energy are compared and presented in Fig. (5.25) for two layouts of heat exchangers. The maximum discrepancies between two results are 22.1% and 15.4% for horizontal and vertical heat exchanger, respectively.

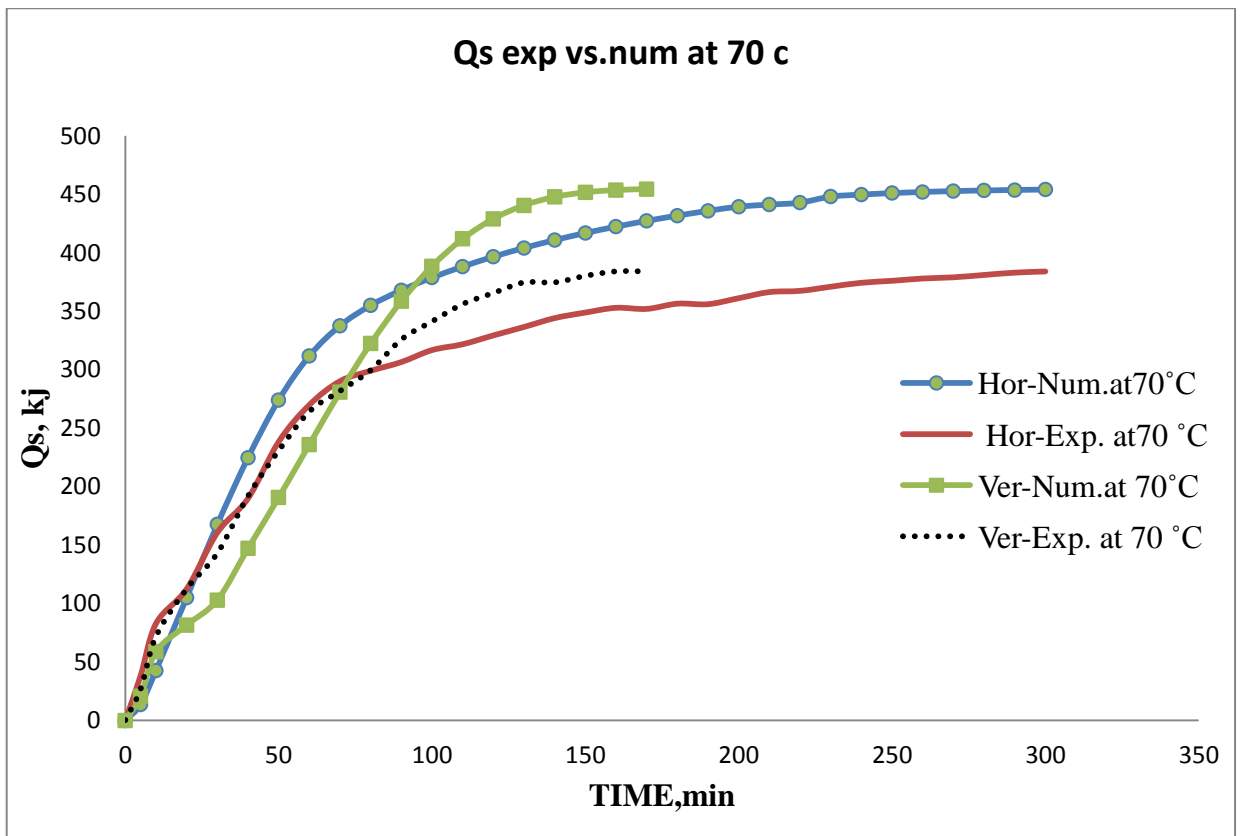


Fig. (5.25) Experimental and numerical stored energy for two orientations of the heat exchanger.

**CHAPTER SIX**  
**CONCLUSIONS AND**  
**RECOMMENDATIONS**

### *Chapter Six: Conclusions and Recommendations*

The experimental and numerical investigation of melting of phase change material inside an annular cavity of horizontal and vertical heat exchanger exhibit the following conclusions and suggestions for future works.

#### **6.1 Conclusions**

According to the experimental findings and numerical predictions, the following concluding remarks are extracted:

- 1- The natural convection is dominated the most periods of melting process, while the role of pure conduction is a privilege only at the initial period of the melting process.
- 2- The melting time was reduced by increasing the inlet temperature of water for both orientations of heat exchanger. It is reduced about 27.5% and 46.3% when the inlet water temperature is changed from 60 to 70 °C and from 70 to 80 °C, respectively for horizontal heat exchanger. For the same temperature increase, the melting times are reduced by 32.6% and 50.2% for vertical heat exchanger.
- 3- The melting rate of PCM in the vertical heat exchanger is higher than that in the horizontal heat exchanger. Also, the required time for melting process in the vertical heat exchanger are reduced by 28.7%, 30.4% and 31.2% than in the horizontal heat exchanger for inlet water temperatures of 60, 70 and 80 °C, respectively.
- 4- The accumulated energy stored by PCM during the melting process in vertical heat exchanger is higher than that obtained in the horizontal orientation of heat exchanger by about 4, 14.2 and 16.3% at water temperatures of 60, 70 and 80 °C, respectively at time of 140 min.
- 5- The temporal variation of the Nusselt number is directly varying with the inlet HTF temperature.

- 6- The melting front is affected by inlet temperature, the orientation of heat exchanger and the dominant mechanisms of heat transfer.

## **6. Recommendations for future works**

The current investigation of the PCM melting inside annular cavity of two orientations leads to the following recommendations and additional suggestions for future researches:

- 1- Studying the melting behavior of PCM inside annular cavity of the inclined heat exchanger of tilt angles of 30, 45° and 60°.
- 2- Investigating the effect of the eccentricity by deviation the location of an internal tube from the center on the melting process of two orientations of the heat exchanger.
- 3- Exploring the influence of using several internal tubes (2, 3 or 4) on the melting process with maintaining the same surface area. Also, studying the effect of the hot pipes arrangement on the melting rate.
- 4- Studying the solidification (discharging) process of liquid PCM under the effect of both the HTF temperature and orientation of heat exchanger.
- 5- Researching the melting process after enhancing the thermal conductivity of PCM by dispersion solid nanoparticles, insertion fins, porous media, etc.

## Reference

- 1- Zalba, B., Marin, J. M., Cabeza, L. F., Mehling, H., Review on thermal energy storage with phase change: materials, heat transfer analysis and applications, *Applied Thermal Engineering*, 23, 2003:pp. 251–283.
- 2- Gasia, J., Steven, N.H., Belusko, M., Luisa, F., Cabeza, Bruno F., Experimental investigation of the effect of dynamic melting in a cylindrical shell-and-tube heat exchanger using water as PCM, *Applied Thermal Energy*, 185, 2017:pp.136–145.
- 3- Tabassum. T., A Numerical Study of a Double Pipe Latent Heat Thermal Energy Storage System, Master Thesis, 2009, McGill University.
- 4- Gao, D., Deng, T., Energy storage: Preparations and physicochemical properties of solid- liquid Phase change materials for thermal energy storage, 2013:pp. 32–44
- 5- Shmueli, H., Ziskind, G., Letan, R., Melting in a vertical cylindrical tube: Numerical investigation and comparison with experiments, *International Journal of Heat and Mass Transfer*, 53, 2010:pp. 4082–4091.
- 6- Waghmare, A. V., Pise, A. T., Numerical investigation of concentric cylinder latent heat storage with / without gravity and buoyancy. *Energy Procedia*, 75, 2015:pp. 3133–3141.
- 7- Bechiri, M., Mansouri, K., Study of heat and fluid flow during melting of PCM inside vertical cylindrical tube, *International Journal of Thermal Sciences*, 135, 2018: pp. 235–246.
- 8- Guo, S.Y., Peng, C., Wang, W., Experimental study of paraffin melting in cylindrical cavity with central electric heating rod, *Energy Procedia*, 237, 2018: pp. 264–271.
- 9- Al Siyabi, I., Khanna, S., Mallick, T., and Sundaram, S., An experimental and numerical study on the effect of inclination angle of

- phase change materials thermal energy storage system, *J. Energy Storage*, 23, 2019:pp. 57–68.
- 10- CHUNG, J., LEE, J. S., Thermal instability during the melting process in an isothermally heated horizontal cylinder, *Heat Mass Transfer*, 16, 1997:pp. 3899-3907.
  - 11- Kawanami, T., Fukusako, S., Yamada, M., Itoh, K., Experiments on melting of slush ice in a horizontal cylindrical capsule. *Heat and Mass Transfer*, 42, 1999: pp. 1870–1879.
  - 12- Regin, F.A., Solanki, S.C., Saini, J.S., Latent heat thermal energy storage using cylindrical capsule: Numerical and experimental investigations. *Renewable energy*, 31, 2006:pp. 2025-2041.
  - 13- Hlimi, M., Hamdaoui, S., Mahdaoui, M., Kousksou, T., Msaad, A. A., Jamil, A., and El Bouardi, A., Melting inside a horizontal cylindrical capsule, *Case Stud. Therm. Eng.*, 8, 2016:pp. 359–369.
  - 14- Ansyah, P. R., Waluyo, J., Najib, S, M., and Anggara, F., Thermal Behavior of Melting Paraffin Wax Process in Cylindrical Capsule by Experimental Study. *American Institute of Physics*, (020008), 2018.
  - 15- Ghasemi, B., Molki, M., Melting of unfixed solids in square cavities, *Heat and Fluid Flow*, 20, 1999: pp. 446–452.
  - 16- Yanxia, D., Yanping, Y., Daiyong, J., Baoyi, C., Jinfeng, M., Experimental investigation on melting characteristics of ethanolamine – water binary mixture used as PCM, *Heat and Mass Transfer*, 34, 2007: pp. 1056–1063.
  - 17- Younsi, Z., Joulin, A., Zalewski, L., Phase Change Materials: A Numerical Method for the Behavior Predictions. *Theory and Applications*, 33, 2009:pp.1–7.
  - 18- El Qarnia, H., Draoui, A., Lakhel, E. K., Computation of melting with natural convection inside a rectangular enclosure heated by discrete protruding heat sources, *Applied Mathematical Modelling*, 37, 2013: pp. 3968–3981.



- 19- Kousksou, T., Mahdaoui, M., Ahmed, A., Msaad, A. A., Melting over a wavy surface in a rectangular cavity heated from below, *Energy*, (64), 2014:pp. 212–219.
- 20- Kamkari, B., Jahedi, H., Numerical simulation and experimental verification of constrained melting of phase change material in inclined rectangular enclosures, *Heat and Mass Transfer*, 88, 2017: pp. 211–219.
- 21- Wang, Y., Dai, J., An, D., applied sciences Numerical Investigations on Melting Behavior of Phase Change Material in a Rectangular Cavity at Different Inclination Angles, *Applied Sciences*, 2018.
- 22- Hong, Y., Ye, W., Du, J., Huang, S., Solid-liquid phase-change thermal storage and release behaviors in a rectangular cavity under the impacts of mushy region and low gravity, *International Journal of Heat and Mass Transfer*, 130, 2019: pp. 1120–1132.
- 23- Faistauer, F., Rodrigues, P., Oliveski, R. D. C., Numerical Study of Phase Change of PCM in Spherical Cavities, *Trans Tech Publications Switzerland*, 372, 2017:pp. 21–30.
- 24- Khodadadi, J.M., Zhang, Y., Effects of buoyancy-driven convection on melting within spherical containers, *International Journal of Heat and Mass Transfer* , 44, 2001: pp1605–1618.
- 25- Tan, F. L., Hosseinizadeh, S. F., Khodadadi, J. M., Fan, L., International Journal of Heat and Mass Transfer Experimental and computational study of constrained melting of phase change materials ( PCM ) inside a spherical capsule, *International Journal of Heat Mass Transfer*, 52. (15–16), 2009:pp. 3464–3472.
- 26- Khot, S. A., Sane, N. K., Gawali, B. S., Experimental Investigation of Phase Change Phenomena of Paraffin Wax inside a Capsule, *International Journal of Engineering Trends and Technology* ,2, 2011: pp. 67–71.

- 27- Hosseinizadeh, S. F., Darzi, A. A. R., Tan, F. L., Khodadadi, J. M., Unconstrained melting inside a sphere, *International Journal of Thermal Sciences* , 63, 2013:pp. 55–64.
- 28- Sattari, H., Mohebbi, A., Afsahi, M. M., Yancheshme, A. A., CFD simulation of melting process of phase change materials ( PCMs ) in a spherical capsule, *International Journal of Refrigeration*, 2016.
- 29- Li, W., Li, S. Guan, S., Wang, Y., Zhang, X., Numerical study on melt fraction during melting of phase change material inside a sphere, *Int. J. Hydrogen Energy*, 2017:pp. 1–8.
- 30- Junior, J. F. R., Olivesik, R. D. C., Rocha, L. A. O., Biserni, C., numerical investigation on phase change materials (PCM):the melting process of Erythritol in spheres under different thermal conditions, *int. j. mech. sci.*, 2018.
- 31- Gao, Z., Yao, Y., . Wu, H., A visualization study on the unconstrained melting of paraffin in spherical container, *Applied Thermal Engineering*, 155, 2019: pp. 428–436.
- 32- Ng, K. W., Gong, Z. X., Mujumdar, A. S., Heat Transfer in free convection-dominated melting of a phase change material in a horizontal annulus, *Heat Mass Transfer*, 25,1998: pp. 631–640.
- 33- Khillarkar, D. B., Gong, Z. X., Mujumdar, A. S., Melting of a phase change material in concentric horizontal annuli of arbitrary cross-section, *Applied Thermal Engineering*, 20, 2000: pp.893–912.
- 34- Ettouney, H., El-dessouky, H., Al-kandari, E., Heat Transfer Characteristics during Melting and Solidification of phase change energy storage process, *Ind. Eng. Chem*, 2004: pp. 5350–5357.
- 35- Wei,L., Xinguo, L., Jun, Z., Numerical Study of Melting in a Square Annulus, *National High Technology Research*, 2006, pp. 5–8.
- 36- Adine, H. A., El Qarnia, H., Numerical analysis of the thermal behaviour of a shell-and-tube heat storage unit using phase change

- materials, *Application Mathematical Model*, 33, 2009: pp. 2132–2144.
- 37- Dutta, R., Atta, A., and Dutta, T. K., Experimental and Numerical Study of Heat Transfer in Horizontal Concentric Annulus Containing Phase Change Material, *The Canada Journal of Chemical Engineering*, 86 2008:pp. 700–710.
- 38- Hosseini, M. J., . Ranjbar, A. A., Sedighi, K., Rahimi, M., A combined experimental and computational study on the melting behavior of a medium temperature phase change storage material inside shell and tube heat exchanger, *Int. Commun. Heat Mass Transf.*, 39(9), 2012:pp. 1416–1424.
- 39- Darzi, A. R., Farhadi, M., Sedighi, K., Numerical study of melting inside concentric and eccentric horizontal annulus, *Appl. Math. Model*,36(9), 2012: pp. 4080–4086.
- 40- Azad, M., Groulx, D., Melting of Phase Change Materials in a Cylindrical Enclosure : Parameters Influencing Natural Convection Onset, proceeding of the 4th international forum on heat transfer. 2016.
- 41- Kurnia, J. C., Sasmito, A. P., Ping, S. I., Investigation of Heat Transfer on a Rotating Latent Heat Energy Storage, *Energy Procedia*, 105, 2017: pp. 4173–4178.
- 42- Faghani, M., Hosseini, M. J., Bahrampoury, R., Numerical simulation of melting between two elliptical cylinders, *Alexandria Eng. J.*, 2017:pp. 1–10.
- 43- Cao, X., Yuan, Y., Xiang, B., Haghghat, F., Effect of natural convection on melting performance of eccentric horizontal shell and tube latent heat storage unit, *Sustain. Cities Soc.*, 38, 2018: pp. 571–581.
- 44- Seddegh, S., Joybari, M. M., Wang, X., Haghghat, F., Experimental and numerical characterization of natural convection in a vertical

shell-and-tube latent thermal energy storage system, Sustain. Cities Soc., 2017.

- 45- Xiong, W., Numerical and Experimental Study of the Melting Process of a Phase Change Material in a Partically Filled Spherical Shell, 2017, Thesis.
- 46- Voller V. R., Prakash, C., A fixed grid numerical modeling methodology for convection-diffusion mushy region phase-change problems, Heat Mass Transfer, 30, 1987.
- 47- Kumar, M., Krishna, D. J., Influence of Mushy Zone Constant on Thermohydraulics of a PCM, Energy Procedia, 109, 2017:pp. 314–321.
- 48- Holman, J. P., Experimental Method for Engineers. Mc.Graw-Hill,2001.

Calibration of Thermocouples and Data Logger

العدد : ٤١٦٢  
التاريخ : ٢٠١٩ / ١ / ١١  
هـ : ١ / ١

جمهورية العراق

وزارة التخطيط  
الجهاز المركزي للقياس والسيطرة النوعية

الدائرة : القياس .  
القسم : المقاييس.

إلى / جامعة كربلاء - كلية الهندسة - الدراسات العليا

م / ابناء مساعدة

بهدي جهازنا أطيب تحياته .....  
أشارة إلى كتابكم المرقم (د.ع / ١٥١٨ / ٦ / ١٠) في ٢٠١٩/٣/٢٠ .  
نود اعلامكم الاتي :  
١- تم معايرة المزدوجات الحرارية الواردة في كتابكم اعسلاء و المييلة اذناه و ينبغي الاخذ  
بنظر الاعتبار النتائج و التصحيحات المييلة عند القياس علما ان المعايرة نافذة لغاية سنة  
من تاريخ اجرائها .  
٢- تم تسديد اجور المعايرة البالغة (١٦٥٠٠٠) مائة و خمسة و ستون الف دينار دينار فقط  
بموجب الوصل المرقم (١٧٢٠٥) في ٢٠١٩/٤/١٦ .

الاجهزة :

- قارئ درجة حرارة مع مزدوج حراري نوع K عدد (٥) بالشهادات المرقمة :  
PHT 420 - 421 - 422 - 423 - 424 /2019  
مع التقدير .

المرقات /

شهادة معايرة عدد (٥) فقط .

فسي ابراهيم خليل  
مدير عام دائرة القياس / وكالة  
٢٠١٩/٤/١١



لمسوخة منه الى /

- قسم الهندسة الميكانيكية - طالب الماجستير وسام عباس نخلان  
- قسم المقاييس / شعبة القياسات الفيزيولوجية.

م . خلدون

# Appendix



## Calibration Certificate Central Organization for Standardization and Quality Control (COSQC) Metrology Department - Physics Section

P.O. Box 13032 Aljadriya street, Baghdad, Tel: 7785180 - E-Mail: cosqc@cosqc.gov.iq

Certificate No: PHT 423/2019  
Date of issue: 20/04/2019

Customer	
Name:	جامعة كربلاء - كلية الهندسة - الدراسات العليا - قسم الهندسة الكهربائية - الطالب وسام همام دنان
Address:	العراق - كربلاء
Item under calibration	
Description:	Temperature Recorder 12 CH SD Card Data Logger + TC (K)
Manufacturer:	Lutron / Taiwan
Model:	BTM - 4208SD
Serial number:	1130093 / TC : ( 4 )
Other identification:	( -200 ----- 1370 ) °C Res. : 0.1 °C
Date of reception:	Order no. (IBD) date : 16/04/2019
Condition of reception:	At Found
Standard(s) used in the calibration	
Description:	Digital Nano volt / Micro Ohm meter
Manufacturer:	Agilent / Malaysia
Model:	34420A
Serial number:	MY42000734
Other identification:	ID : PHT-01-17 ID : PHT-01-04, 85, 86
Calibration information	
Date of calibration:	17/04/2019 Due to: 17/04/2020
Place of calibration:	PH LAB 1
Method(s) of calibration:	Calibration method using - PtDC-TC-012 (C)
Calibrated quantity:	Temperature °C
Results of calibration:	Attached a complete result in Annex 1 to 2 of this certificate
Measurement uncertainty:	The reported expanded uncertainty is based on UKAS M3003 Standard and the standard Uncertainty multiplied by coverage factor k=2 to give confidence level of 95%
Metrological traceability:	The traceability of measurement results to the SI units is assured by the National standard maintained at Central Organization for standardization and Quality Control through calibration at - UNE /CER, NO (G1KS-0127)
Environmental conditions of calibration:	Temp: 25.65 °C RH: 30.9%
Observations, opinions or recommendations:	The results and corrections in Annex 1 should be taken into consideration

Approved by:



*Moyasser Ali Taher*  
Moyasser Ali Taher  
20/04/2019

1 of 2

This certificate is issued in accordance with the laboratory accreditation requirements. It provides traceability of measurement to recognized national standards in the units of measurement realized at the COSQC or other recognized national standards laboratories. This certificate may not be reproduced other than as led by photographic process. This certificate refers only to the particular item subjected for calibration.

Ref. Proc.Tc-012

# Appendix



**Calibration Certificate**  
**Central Organization for Standardization and Quality Control (COSQC)**  
**Metrology Department - Physics Section** (Proc.TC-012)  
P.O. Box13032 Aljadriya street, Baghdad , Tel:7785180 - - E-Mail : cosqc@cosqc.gov.iq


Annex 1

Certificate No.: PHT 423/2019  
Date of issue : 28/04/2019

## Results

The results of the measurements are given on table below.

Set	Ref. C* (R)	UUC C* (M)	Error C* (M) (R)	Uncertainty $\pm C^*$
0	-0.21	0.06	0.27	0.48
50	49.72	49.34	-0.38	0.43
100	100.48	99.86	-0.62	0.48

  
Calibrated by :  
Khalid Naser  
28/04/2019

  
Revised by :  
Moyasser Ali Taher  
28/04/2019



  
Approved by:  
Moyasser Ali Taher  
28/04/2019

2 of 2

This certificate is issued in accordance with the laboratory accreditation requirements. It provides traceability of measurement to recognized national standards to the units of measurement realized at the COSQC or other recognized national standards laboratories. This certificate may not be reproduced other than in full by photographic process. This certificate refers only to the particular item submitted for calibration.

Ref. Proc.TC-012

## Appendix

### Appendix B

#### Evaluation of the effect of water flow rate on the melting process

It was observed experimentally and numerically that the flow rate has an insignificant effect on the melting characteristics of PCM inside an annular cavity of two orientations of the heat exchanger. The time-variation of the liquid fraction of PCM in two orientations of heat exchanger is evaluated experimentally (Fig. (B.1)) and numerically (Fig. (B.2)) for two values of volumetric flow rate. The results prove that the weak effect of water flow rate on the melting process.

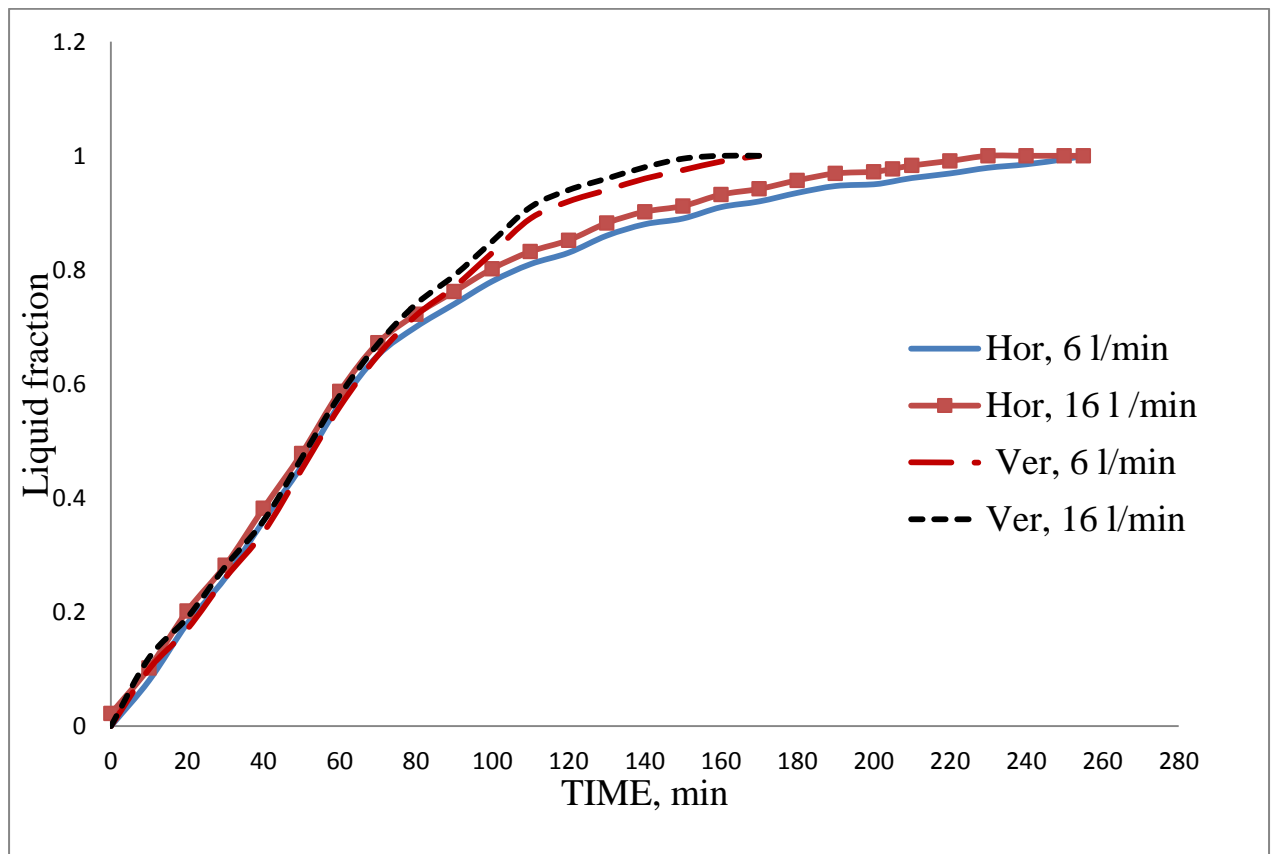


Fig. (B.1) Experimental result of the melt fraction for two values of water flow rates.



## Appendix

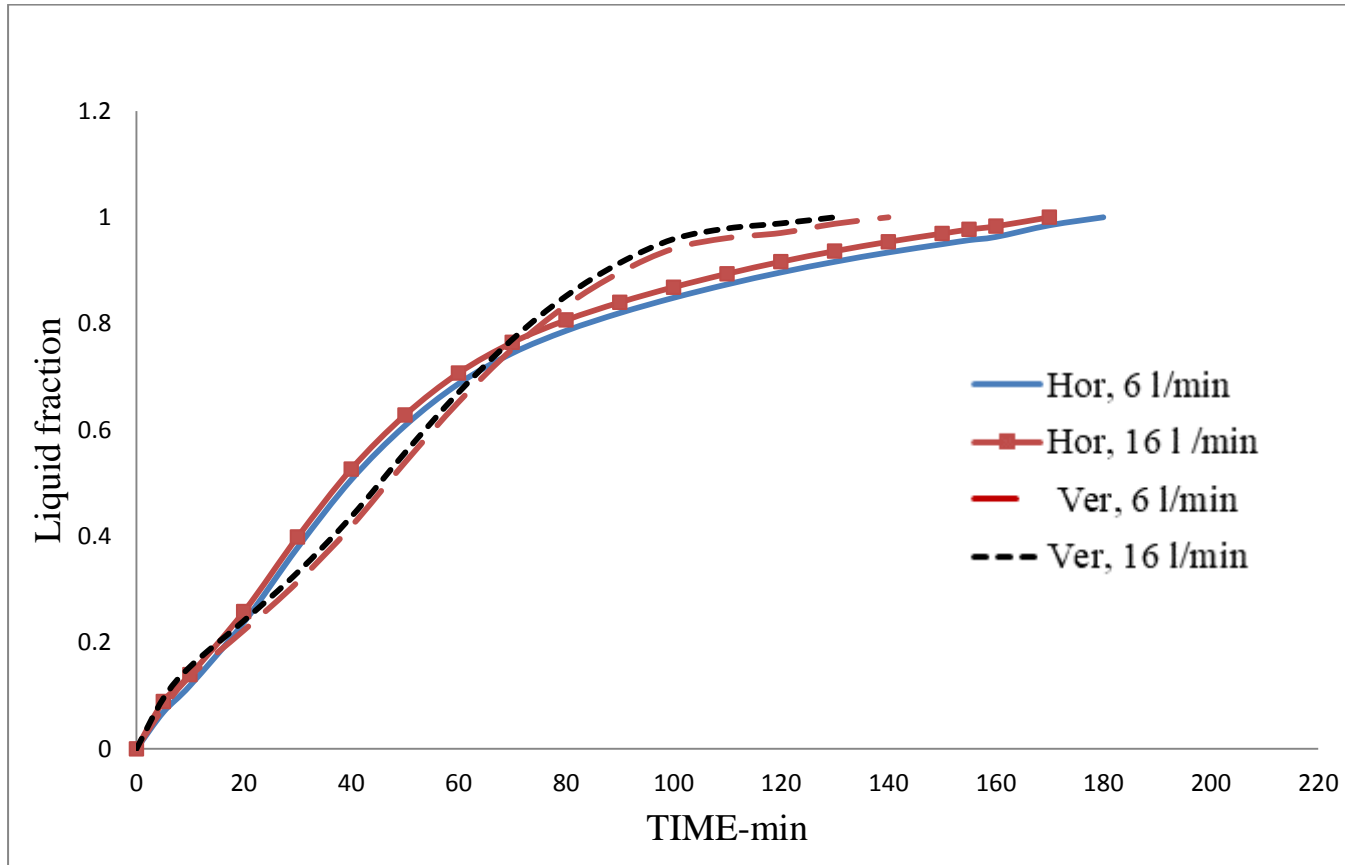


Fig. (B.1) Numerical result of the melt fraction for two values of water flow rates.

## المستخلص

تتضمن الدراسة الحالية تحقيقاً تجريبياً وعداداً للأداء الحراري لمواد تغيير الطور (PCM) داخل مبادل حراري مركزي ثنائي الأنابيب. تم استخدام شمع البارافين RT-42 Rubitherm لملء الفراغ الحلقي بين الأنبوب الداخلي النحاسي الساخن بقطر ٢٥ ملم وقذيفة الأكريليك الخارجية المعزولة بقطر ٧٥ ملم. يتضمن الإعداد التجريبي اثني عشر مزدوجاً حرارياً لتسجيل درجات الحرارة العابرة لـ PCM في مواقع مختلفة. أيضاً ، يتم تتبع تقدم الجبهة الصلبة السائل أثناء عملية الانصهار فوتوغرافياً بواسطة كاميرا رقمية. طبق المحاكاة العددية ثنائية الأبعاد الطريقة المستخدمة في مسامية التثبيت لحل مشكلة ذوبان PCM. يتم فحص تأثير درجات حرارة مختلفة (٦٠ و ٧٠ و ٨٠ درجة مئوية) من الماء الساخن مثل سائل نقل الحرارة (HTF) الذي يتدفق داخل الأنبوب الداخلي على عملية الصهر. أيضاً ، تم بحث تأثير الاتجاهين (الأفقي والرأسي) للمبادل الحراري على سلوك ذوبان PCM.

أظهرت النتائج التجريبية والعددية أن الطبقة الذائبة من PCM تتشكل بشكل متماثل حول الأنبوب الداخلي لكلا اتجاهي نقل الحرارة بسبب هيمنة التوصيل في المرحلة الأولى من عملية الانصهار. في وقت لاحق ، تنمو طبقة ذوبان PCM ويتم تطوير تأثير الحمل الحراري الطبيعي مما يؤدي إلى ارتفاع معدل الانصهار في الجزء العلوي من التجويف. لقد بدا أن وقت الذوبان ينخفض بشكل واضح عن طريق زيادة درجة حرارة مدخل الماء في كلا المبادلات الحرارية. أيضاً ، فإن معدل انصهار PCM في الاتجاه العمودي أسرع من معدل الانصهار في الاتجاه الأفقي. كشفت النتائج التجريبية أن زمن الانصهار في المبادل الحراري الأفقي الحلقي PCM الحلقي انخفض حوالي ٢٧.٥ ٪ و ٤٦.٣ ٪ عندما ارتفعت درجة الحرارة من ٦٠ إلى ٧٠ درجة مئوية ومن ٦٠ إلى ٨٠ درجة مئوية ، على التوالي. لنفس الزيادة في درجة الحرارة ، يتم تسريع وقت الذوبان بحوالي ٣٢.٦ ٪ و ٥٠.٢ ٪ في المبادل الحراري العمودي. كذلك ، فإن قيم الطاقة المخزنة بواسطة PCM في المبادل الحراري العمودي أعلى حوالي ٤ و ١٤.٢ و ١٦.٣ ٪ من تلك التي تم الحصول عليها في الاتجاه الأفقي عند ١٤٠ دقيقة عند ٦٠ و ٧٠ و ٨٠ درجة مئوية على التوالي. بالإضافة إلى ذلك ، فإن رقم Nusselt العابر له نفس السلوك في اتجاهين ويتغير بشكل إيجابي مع كمية الطاقة الحرارية المنقولة من HTF والتي بدورها تختلف بالتناسب مع درجة حرارة مدخل HTF.

أظهرت النتائج العددية والتجريبية اتفاق جيد. تم العثور على الحد الأقصى للاختلافات بين النتائج العددية والتجريبية لوقت الانصهار ، وعدد نسلت وتخزين الطاقة لتكون ١٢.٤ ، ٢٢.٥ و ٢٢.١ % لمبادل حراري أفقي عند ٧٠ درجة مئوية من درجة حرارة المياه مدخل. في حين أن هذه الاختلافات هي ١٠.٧ ، ١٤.٩ و ١٥.٤ % للمبادل الحراري العمودي.



وزارة التعليم العالي والبحث العلمي

جامعة كربلاء

كلية الهندسة

قسم الهندسة الميكانيكية

## دراسة الأداء الحراري لمواد متغيرة الطور لمبادل حراري.

رساله مقدمه الى كلية الهندسة- جامعه كربلاء كجزء من متطلبات نيل  
درجه الماجستير في علوم الهندسة الميكانيكية.

من قبل

وسام عباس دخان

بأشراف

أ.د. تحسين علي حسين الحطاب

أ.م.د. نبيل شهيد ضيدان

٢٠١٩